ANALYSES OF ATMOSPHERIC AND MARINE OBSERVATIONS ALONG THE TURKISH COAST

A THESIS SUBMITTED TO
THE GRADUATE SCHOOL OF THE INSTITUE OF MARINE SCIENCES
OF
THE MIDDLE EAST TECHNICAL UNIVERSITY

BY

ERSİN TUTSAK

IN PARTIAL FULFILLMENT OF THE REQUIREMENTS
FOR
THE DEGREE OF MASTER OF SCIENCE
IN
THE DEPARTMENT OF PHYSICAL OCEANOGRAPHY

SEPTEMBER 2012

Approval of the thesis

"**ANALYSES OF ATMOSPHERIC AND MARINE OBSERVATIONS ALONG THE TURKISH COAST**"

submitted by **Ersin Tutsak** in partial fullfillment of the requirements for the degree of **Master of Science in Physical Oceanography** by,

Prof. Dr. Ahmet Kideyş _____
Director, **Graduate School of The Institue of Marine Sciences**

Prof. Dr. Emin Özsoy _____
Head of Department, **Physical Oceanography**

Prof. Dr. Emin Özsoy _____
Supervisor,

Examining Committee Members:

Assoc. Prof. Dr. Bettina Fach Salihoğlu _____

Prof. Dr. Emin Özsoy _____

Assoc. Prof. Dr. Mustafa Koçak _____

Date: _____

I hereby declare that all information in this document has been obtained and presented in accordance with academic rules and ethical conduct. I also declare that, as required by these rules and conduct, I have fully cited and referenced all material and results that are not original to this work.

Name, Last name : Ersin Tutsak

Signature :

ABSTRACT

ANALYSES OF ATMOSPHERIC AND MARINE OBSERVATIONS ALONG THE TURKISH COAST

Tutsak, Ersin

M.Sc, Department of Physical Oceanography

Supervisor: Prof. Dr. Emin Özsoy

September 2012, 125 pages

Time series and spectral analyses are applied to meteorological data (wind velocity, air temperature, barometric pressure) and sea level measurements from a total of 13 monitoring stations along the Turkish Coast. Analyses of four-year time series identify main time scales of transport and motion while establishing seasonal characteristics, i.e. distinguishing, for instance, between winter storms and summer sea-breeze system. Marine flow data acquired by acoustic doppler current profilers (ADCP) is also analyzed to better understand the response of the Turkish Strait System dynamics to short-term climatic variability. The cumulative results obtained from these analyses determine temporal and spatial scales of coastal atmospheric and marine fluxes as affected by the regional climate system.

Keywords: Timeseries, sea level, atmospheric observations

ÖZ

TÜRKİYE KIYILARI BOYUNCA ATMOSFERİK VE DENİZEL GÖZLEMLERİN ANALİZLERİ

Tutsak, Ersin

Yüksek Lisans, Fiziksel Oşinografi Bölümü

Tez Yöneticisi: Prof. Dr. Emin Özsoy

Eylül 2012, 125 sayfa

Zaman serisi ve spektral analizleri, Türk kıyıları boyunca bulanan 13 tane kıyısal izleme istasyonundan toplanan meteorolojik (rüzgar hızı, hava sıcaklığı, barometrik basınç) ve deniz seviyesi verilerine uygulandı. Dört yıllık zaman serilerinin analizleriyle, hareket ve taşınımların ana zaman ölçekleri tespit edilirken, mevsimsel özellikler örneğin kış fırtınaları ve deniz meltemi sistemleri arasındaki farklılıklar ortaya konuldu. Akustik doppler akıntı profileyicisi (ADCP) tarafından elde edilen akıntı verileri, Türk Boğazlar Sistemi dinamiklerinin kısa vadeli iklim değişikliklerine verdiği yanıtı anlayabilmek için analiz edildi. Bu analizlerden elde edilen kümülatif sonuçlar, bölgesel iklim sistemi tarafından etkilenen kıyısal atmosferik ve deniz akıların zamansal ve mekansal ölçeklerini belirledi.

Anahtar Kelimeler: zaman serileri, deniz seviyesi, atmosferik ölçümler

ACKNOWLEDGMENTS

I would like to express my deepest gratitude to my supervisor Prof. Dr. Emin Özsoy for his advice, criticism and encouragements throughout this study.

I would like to thank Assoc. Prof. Dr. Mustafa Koçak and Assoc. Prof. Dr. Bettina Fach Salihoğlu for their valuable suggestions and comments at every stage of the study.

I would also like thank to Adil Sözer, Ali Aydoğdu and Özgur Gürses for their valuable discussion and help. I would also extend my sincere thanks to my friends living in Setustu for making there a nice place.

Lastly, I would like to express my heartfelt thanks to Gül Akgül for her patience and support.

This study was supported by the Turkish Scientific and Technical Research Council (TUBITAK); Meteorology and Oceanography Network Pilot Project, Project No:105G029.

To My Family,

Contents

List of Figures

FIGURES

List of Tables

TABLES

LIST OF SYMBOLS

AH Air Humidity

AT Air Temperature

AP Atmospheric Pressure

ADCP Acoustic Doppler Current Profiler

BS Black Sea

BOS Bosphorus

CIL Cold Intermediate Layer

ECMWF European Centre for Medium-Range Weather Forecasts

TSS Turkish Straits System

TNVCN Turkish National Vertical Control Network

FFT Fast Fourier Transform

MEM Maximum Entropy Method

Chapter 1

INTRODUCTION

1.1 Objectives of the current study

The Turkish Straits System (TSS) is a unique channel system between the Black Sea and the Mediterranean Sea, which plays key role in exchanging water bodies through the Dardanelle (DS) and Bosphourus (BOS) straights (Ünüata *et al.*,1990). The channel system is vital for both Black Sea and Mediterranean Sea since the TSS demonstrates sensitivity to climatic changes and contrasts (Özsoy, 1998). It is also capable of driving environmental changes in the adjacent basins disproportionate to its relative size (Özsoy *et al.*, 2001). The main objective of the present study is to obtain long-term surface atmospheric and ocean data in an attempt to understand and quantify regional climatic variability in the Turkish coastal system as well as assess the effects of such variability on the Mediterranean-Black Sea coupling through the Turkish Straits System. More specifically the main aims of the present to study are to:

-identify the scales of motion detected by surface meteorological, sea level and current profile measurements
-determine the changes along the coast and at each station and quantify processes which can be identified
-evaluate local meteorological characteristics and their relation to regional processes
-study effects of local meteorology on sea level
-assess the interactions between sea level and Bosphorus currents

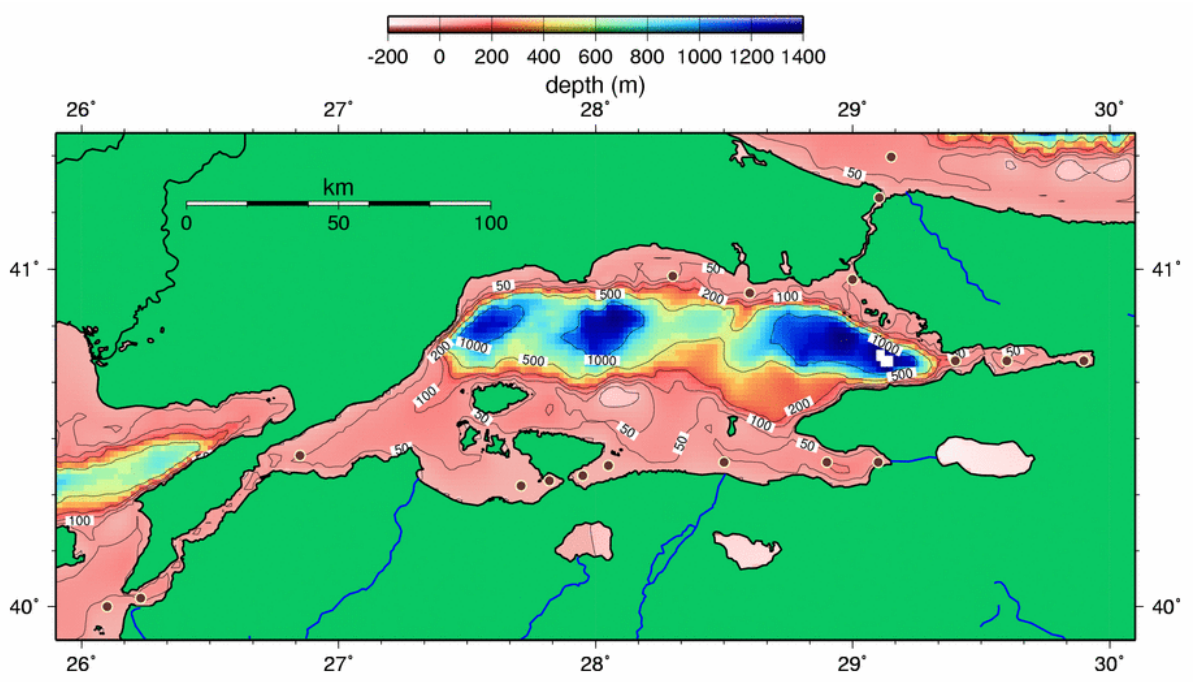

Figure 1.1: The bathmetry of Turkish Straits System

1.2 Turkish Straits System

The Turkish Straits System (Figure 1.1), formed by the Bosphorus and Dardanelles Straits and the sea of Marmara constitutes a water passage system between the Eastern Mediterranean and the Black Sea. The heavier Mediterranean water flows towards the Black Sea at the bottom while brackish water of Black Sea flows towards to the Eastern Mediterranean. The Sea of Marmara is a small basin (size 70 x 250 km, surface area: 11500 km^2, maximum depth 1390 m) with three depressions interconnected by sills. The Turkish Straits has narrow and shallow geometries; the depth of the Bosphorus varies between 30 m and 110 m with an average depth of 35 m. Its width changes between 0.7-3.5 km and its length is approximately 31 km. The contraction occurs at about 12 km north of the southern end of BOS. A sill is located about 3 km north of south end of BOS while another sill is located at the 4km north of north end of BOS. The Dardanelles Strait's length is 62 km where its width varies between 1.2-7 km with a mean of 4 km. The average depth of DS is 55m and its narrowest width occurs at about 25 km east of its junction with Aegean Sea (Unluata *et al.*, 1990).

The TSS is affected by two different seasonal climatic regimes. During the winter, the weather is dominated by an almost continuous passage of cyclonic systems. During the

summer, North east winds are dominant. When not blowing from the NE direction, winds most often come from the South West. In Figure 2, Paths 1 and 2 are typical summer-time trajectories that causes summer storms over the northern parts of Turkey and they result in abundant rain in the region. In winter, cold air masses from the Balkan Region and northern Europe are associated with these trajectories. They are characterized by substantial amplification of the planetary-scale flow waves during the development phase of the cyclone moving cold air to very low latitudes. The frequency of Paths 3 and 4 is greater in winter months than in other months. These types of cyclones are generally associated with above normal temperatures in their warm sector and normal temperatures at the back of the cold front (Karaca *et al.*, 2000).

The mass balance estimates reported by Unluata *et al.* 1990 indicate an average upper layer outflow of 600 km^3 per year and a lower layer inflow of 300 km^3 in the Bosphorus, However the instantaneous fluxes, calculated by ADCP measurements are greatly different from these estimates due to the transient meteorological and hydrological forcings (Latif *et al.*, 1991).

The exchange flow through the Bosphorus Strait is principally determined by geometry and stratification, and exhibits a complex nonlinear response to forcing by the net water budget, pressure and wind setup effects in adjacent basins (Unluata *et al.*, 1990; Ozsoy *et al.*, 1998; Gregg *et al.*, 1999; Gregg and Ozsoy, 2002). Time-dependent forcing creates daily to inter-annual variability in the currents and extreme conditions result in temporary blocking of the flows in either direction (Ozsoy *et al.*, 1996, 1998).

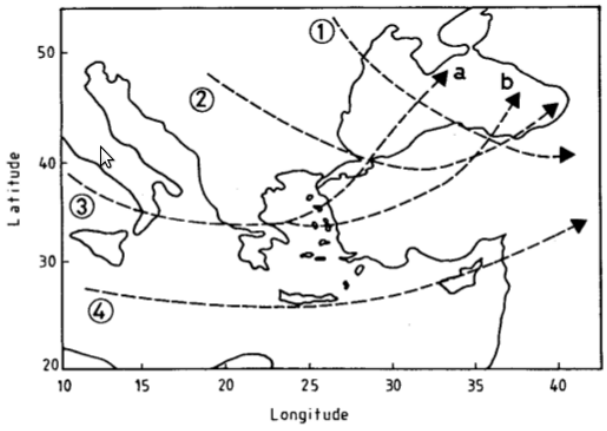

Figure 1.2: The paths of atmospheric cyclones over Turkey (reproduced from Karaca *et al.*, 2000)

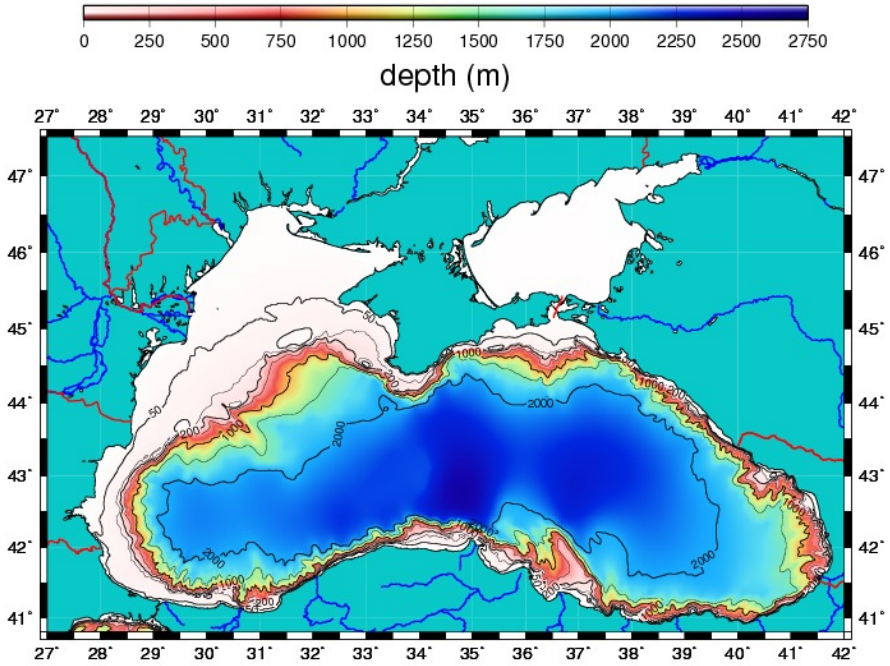

Figure 1.3: The bathmetry Of Black Sea

1.3 An Overview of Black Sea Oceanography

The Black Sea is an example of a landlocked sea with a surface area of 4.23x105 km^2 and a total volume of 5.47x105 km^3. That's connected to the other Seas only via the Bosporus Strait (Figure 1.3). The average depth with a maximum of 2200 m is estimated to be about 1240 m (Ross *et al.*, 1974). The abyssal plain is separated from the margins by steep continental slopes and the continental shelf is narrow expect the North Western (Ozsoy *et al.*, 1997)

The Black Sea region is affected by seasonal changes of atmospheric pressure patterns over the adjoining lands of Europe and Asia and frequented by eastward-travelling depressions especially during the October-March Period. The dominant wind direction is northeast in the western part, whereas southerlies dominate the eastern part of the basin.

The surface waters are strongly influenced by rivers; namely the Danube, Dniester and Dnieper. The Danube River contributes about half of the total river runoff to the Black Sea and the Dnieper and the Dniester Rivers provides aproxiamately 17 percent of the total river runoff(Sur, 2004). The Black Sea water budget contists of 350 km^3/yr river runoff, 350 km^3/yr precipitation and 350 km^3/yr evaporation (Unluata *et al.*, 1990). Seasonality of

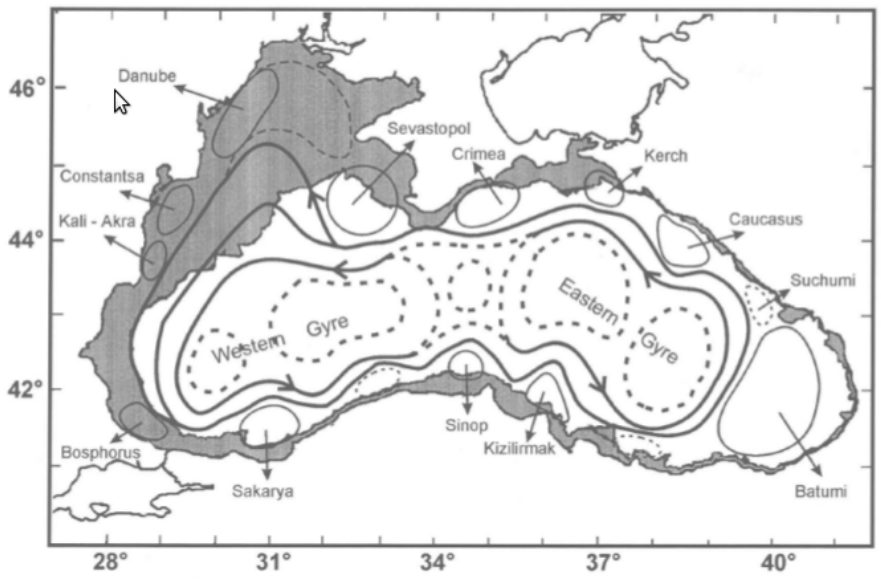

Figure 1.4: Schematic diagram illustrating the general circulation features of the Black Sea (Oguz *et al.*, 2005).

Danube River discharge obtained from 1996-2005 (Fig. 1.5) shows that the rate of runoff is maximal in the spring whereas it is minimal in winter.

The river origin low salinity surface waters overlay the warmer and more saline Mediterranean influenced waters. In between them, there exits a permanent cold intermediate layer (CIL) with the typical temperature less than 8^o C. The mechanism of formations of CIL is still not well known. The upper layer circulation system exhibits some major formations such as the Rim Current, a cyclonic boundary flow system that is flowing over the steep continental shelf topography, further intensifying in winter.

Based on Acoustic Doppler Current Profiler (ADCP) measurements, it is observed that the speed of the Rim Current is 50-100 cm/s at the surface and 10-20 cm/s between 150 meters and 300 meters (Oguz and Besiktepe, 1999). Figure 1.4 shows there are two cyclonic gyres circling within the peripheral flow with a number of anti-cyclonic eddies located at the coastal side of the Rim Current; namely the Bosphorus, Sakarya, Sinop, Kizilirmak, Batumi, Sukhumi, Caucasus, Kerch, Crimea, Sevastopol, Danube, Constantsa and Kaliakra eddies (Oguz *et al.*, 1998). Moreover, the Rim Current divides into two branches near the southern tip of Crimea. They converge and unite again at the south eastern coast. Additionally there is a meso-scale anti-cyclonic formation in the northwestern shelf (Oguz *et al.*, 1998b).

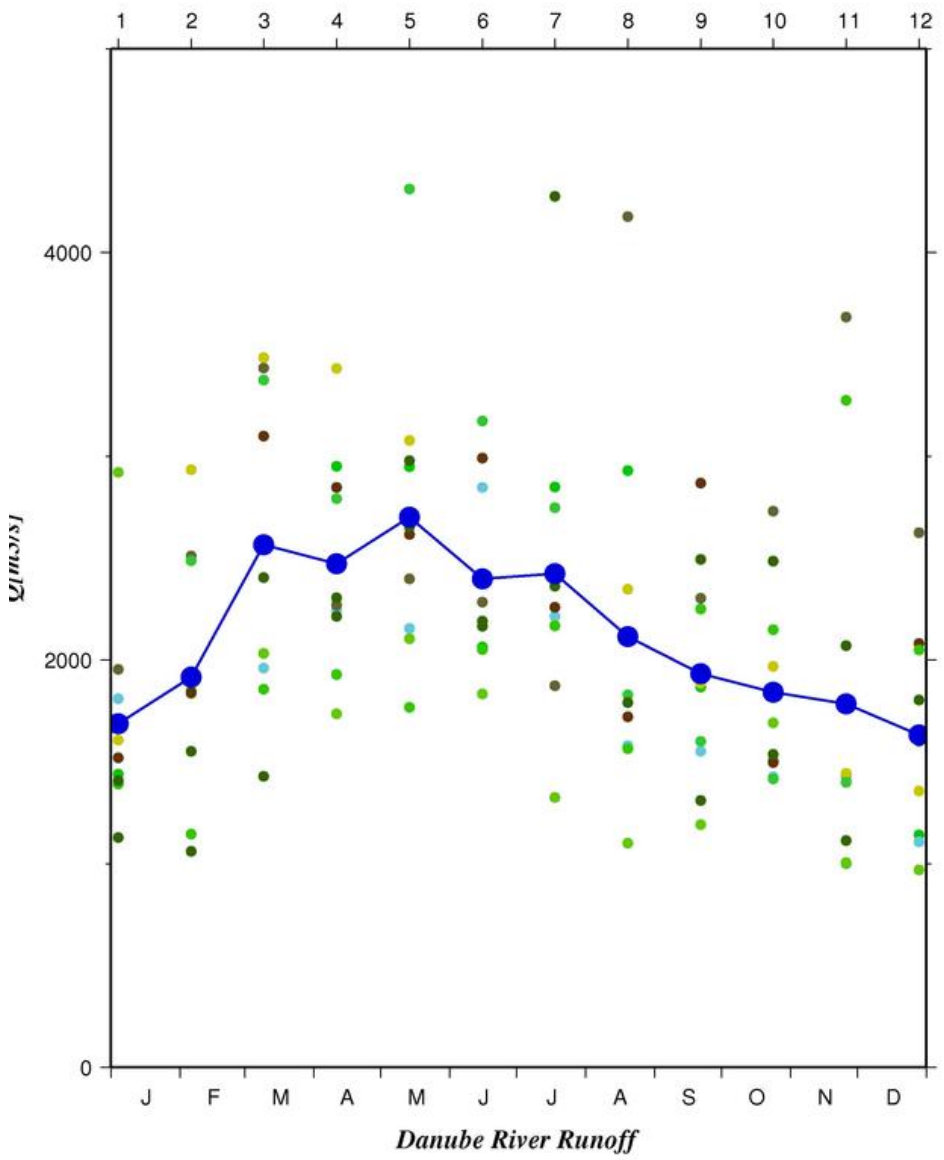

Figure 1.5: Average 10- year monthly discharge of the Danube from 1996 to 2005 (Pekarova *et al.*, 2008)

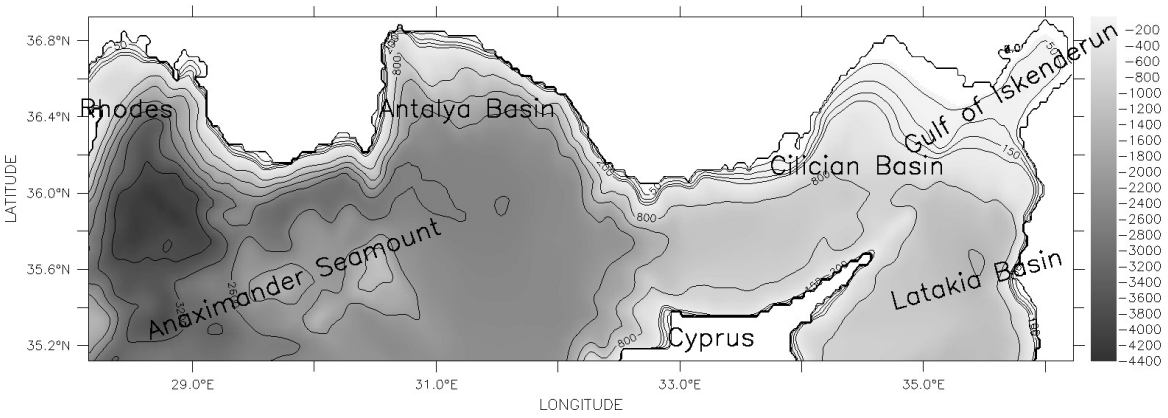

Figure 1.6: Bathymetry of the Northern Levantine Basin

1.4 An Overview of Mediterranean Oceanography

The Mediterranean is a semi-enclosed sea connected to the Black Sea by Turkish Straits System and the North Atlantic by Gibraltar Strait with an area of 2.5 million km^2. It is divided by Strait of Sicily into two as eastern and western basins. In this study, the region of interest of Mediterranean is Northern Levantine Basin located in northeastern corner of the sea hat stays in between 35^oN - 37^oN latitudes and 28^oE - 37^oE longitudes (Fig. 1.6).

Meteorologically, the Northern Levantine basin is under the influence of strong cyclones originated in Ionian Sea. Combination of the northerly Etesians coming over Aegean Sea and the westerly cyclones over Southern Levantine dominates the wind patterns on Northern Levantine in summer. On the other hand, in winter, the northerly Poyraz winds passing from the channels in Taurus Mountains strongly effects the atmosphere over the basin (*Özsoy, 1981*).

These cold Poyraz winds have a strong influence on the hydrology of Northern Levantine Basin. Levantine Intermediate Water (LIW) formation is directly related to the sudden cooling of the warm and saline Levantine Surface Water (LSW) (*Ovchinnikov, 1966*). Formation of LIW initiates a thermohaline cell which travels along European coasts of the Mediterranean and reaches to the Atlantic Ocean. Atlantic water flowing into the Mediterranian from the Gibraltar Strait meanders the coasts of North Africa and reaches to the Levantine Sea as Modified Atlantic Water (MAW) (*Zavatarelli and Mellor, 1995*).

Basic circulation features appear that in Northern Levantine are the permanent Asia Minor Current (AMC) and the cyclonic Rhodes Gyre, and quasi-permanent West Cyprus Eddy (Fig. 1.7). These upwelling processes and strong circulation structures result in a

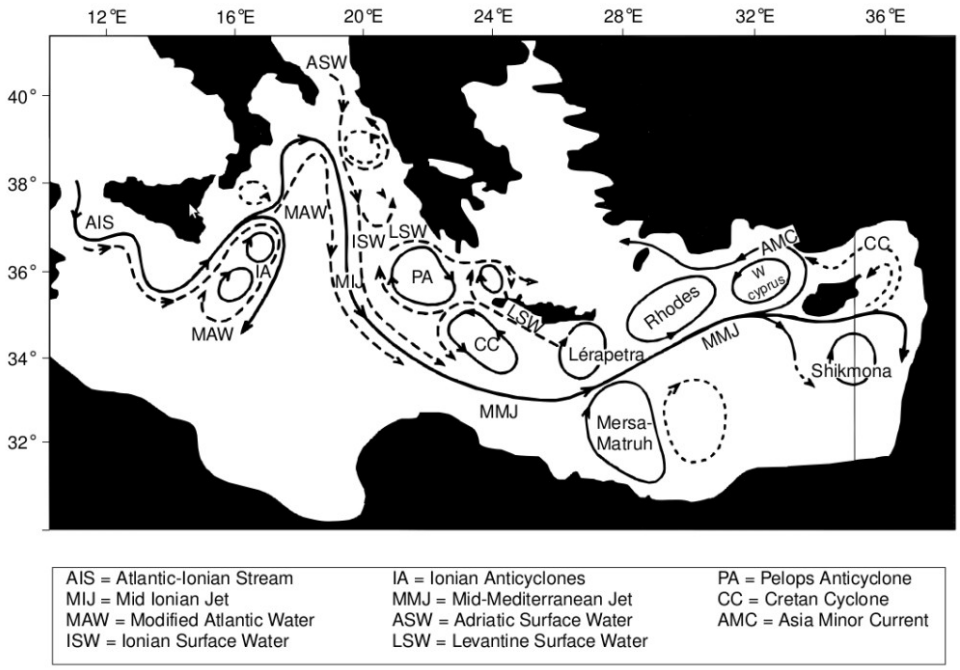

Figure 1.7: General Surface Circulation of Eastern Mediterranean (Robinson et al., 2001)

variation of sea surface height along the basin. The model used in Alhammoud *et al.* (2005) calculated a variation in the sea surface height anomaly amplitude values of 18 cm (from -8 cm to +10 cm). Moreover, Ayoub et al. (1998) found a range of 16 cm (from -6 cm to +10 cm) and Larnicol et al. (2002) of 27 cm (from -12 cm to +15 cm). Finally, MFS team (2001) proposed a 22 cm (from -6 cm to +16 cm) SSH anomaly amplitude.

Chapter 2

MATERIALS AND METHODS

2.1 Description of Sampling Sites

Meterological and marine physical parameters were obtained between January 2008 and December 2011 from 13 stations located on the coast of Turkey. These stations were installed within the framework of the Turkish Meteorology and Oceanography Excellent Network (MOEN) project in order to observe sea level, current direction and velocity and meteorological parameters namely; atmospheric pressure, air temperature, air humidity, wind velocity and wind direction. A total of 8 Coastal Monitoring Stations (CMS) were start-up on the coastal sites of Turkey and Turkish Republic of Northern Cyprus (TRNC), at the same time, 5 of the General Commander of Mapping stations were modified for this purpose from January 2008 and April 2008. Figure 2.1 and Table 2.1 present locations and geographical coordinates of the stations, respectively. As can be seen from Figure 2.1, Iskenderun, Erdemli, Taşucu, Bozyazı, Girne and Mağusa for Mediterranean Sea, Aksaz and Gökçeada for Aegen Sea, Erdek, Marmara Ereğlisi and Yalova for Marmara Sea and Şile and İğneada for Black Sea were selected to identify interactions of these region respect to each other. Except at Marmara Ereğlisi, meteorological parameters (atmospheric pressure, air temperature, air humidity, wind velocity and wind direction) and sea level were measured at all sites. In addition to these parameters, current data were obtained from Bosphourus.

2.2 Mean Observational Coverage

The sampling campaigns commenced in January 2008 and finished in December 2011. Over the sampling period at least a total of 1028 daily parameters were collected for each station. The sampling were at times interrupted owing to equipment failure. The percentage of mean observational coverage for each site over the whole sampling period is highlighted

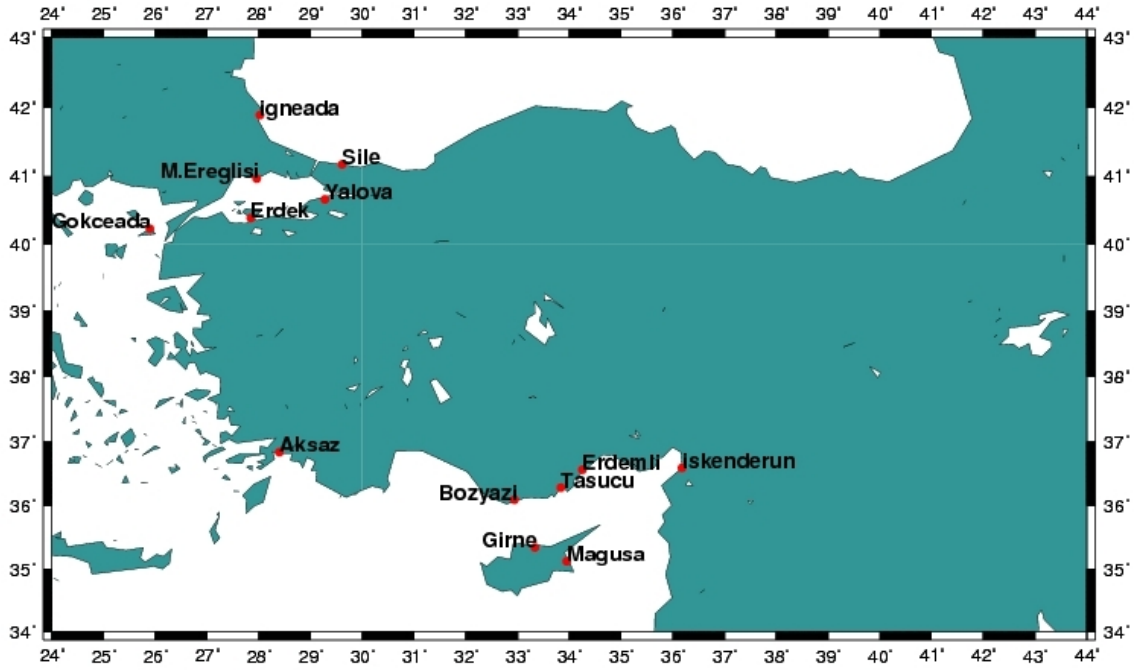

Figure 2.1: Locations of Stations on coastal sites of Turkey and TRNC

Table 2.1: Coordinates of Coastal Monitoring Stations

Region	Station	Latitude	Longitude	Establishment Date
Mediterranean	Iskenderun	36.5932	36.1802	24/05/2008
	Erdemli	36.5634	34.250	21/05/2008
	Tasucu	36.2814	33.8361	23/08/2008
	Bozyazi	36.0961	32.9400	21/08/2008
	Girne	35.3408	33.3342	24/10/2008
	Magusa	35.1233	33.9503	25/10/2008
Agean Sea	Aksaz	36.8378	28.3978	17/01/2008
	Göçkeada	40.2325	25.8939	14-01-2008
Marmara	Erdek	40.3898	27.8451	27/05/2008
	MarmaraEreglisi	40.9702	27.9602	28/05/2008
	Yalova	40.6628	29.2781	30/01/2008
Black Sea	Şile	41.1767	29.6117	30/01/2008
	Igneada	41.8897	28.0238	29/05/2008

in Figure 2.2. It is apparent from Figures 2.2 that the mean observational coverage within four years was different at the each sampling sites. During the study period mean sampling coverage were found to be lowest at İğneada and Taşucu ranging between % 70 and % 75. Mean coverage for Girne, Magusa and Erdemli was around % 80 while Iskenderun, Bozyazı, Göçkeada, Erdek and Marmara Ereğlisi demonstrated sampling coverages approximately %90. On the other, the highest mean sampling coverages were found for Aksaz, Yalova and Şile with values larger than % 98.

These recovery percentages given in Fig. 2.2 mainly based on average sampling periods of all parameters for each station. At times, there could be gap in one parameter while other parameters exist during that time. Moreover, sea level collected from Iskenderun Station during the study period is not used due to bad quality (See Appendix, Fig. 6.1).

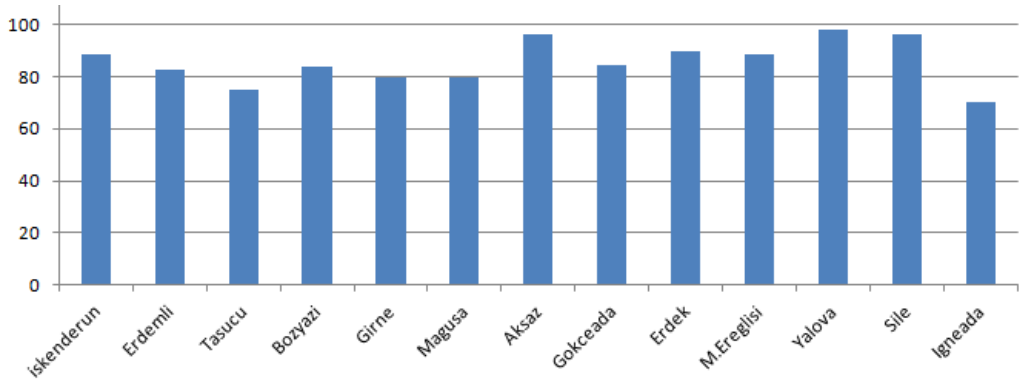

Figure 2.2: Data Recovery Percentage

2.2.1 Ancillary Data

In addition to observations, model outputs are utilized in this study, which are ROMS Model adapted for Bosphorus by Sözer (2012) and ERA-Interim produced by the European Centre for Medium-Range Weather Forecasts (ECMWF).

ROMS, three-dimensional free-surface, hydrostatic primitive equation model with stretched terrain-following coordinates in vertical is used (ROMS, Hedström 1997; Shchepetkin and McWilliams, 2005). Simulations are performed under two groups, idealized and real configuration.

In the ideal case, the geometry of the Bosphorus Strait is idealized with a contracting

channel, 34 km in length and 1300 m in width, a lateral constriction is laid at one-third of its length from the south end of the channel with a width of 700 m at the narrowest section. The abrupt openings to the Marmara and the Black Seas are represented by two relatively large reservoirs. A sill is located between the lateral constriction and the north reservoir. The channel has a constant depth of 70 m at every point of the model domain, except at the sill where the depth reduces to 57 m in 500 meters. The model domain is discretized with a 55 x 512 x 35 rectilinear grid. Temperature is taken as constant and the initial conditions of the model domain consist of water masses only with contrasting salinity values of 19 and 38 at south and north, respectively meeting at mid-channel. Model was run from the lock-exchange initial to the steady-state condition.

In the real case, the realistic topography of the Bosphorus is discretized with a variable resolution rectilinear grid with cross and along channel dimensions of 163 and 716, respectively. There are 35 s-levels following the topography, the vertical resolution varies between 0.7 to 2.85 m. The model domain is extended into the neighboring seas with two 10 km x 17.5 km rectangles with closed boundaries in east-west directions and open boundaries in north-south directions. The bathymetry is minimally smoothed, however the minimum depth is set as 25 m due to stability reasons, another simplification for the bathymetry is the constant depth relaxation at the open boundaries. The model is started from a lock-exchange initial condition with contrasting water masses meeting at the mid-channel, the salinity and temperature fields are set to (T=13.0, S=38.0), (T=24.1, S=17.6) at the south and north sections of the model domain, respectively. The model is started by the removal of an imaginary wall at the mid-channel to the steady-state condition and restarted again with nudged boundary conditions for temperature and salinity fields producing two-layer stratification of Marmara Sea and the CIL of Black Sea.

ERA-Interim is the latest global atmospheric reanalysis produced by the ECMWF (Dee *et al.*, 2011). In this study, atmospheric pressure and wind from ERA-Interim are used to better understand process involved with observations from stations.

2.3 Instrumentation

Over the sampling period meteorological parameters, sea level and current were obtained by instruments purchased from Campbell Scientific, Bartex and Nortek Companies,respectively. Meteorological and sea level instrumental equipment are powered by rechargeable batteries with approximately 10 days battery life, which are supplied by so-

lar electric panels. These instrumental equipment can be summarized as follow:

a) Meteorological parameters: Meteorological sensors accompanying with the tide gauge sensor at each station except for Marmara Ereglisi station are measuring atmospheric pressure (AP), air temperature (AT), air humidity (AH), wind speed (WS) and wind direction (WD) and of the output specifications are given table 2.2. These sensors have simple and well-known methodologies to observe the related parameters. To sum up, the atmospheric pressure sensor has a transducer to give an electronic signal indicating the amount of atmospheric pressure in the environment and also has a vibrating part affected by atmospheric pressure fluctuations. With the help of the vibrating part, the changes in the atmospheric pressure are detected. The relative humidity and the air temperature sensors are combined. The relative humidity is measured by a hygrometer having two thermometers mounted side-by-side. One thermometer bulb called the dry bulb is exposed to the open air and the other called the wet bulb is wrapped in a damp cloth. The relative humidity is calculated reading the temperature differences between the two thermometer. Because the wet bulb thermometer is cooled by the evaporation of water from the cloth and the rate of evaporation and cooling depends on the humidity in the air. Air direction is measured by a weather vane and its speed by an anemometer. An anemometer has small cups which catch the wind and spin around at different speeds with the respect to the strength of the wind. The wind speed therefore is calculated counting the amount of spins in a certain time.

b) Marine Physical parameters: The system at each station consists of a tide gauge and meteorological sensors and is powered by a rechargeable battery with approximately 10 days battery life, charged by solar electric panels. Sea level measurements in a station are made by the acoustic tide gauge sensor that sends an acoustic pulse by the help of a transducer towards the sea surface through a 13 mm diameter sounding tube. The time elapsed from transmission until reflection of pulse from the sea surface to the transducer is calculated in order to determine the vertical distance above the sea surface. The sounding tube protecting the acoustic energy from such adverse environmental effects as wind, rain, and snow comprises various tubes such as calibration tube providing a return echo from a known distance, the range tube being channel the acoustic pulses to and from the surface, the trim tube allowing minor corrections to the tube so that the overall tube length is flexible and the red brass tube providing a measure of anti-fouling to keep the end of the tube free of marine growth and algae. The calibration method is quite simple with a reference point whose distance to the transducer is known and also the acoustic pulse coming from the transducer has reflection from the reference point. Therefore, the travel time between the

reference point and the transducer is used to calculate the sound speed in the sounding tube, which enables the acoustic sea level sensor to calibrate itself in order to offset the changes in the velocity of the sound due to the the temperature changes along the sounding tube. A 15 cm diameter protective well is used so as to protect the sounding tube (Bartex,1995).

Table 2.2: Output Specifications of Meteorological Sensors

Sensor	Range	Accuracy	Unit
Atmospheric Pressure	600 - 1060	±0.5	mbar
Air Temperature	-40 - 60	±2	°C
Air Humidity	0 - 100	±2	%
Wind Speed	0 - 50	±0.12	m/s
Wind Direction	0 - 360	±4	°

Sampling rate is 10 seconds for the sea level and meteorological data. The sea level and meteorological data are collected at the intervals of 15-minute, hourly and daily averages are calculated from 10-seconds samples. Data collected at each station are stored at a data logger and then transferred to the data center using GPRS connection through a data transfer software (Cambell Scientific, 1997). When collected data are plotted for quality control by using graphics software, it appears that the sea level sensors in some stations are subject to the noises. In order to remove spikes from the sea level measurements , a de-spiking filter are applied to the data. In Figure 2.3, sea level measurements from Erdek station are plotted as an example before and after applying differences smoothing and median smoothing de-spiking filters.

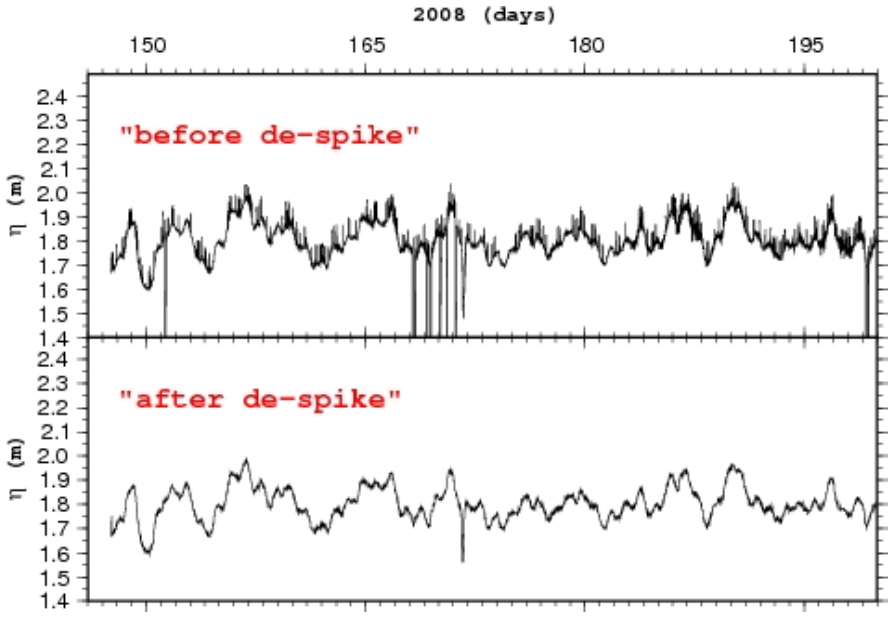

Figure 2.3: Sea level measurements from Erdek Station before (upper panel) and after (lower panel) applying de-spiking filter

In addition to the Coastal Monitoring Stations within the MOEN project, an Acoustic Doppler Current Profiler (ADCP) was mounted at the bottom of Bosphorus shown in Figure 2.4. It was deployed at depth of $\simeq$70 meters and connected with a cable to a computer situated in the shore in order to obtain the real-time data.

ADCP uses the doppler effect to measure the current velocity in the water column. Simply, it transmits a sound pulse, then listens the echo of the pulse. Having the information of the change in pitch or frequency of the echo enables to calculate the current velocity. Actually, sound itself does not reflect from the water. Small particles in the water, for examples, zooplanktons or suspended sediments make sound reflect and create an echo. ADCP has a transducer transmitting 3 beams at width of 3^o, sensors (tilt, temperature, pressure) and a compass. Each beam measures velocity parallel to itself and does not sense the velocity perpendicular to itself at all. ADCP senses the 3D velocity with three beams and first gives the velocity data in an orthogonal coordinate system then converts into components relative to the earth or ENU (East,North,Up) coordinates using tilt and compass. Data is collected at the interval of 10 minutes and 60 seconds of this interval ADCP measure the current velocity actively. In the remaining part of the interval, ADCP is in sleep mode.

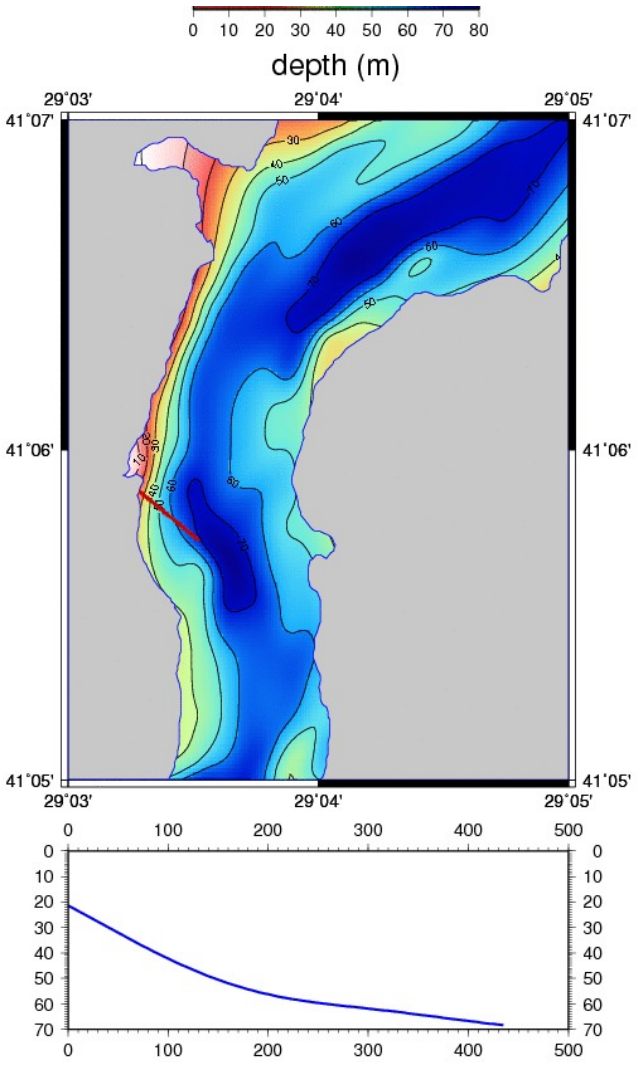

Figure 2.4: Location of Adcp mounted in bosphorus with bathmetry of the region

2.4 Data Analysis Techniques

2.4.1 Time series Analysis

As a definition, a time series is a sequence of observations ordered in time or space. Time series analysis are applied to data sets in order to identify the phenomenons represented by the successive measurements taken at same time intervals and also predict the events which can be occurred in the future based on the patterns of the observed time series identified in the past.

In this study, based on measurements made during the years from 2008 to 2012, time series analyses (correlation ,auto-, cross-, and rotary spectra) are performed to exhibit the

measurements in both time and frequency domains, which enable to detect temporal and spatial scales of phenomena, oscillations and correlations of the observations in distinct areas.

2.4.2 Correlation Analysis

If x_k is a time series, discretely defined at equally spaced points (k = 1,2,..., N), we can calculate the autocovariance function at lag L.

$$\phi_x(L) = \frac{1}{N-2L} \sum_{k=L}^{N-L} x_k^{'} x_{k+L}^{'} = \overline{x_k^{'} x_{k+L}^{'}} \; ; \;\; \text{L=0,}\pm1,\pm2,\pm3,... \qquad (2.1),$$

where the primes show deviations from the mean value. The autocovariance is the covariance of a variable with its other time, quantified by a time lag τ. As seen in formula 2.1, autocovariance at lag zero gives the variance of the variable. The Autocorrelation function is obtained normalizing autocovariance function. The value of this normalized function shown in 2.2 is sometimes referred to as the autocorrelation coefficient.

$$\phi_x(\tau)/\phi_x(0) = r(\tau);\; -1 < r(\tau) < 1;\;\; \text{r(0)} = 1 \qquad (2.2)$$

if x is not periodic, $r(\tau)$ goes to zero as τ goes to infinity. It is normally assumed that data sets applied to time series analysis are stationary. The term stationary implies that statistical properties of time series such as the mean value of any variable, its higher-order statistical moments and variance will not change over time.Therefore it is usually necessary to remove any trends in the time series before analysis. It is also inferred that the autocorrelation function can be assumed to be symmetric, if it is now replaced x_k in the formula 2.1 relations with another function y_k, the cross-covariance function is obtained.

$$\phi_{xy}(L) = \frac{1}{N-2L} \sum_{k=L}^{N-L} x_k^{'} y_{k+L}^{'} = \overline{x_k^{'} y_{k+L}^{'}} \; ; \;\; \text{L=0,}\pm1,\pm2,\pm3,... \qquad (2.3)$$

Similarly to the previously mentioned case, the crosscorrelation function is obtained normalizing crosscovariance function as well.

2.4.3 Fourier Series and The Fourier Transform

In mathematics , Fourier Series are used to decompose periodic signal into the sum of the sinusoid functions. Consider a function of time t with a period T , such that

$$f(t) = f(t+T) = f(t+2T) \tag{2.4}$$

it can be written this function as composition of sine and cosine waves with various frenquencies having amplitudes a_k and b_k ,

$$f(t) = a_0 + \sum_{k=1}^{\infty}(a_k cos(wt) + b_k sin(wt)) \tag{2.5}$$

or in a complex form ,

$$f(t) = \sum_{k=-\infty}^{\infty} c_k e^{iwt} \ , \ w = \frac{2\pi k}{T} \tag{2.6}$$

$$c_k = \int_0^T f(t)e^{-iwt} \tag{2.7}$$

Using these formulas , it can be obtained the variance in $f(t)$ is $V_{ff} = \sum |c_k|^2$. The term $|c_k|^2$ is the contribution of the variance(power) of the Fourier series made by the component with angular frequency w. A plot of that variance contribution in each angular frequency , called a periodogram, is a representation of the power (variance) spectrum of time series. A algorithm called Fast Fourier transform are performed by the help of computers to obtain $|c_k|^2$. Moreover, in order to obtain more reliable estimations in the spectrum analysis, Maximum Entropy Method (MEM) is applied (Ulrych and Bishop, 1975).

2.4.4 Rotary Spectra

Rotary spectra formulated by Gonella (1972) is applied to a vector time series such as current or winds and a representation in frequency space of the variance spectrum of a two-dimensional time series. The advantage of this method is that is not dependent on the orientation of the coordinate system and also gives information about the rotational characteristics of the analyzed data. The variance for each frequency band is divided into two components which are interpreted as the clockwise rotating variance (at negative frequency) and the counterclockwise rotating variance (at positive frequency). The analyzed time series may be reconstructed in a new coordinate system which depends on frequency such that the cospectrum is theoretically zero for all frequencies. Since the rotary spectrum for a vector time series is invariant under a coordinate rotation, it is a fundamental frequency representation of the time series (O'Brien and Pillybury, 1974).

The paremeters given in this study are rotation coefficient(C_r), E_ϵ(ellipse stability),orientation angle(ϕ) and the ratio of major axis to minor axis (B/A). C_r gives information about the

rotation. For $C_r > 0$, the rotation is clockwise whereas for $C_r < 0$ the rotation is counterclockwise. B/A is a measure of circular, elliptical or rectilinear oscillation. An B/A of zero corresponds to rectilinear motion. On the other hand,an B/A of 1 corresponds to circular motion. ϕ is the orientation angle where $\phi = 0$ indicates east and increase in the counterclokwise direction. Lastly, E_ϵ represents the confidence of the measure.

Chapter 3

RESULTS & DISCUSSION

The results obtained during the sampling period in this study are reviewed with respect to the times series of atmospheric parameters, sea level and current data in section 3.1. Moreover, spectra analysis applied to time-series are introduced in section 3.2.

3.1 General description of the Time Series

The time series obtained from all stations are given in Figures 6.1-6.13 and also statics summary of data are give in Table 3.1. The main characteristics of sampling sites are briefly discussed below. Time unit of the time series is in Julian days that starts from zero at the being of 2008. The Figure 3.14 demonstrates the wind direction distributions for sampling sites and the dominant directions at stations are clearly seen.

3.1.1 Atmospheric Parameters

The Mediterranean :

As seen in Figure 2.1 the coastal stations in the Mediterranean are Iskenderun(Fig. 6.1), Erdemli (Appendix, Fig. 6.2), Tasucu(Fig. 6.2), Magusa (Fig. 6.4), Girne (Fig. 6.5), Bozyazi(Fig. 6.6) and Aksaz(Fig. 6.7).

During the summer, the sea breeze modified westlies are prevailing, whereas in the winter, cyclonic winds with several days period are dominant. The average wind speed over the sampling period in the region is approximately 1.4 m/s, except Iskenderun and Tasucu(table 3.1). the wind speed at the Iskenderun station (Fig 3.1) is relatively weak compared to other nearby stations but even the mean value of wind speed is low, the observed maximum wind speed at Iskenderun station can exceed 17 m/s. Contrary to Iskenderun, the mean of 3.4 m/s with a maximum speed of 18.8 m/s at Tasucu station is found as highest mean of wind

speed in the region.

During the winter and the spring, low-frequency oscillations in atmospheric pressure with a period of several days are observed due to the depressions .In summer and autumn diurnal oscillations are observed due to the sea breeze.

The air temperature ranges from 0.49 C in winter to 41.66 C in summer with a record mean temperature of about 21.55 C. With respect to the inter-annual variability, 2010 is the warmest year in the region, which is 0.6 C and 1.3 C more than 2009 and 2011, respectively.

The Turkish Straits System :

The coastal stations in the Turkish Straits system and its neighboring region are Gokceada (Fig. 6.8), Erdek (Fig. 6.9), Meregli (Fig. 6.10), Yalova (Fig. 6.11) and Sile (Fig. 6.12). Even Gokceada, Sile and Igneada stations is at northeastern side of Agean Sea and Black Sea side, respectively, they are considered as part of Turkish Straits System in view of atmospheric features .

During summers northeasterly winds are found to be dominant in the region. In addition to the northeasterly, the winds coming from southwest is secondary importance in the summer. In winter time, cyclones passage lasting several days are frequently seen in the time series,which results in southerly winds.

The average wind speed (Table 3.1) is around 2.5 m/s with a maximum of 16 m/s at Erdek and Yalova Stations, 2 m/s at Sile and Yalova stations and 3.8 m/s with a maximum of 19 m/s at Gokceada Station. As it is seen, wind at Gokceada station is remarkably higher than nearby stations; especially in the cool season the northeasterly winds exceeding 15 m/s frequently occur and can last upto fifteen days.

The mean air temperature in the region is found as 15 C ranging from -12 C in winter to 33 in summer. Inter-annual variability indicate that the warmest year is 2010 , which is 0.7 C and 1.8 C more than 2009 and 2011,respectively.

Case Studies with respect to the Atmospheric Event:

Because of the high numbers of stations and four-year records, events are grouped according to their characteristics. Some of them are selected to be presented here.

During winter seasons, cyclonic events with a general life span of around 3 days (although they may last much longer) are frequently seen at all sampling sites. According to the position of cyclone passage path, the wind direction at stations are so variable that if a station is at the south of the passing low pressure system, the wind generally comes from southeast firstly, then south, southwest and finally northwest whereas if a station is at north of a low pressure system , the wind usually starts to come from east and change from easterly to northeast to

north then ending as northwest. An example of low pressure system passing over Erdemli station between 490-492 days (04-07 May 2008) is given and the path of cyclone is can be seen in Figure 3.18-21, which suggests that the Erdemli station was at north of the system center (Figure 3.4-5) but one day later the station remained at the south of system center (Figure 3.6-7) and correspondingly, wind direction at the station changed according to the pressure system movement (Fig. 3.3).

During summer the sea-breeze is dominant along Turkish costs, especially in the Mediterranean. Times series shows that the sea-breeze can be observed from April to September and intensifies on August since temperature gradients between the sea and the land becomes larger on August. The sea-breeze can exceed 10 m/s whereas the land-breeze can be around 3 m/s. An example of Sea-breeze at Erdemli Station is given between 17-25 September of 2008 in Figure 3.7. It is clearly seen that sea breeze is well-established as long as the land is warmed during day time. On the other hand, sea breeze isn't observed on 264.5 day due to the decreasing air temperature on that day.

At Tasucu station, strong winds coming from Northwest named "Poyraz" are dominant (Figure 3.1-c) and can be seen during the year. Atakturk (1980) studied this phonema in detail and showed that Poyraz winds occur due to the channel type geometry of Goksu valley. In this study, Poyraz winds are clearly seen during the year. In winter time, the Poyraz winds is triggered by cyclone passage. Such a case is shown in Fig. 3.9 that a cyclone is observed between 1076 and 1079 days. Right after cyclone passage over Tasucu site in 1079 days, Poyraz wind started to blow. As for Poyraz winds in summer time, the temperature gradients between coastland and interior part of the region is the main factor causing these winds. An example of such kind of formation is given Fig. 3.10. It is clearly seen that a warm and dry air masses arrived to region from the interior part on 862 day and increased air temperature by 10 C and shortly after, on 863 day the Poyraz winds occurred. Moreover, Poyraz winds bring cold and dry air into the region. It can be concluded that regional winds are related to the meteorological and topographic features.

Table 3.1: Statistical Summary of Measurements

a) Region	Station(N)	Air Temperature(°C)		R.Humidity(%)		Sampling Period
		Mean($\pm\sigma$)	Min-Max	Mean($\pm\sigma$)	Min-Max	From - To
Mediterranean	Iskenderun(1296)	21.07±6.5	0.49-37.80	64.0±13.0	29.2-100	02/2008-12/2011
	Erdemli(1203)	20.37±6.5	2.42-41.66	68.3±18.2	29.9-100	02/2008-12/2011
	Tasucu(1091)	21.18 ±6.4	2.17-38.81	56.7±14.2	21.1-100	08/2008-12/2011
	Bozyazi(1226)	20.30±6.3	3.50-36.64	63.4±11.4	26.3-89.2	08/2008-12/2011
	Girne(1164)	20.47±5.7	5.01-38.03	63.7±8.9	38.4-85.8	10/2008-12/2011
	Magusa(1162)	20.02± 6.6	1.37-39.01	67.6±9.4	38.8-88.1	10/2008-12/2011
Agean Sea	Aksaz(1403)	20.15±7.3	0.51-40.86	62.0±14.6	25.6-95.0	02/2008-12/2011
	Gokceada(1229)	15.44±7.1	-5.54-33.20	98.1±5.7	54.0-100	02/2008-12/2011
Marmara Sea	Erdek(1314)	14.31±7.6	-6.16-33.93	88.0±9.8	52.2-100	05/2008-12/2011
	M.Ereglisi(1292)	*	*	*	*	05/2008-12/2011
	Yalova(1431)	15.44±6.7	-3.75-33.28	74.8±9.6	30.3-97.4	02/2008-12/2011
Black Sea	Sile(1407)	15.23±6.9	-4.01-32.69	82.312±12.8	42.8-100	02/2008-12/2011
	Igneada(1028)	14.44 ±7.8	-12.18-33.94	78.9±8.4	54.4-97.7	05/2008-12/2011

b) Region	Station(N)	Air Pressure(mbar)		Wind(m/s)		Sea level(m)		Sampling Period
		Mean($\pm\sigma$)	Min-Max	Mean($\pm\sigma$)	Min-Max	Mean($\pm\sigma$)	Min-Max	From - To
Mediterranean	Iskenderun(1296)	1013.7±5.3	1002.1-1030.9	1.3±1.2	0-17.53	1.967±0.205	0-2.233	02/2008-12/2011
	Erdemli(1203)	1011.2±5.7	1000.5-1029.6	2.2±1.8	0-15.3	1.201±0.102	0-1.469	02/2008-12/2011
	Tasucu(1091)	1013.1±5.5	1001.7-1030.6	3.4±3.2	0-18.8	1.185±0.103	0-1.430	08/2008-12/2011
	Bozyazi(1226)	1012.6±5.4	1002.0-1030.2	2.0±1.6	0-14.6	1.588±0.126	0-1.885	08/2008-12/2011
	Girne(1164)	1013.6±5.5	1003.1-1027.4	2.3±1.7	0-15.2	1.636±0.121	0-1.791	10/2008-12/2011
	Magusa(1162)	1014.3±5.5	1003.3-1031.1	2.3±1.7	0-13.0	2.081±0.128	0-2.192	10/2008-12/2011
Agean Sea	Aksaz(1403)	1011.6±5.7	998.9-1031.5	1.8±1.9	0-16.5	1.240±0.113	0-1.642	02/2008-12/2011
	Gokceada(1229)	1015.1±6.8	991.8-1036.5	3.8±2.6	0-18.8	2.104±0.144	0-2.345	02/2008-12/2011
Marmara Sea	Erdek(1314)	1014.9±6.0	993.3-1035.4	2.7±1.9	0.1-15.6	1.804±0.118	0-2.362	05/2008-12/2011
	M.Ereglisi(1292)	1014.346±6.1	991.9-1036.4	*	*	1.456±0.205	0-2.233	05/2008-12/2011
	Yalova(1431)	1015.0±6.1	992.0-1036.0	2.5±2.4	0-17.7	1.877±0.145	0-2.344	02/2008-12/2011
Black Sea	Sile(1407)	1015.0±6.3	991.8-1036.5	2.0±2.2	0-14.6	1.645±0.100	0-1.922	02/2008-12/2011
	Igneada(1028)	1016.0±7.0	975.0-1037.9	1.9±1.7	0-11.7	1.872±0.120	0-2.150	05/2008-12/2011

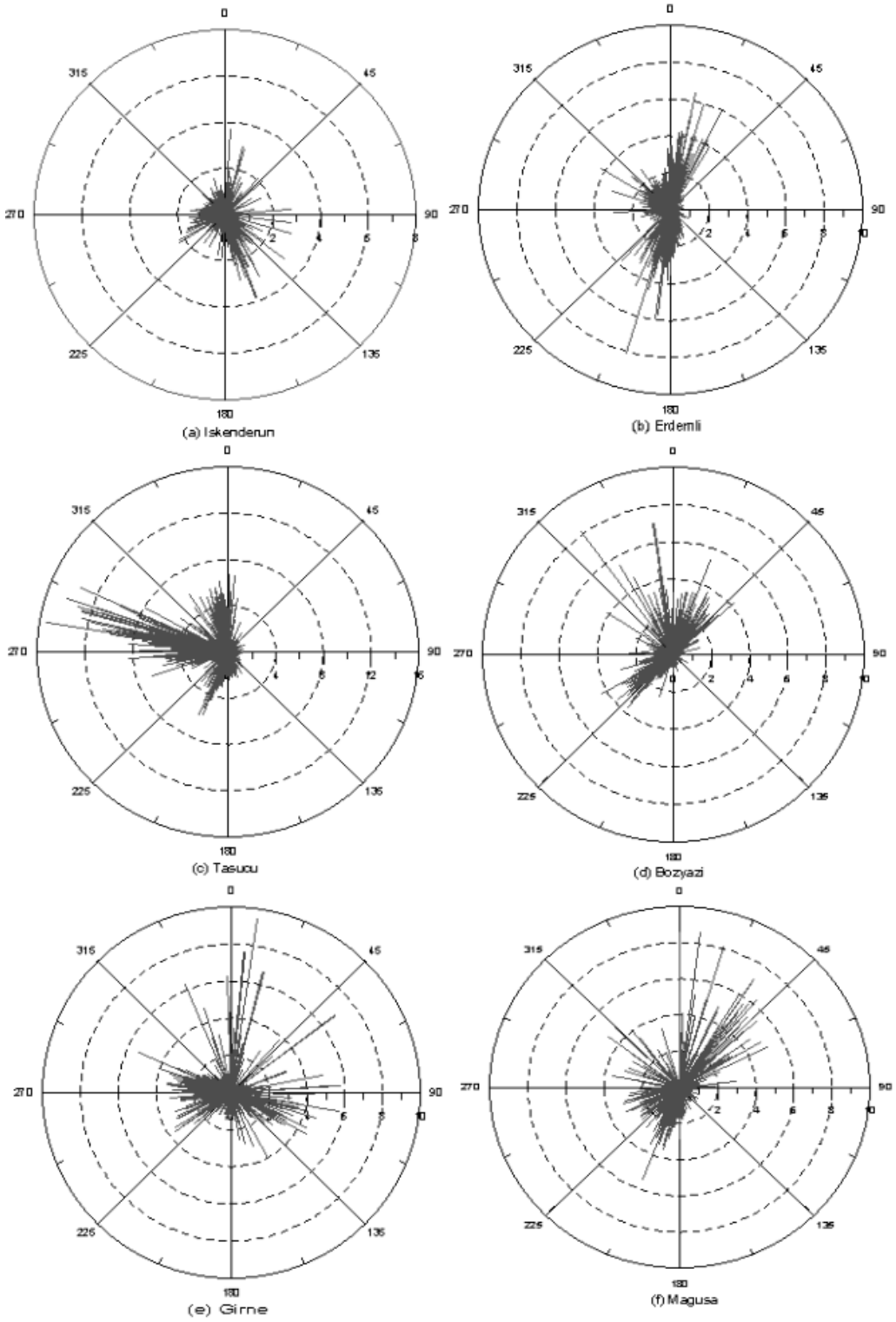

Figure 3.1: Polar Diagram of Wind data from Stations; a)Iskenderun b)Erdemli c)Tasucu d)Bozyazi e)Girne f)Magusa

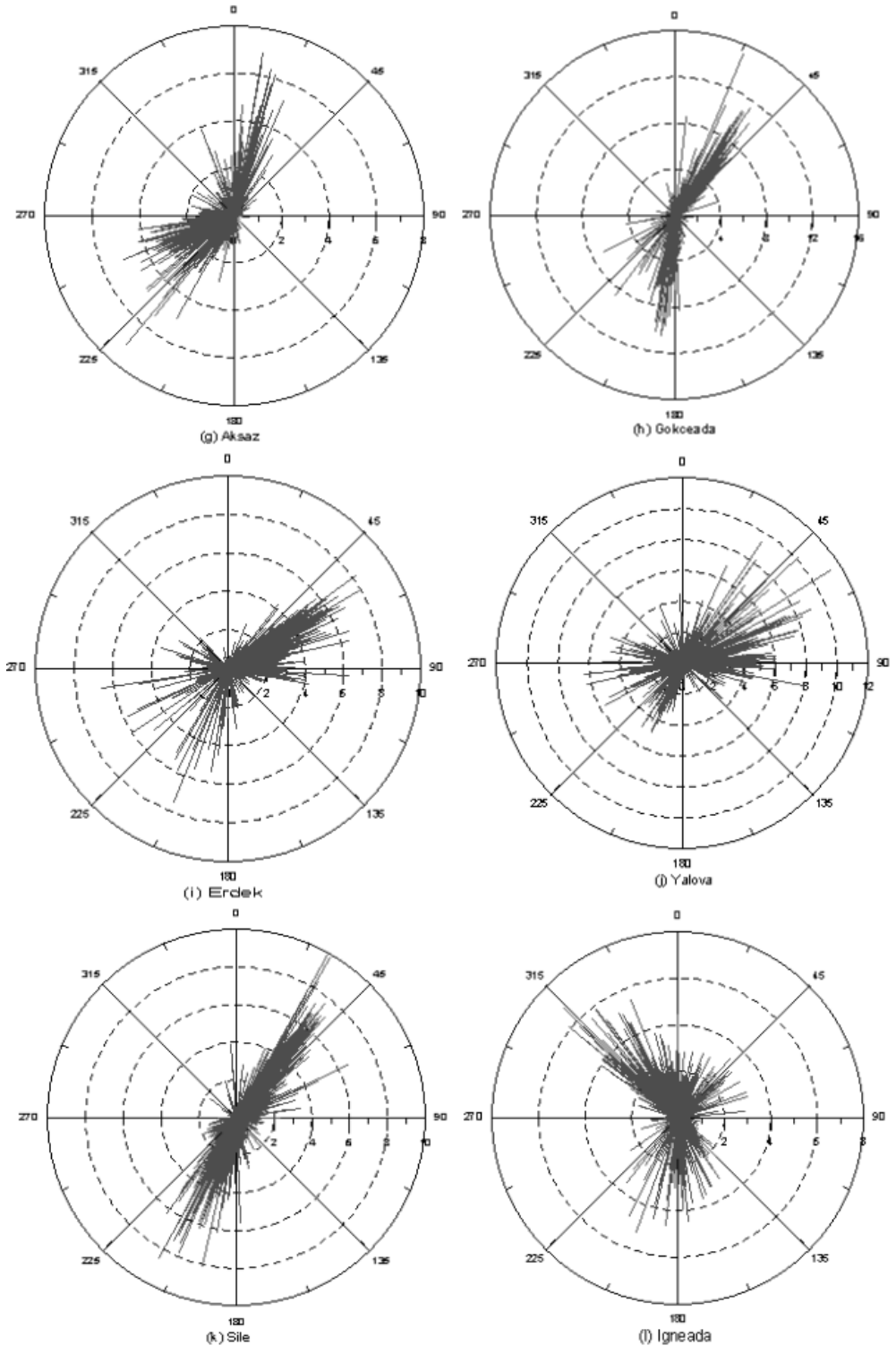

Figure 3.2: Polar Diagram of Wind data from Stations; a)Aksaz, b) Gokceada, c)Erdek, d)Yalova, e)Sile, f)Igneada

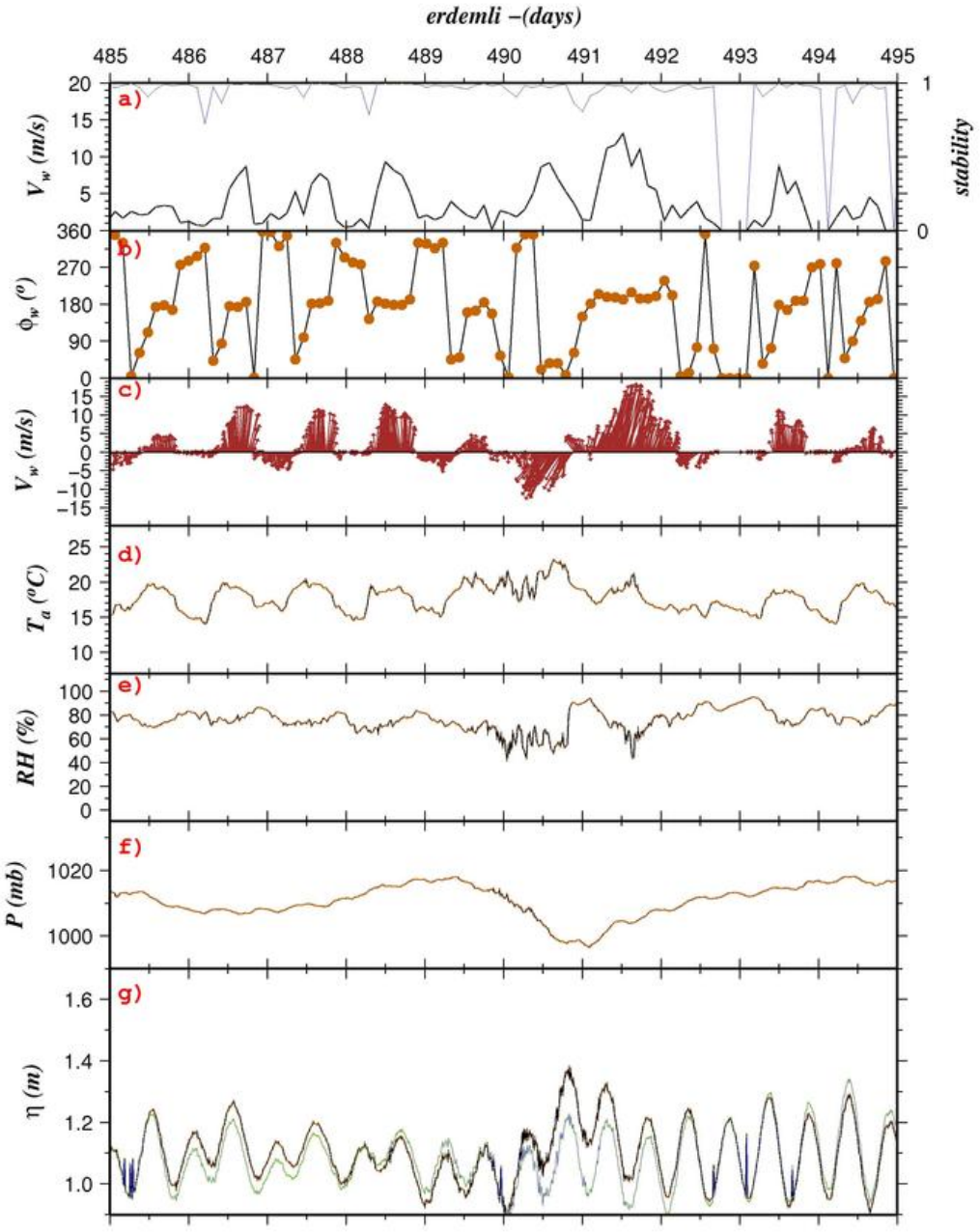

Figure 3.3: Erdemli station time-series between 485 day and 495 day; a)Wind speed, b)wind direction, c)downwind vector diagram, d)air temperature, e)relative humidity, f)atmospheric pressure and g)sea level

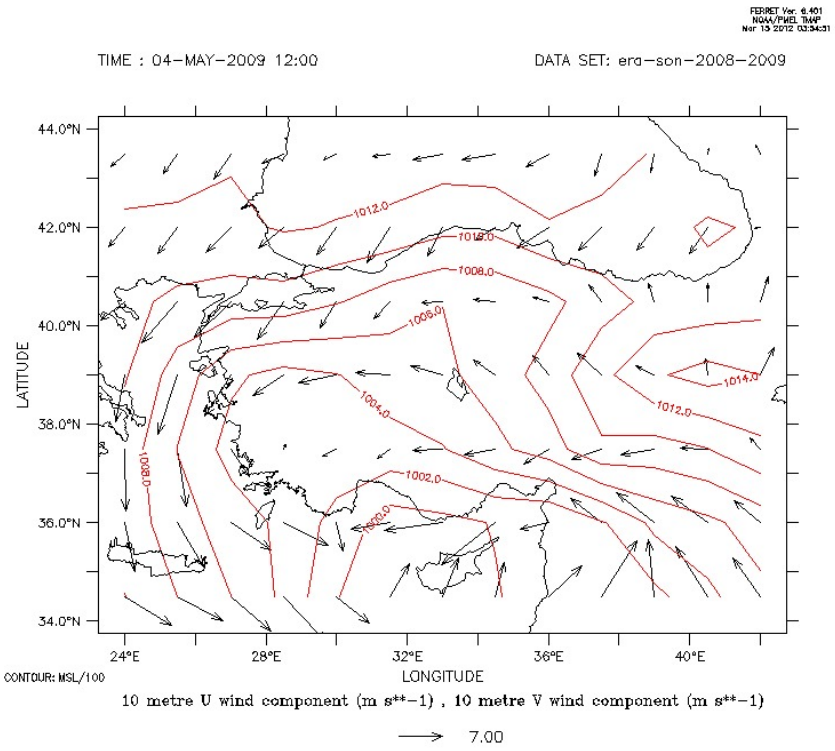

Figure 3.4: ECMWF ERA-Interim surface pressure and wind at 12:00,04 May 2009

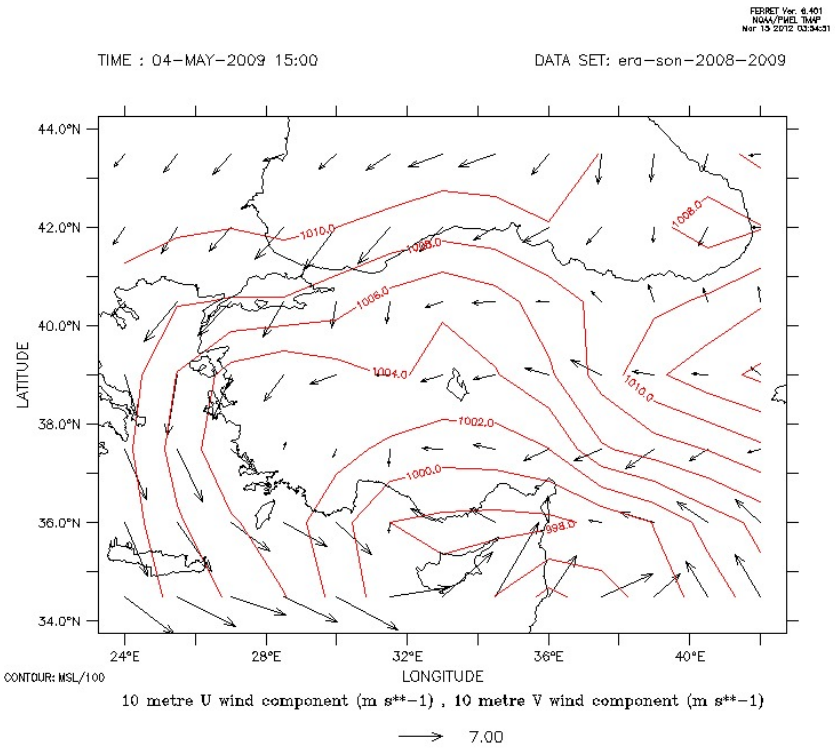

Figure 3.5: ECMWF ERA-Interim surface pressure and wind at 15:00, 04 May 2009

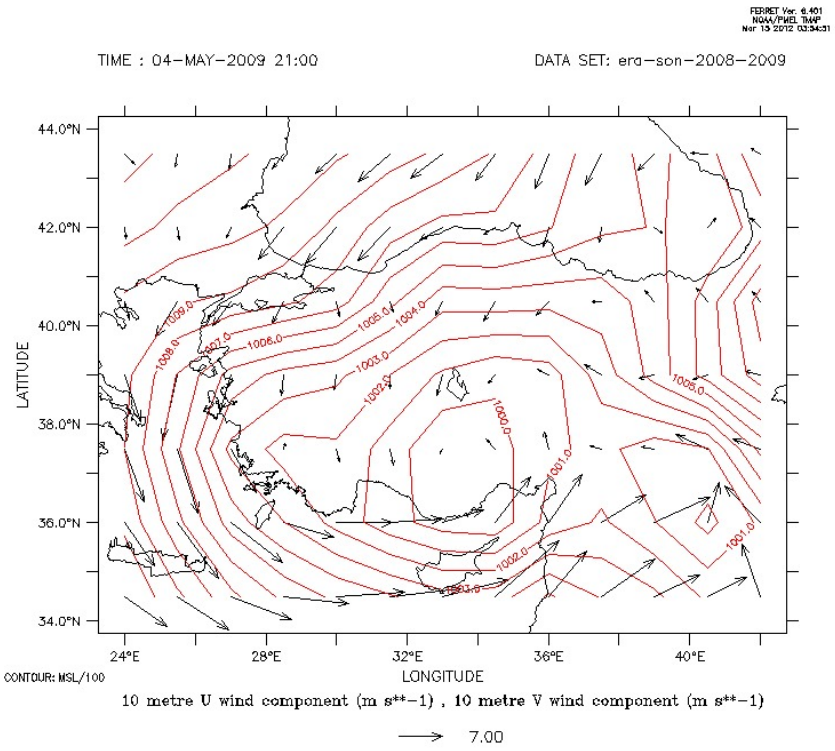

Figure 3.6: ECMWF ERA-Interim surface pressure and wind at 21:00, 04 May 2009

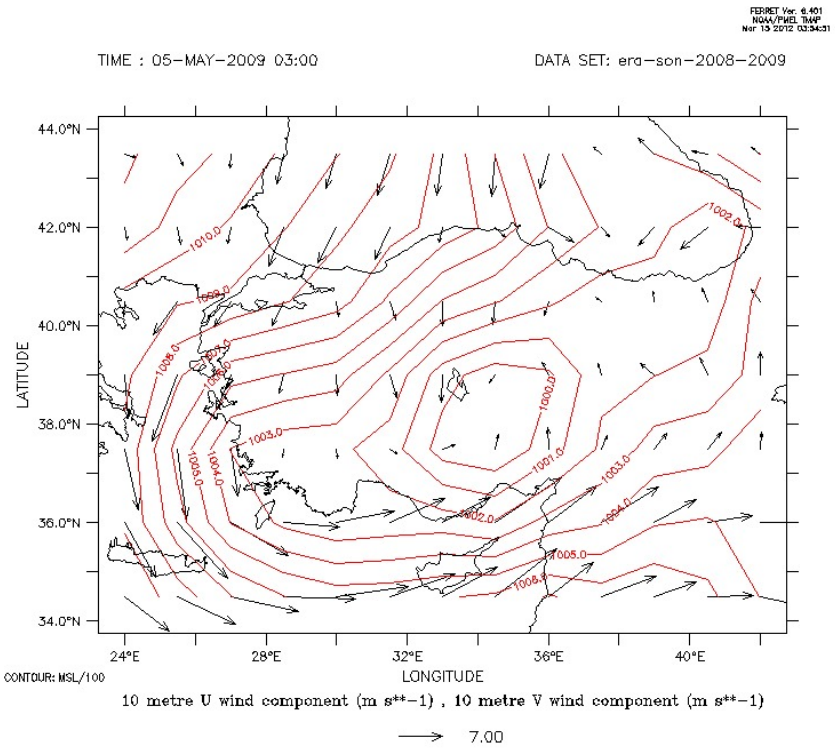

Figure 3.7: ECMWF ERA-Interim surface pressure and wind at 03:00, 05 May 2009

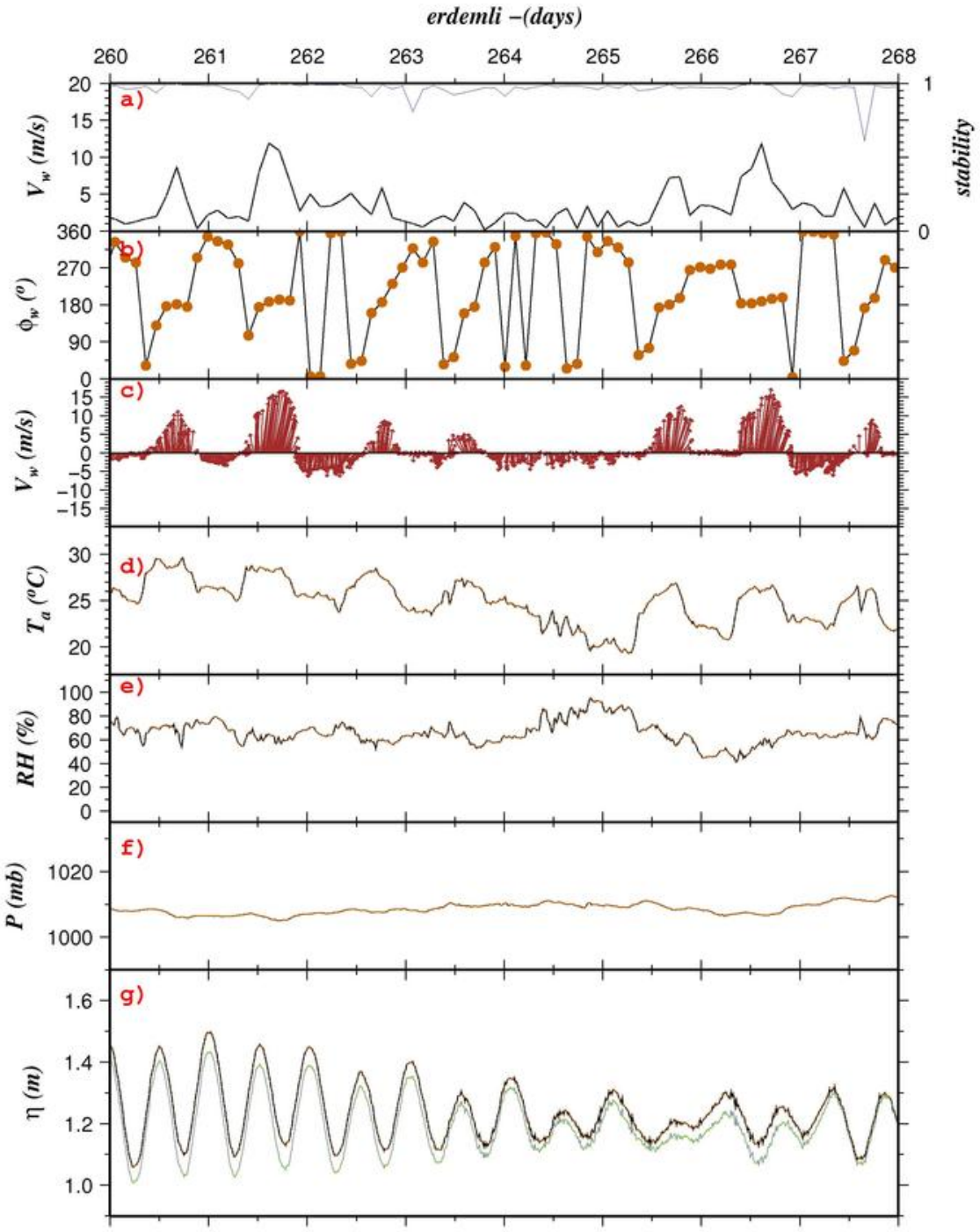

Figure 3.8: Erdemli station time-series between 260 day and 268 day; a)Wind speed, b)wind direction, c)downwind vector diagram, d)air temperature, e)relative humidity, f)atmospheric pressure and g)sea level

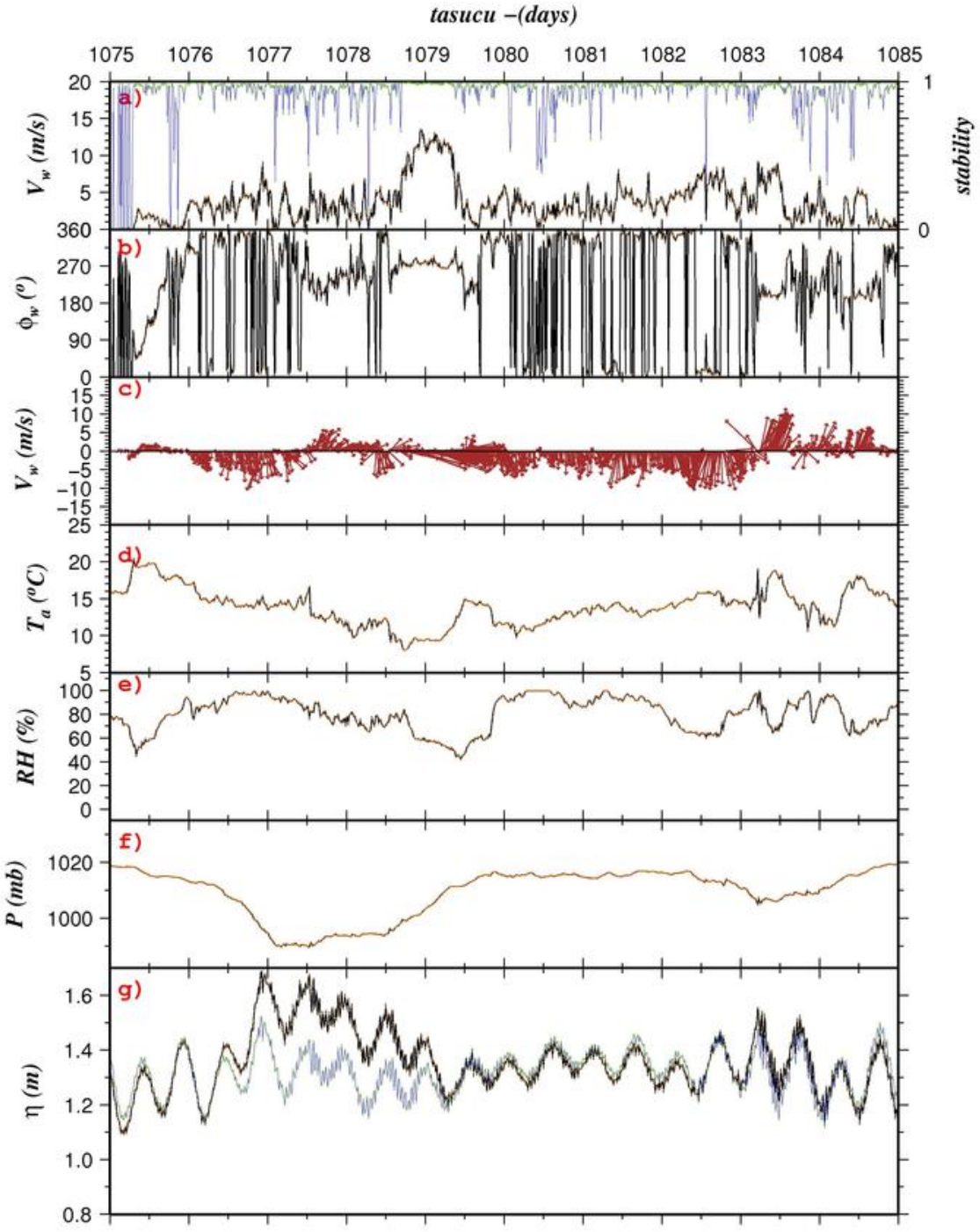

Figure 3.9: Tasucu station time-series between 1075 day and 1085 day; a)Wind speed, b)wind direction, c)downwind vector diagram, d)air temperature, e)relative humidity, f)atmospheric pressure and g)sea level

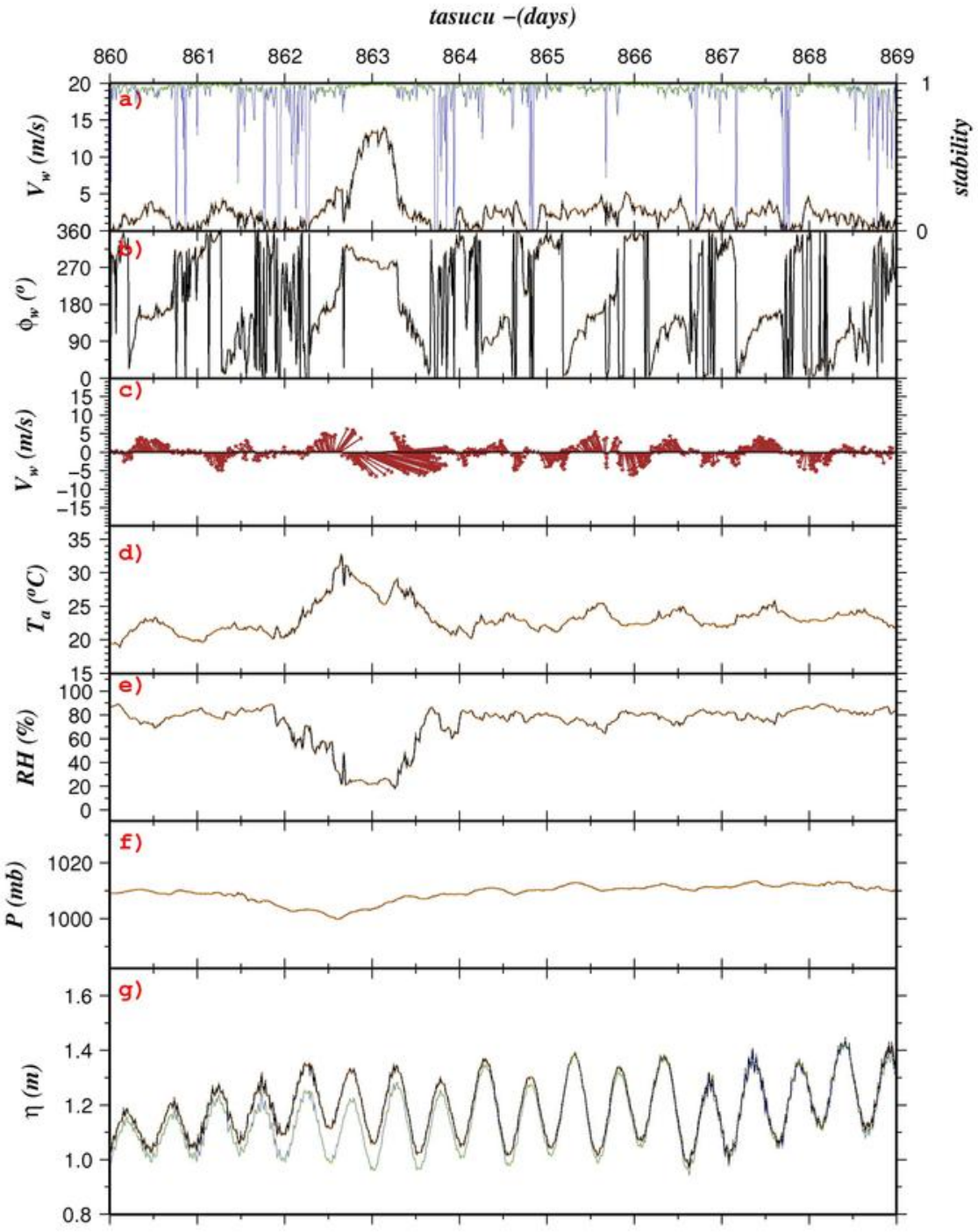

Figure 3.10: Tasucu station time-series between 860 day and 869 day; a)Wind speed, b)wind direction, c)downwind vector diagram, d)air temperature, e)relative humidity, f)atmospheric pressure and g)sea level

3.1.2 Sea Level

Sea level is a complex signal, which is affected by various phenomena. In this study short term sea level responses to the atmospheric variability mainly wind, atmospheric pressure and air temperature are examined. Additionally, seasonal, inter-annual variability and the local mean sea level differences are described. Moreover, analytically calculated free surface and internal oscillations in the Turkish Strait System are examined to find in the sea level records obtained from coastal stations.

Seasonal and Inter-annual Variability:

The monthly mean seal level in Mediterranean and Turkish Straits System are given in Tables 3.2 and 3.3, respectively. The values in tables 3.2 and 3.3 are also plotted in Fig. 3.11 and 3.12, moving them to a common datum. The means indicate that seasonal sea levels in the Mediterranean occur with maximum values observed in the period July-August. On the other hand, the lowest sea level occurs in the period March-April. There is a 17 cm typical difference between the lowest and highest period in the Mediterranean. A great amount of this variation is attributable to the seasonal steric effect that is the thermal expansion of sea water. On the other hand, this situation is not valid for the Turkish Strait System, especially in the Black Sea where the lowest monthly sea level means are found in Autumn whereas the highest occurs in March-April. As for Marmara Sea, the highest monthly sea level is seen in June and the lowest means are observed in Autumn season.

With respect to inter-annual variability, the annual mean sea level in 2010 is higher than other years at all stations. In Mediterranean there is about 4.5 cm difference between 2010 and other years so that the annual mean of 2009 and 2011 is almost same in the Mediterranean. In the Marmara Sea, the mean of 2010 is more than 10.2 cm and 13.5 cm more than 2009 and 2011, respectively. Lastly, the mean of Black Sea in 2010 is 12.3 cm and 14.8 larger than 2009 and 2011, respectively. Again 2008 isn't taken into account in annual scale due to the low data coverage. It is clearly seen that there is drastic sea level rising in 2010, especially in Black Sea (See Fig. 6.12 and Fig. 6.13). In order to identify the factor of this increasing of sea level, North Atlantic Oscillation (NAO) is examined since the river discharge related to this study period doesn't exist. The NAO index means shift air masses between Azore high and Iceland low. The positive winter NAO index results in cold and dry air masses to southern Europe and Black Sea region by strong northwesterly winds whereas the negative winter NAO brings milder winters with warmer air temperatures and more wet atmospheric conditions transported over the Black Sea from the southwest (Hurrell *et al.*,

2003). Stanev(2002) showed every river maximum runoff coincides in time with the negative extreme in the NAO index based on decades of observations. As seen in Fig. 3.13, the NAO index in 2010 is mostly negative. Since atmospheric pressure and wind mean values didn't exhibit variability during 2010, the possible reason of this increasing in sea level can be the river input.

The Local Mean Sea Levels in Turkish National Vertical Control Network (TNVCN-99) Datum :

For each coastal station, tide gauge is linked to a local datum based on the benchmarks creating a local levelling network. The levelling measurements are performed annually between tide gauge zero and local levelling network in order to provide sea level data continuity and keep it on a common datum. An level difference between TNVCN-99 and the local datum occurs in each coastal station. In order to determine the sea level difference between two tide gauges station, the level difference between the TNVCN-99 and the local datum must be known. These measurements provided by General Mapping Of Commander are used to detect the sea level difference between the sampling sites.

The local mean sea level differences are found averaging four years data from stations, which contains geoid and mean dynamic topography .The results (Fig. 3.14) show that local sea level differences between sampling sites.To sum up, there are 19 cm,13 cm,3.85cm, 2.33 cm,38.62cm and 21.43 cm differences between Igneada-Sile, Sile-Yalova, Meregli-Yalova, Meregli-Erdek, Erdek-Gokceada, Tasucu-Girne stations,respectively.

Table 3.2: Monthly mean sea level from 2008 to 2011 in the Mediterranean

Month/Stat.	Erdemli	Tasucu	Bozyazi	Girne	Magusa	Aksaz
January	1.214	1.204	1.559	1.535	2.04	1.285
February	1.213	1.204	1.592	1.574	2.076	1.267
March	1.168	1.159	1.505	1.499	2.004	1.185
April	1.13	1.12	1.489	1.518	2.035	1.171
May	1.156	1.146	1.542	1.592	2.082	1.194
June	1.229	1.232	1.636	1.691	2.13	1.264
July	1.294	1.281	1.697	1.697	2.128	1.306
August	1.308	1.296	1.709	1.689	2.125	1.342
September	1.288	1.275	1.687	1.692	2.125	1.334
October	1.211	1.2	1.61	1.672	2.133	1.272
November	1.201	1.191	1.599	1.624	2.119	1.276
December	1.25	1.239	1.633	1.614	2.107	1.325

Table 3.3: Monthly mean sea level from 2008 to 2011 in the Turkish Strait System

Month/Stat.	Gokceada	Erdek	Meregli	Yalova	Sile	Igneada
January	2.138	1.816	1.364	1.905	1.73	1.956
February	2.094	1.862	1.409	1.882	1.722	2.017
March	2.103	1.765	1.354	1.883	1.713	2.032
April	2.109	1.767	1.352	1.897	1.726	2.028
May	2.128	1.829	1.392	1.935	1.706	1.972
June	2.19	1.871	1.439	1.986	1.718	1.991
July	2.203	1.859	1.404	1.966	1.732	2.007
August	2.193	1.832	1.362	1.913	1.704	1.968
September	2.202	1.823	1.363	1.908	1.634	1.874
October	2.14	1.793	1.363	1.888	1.624	1.858
November	2.155	1.79	1.386	1.892	1.596	1.813
December	2.17	1.851	1.547	1.958	1.634	1.868

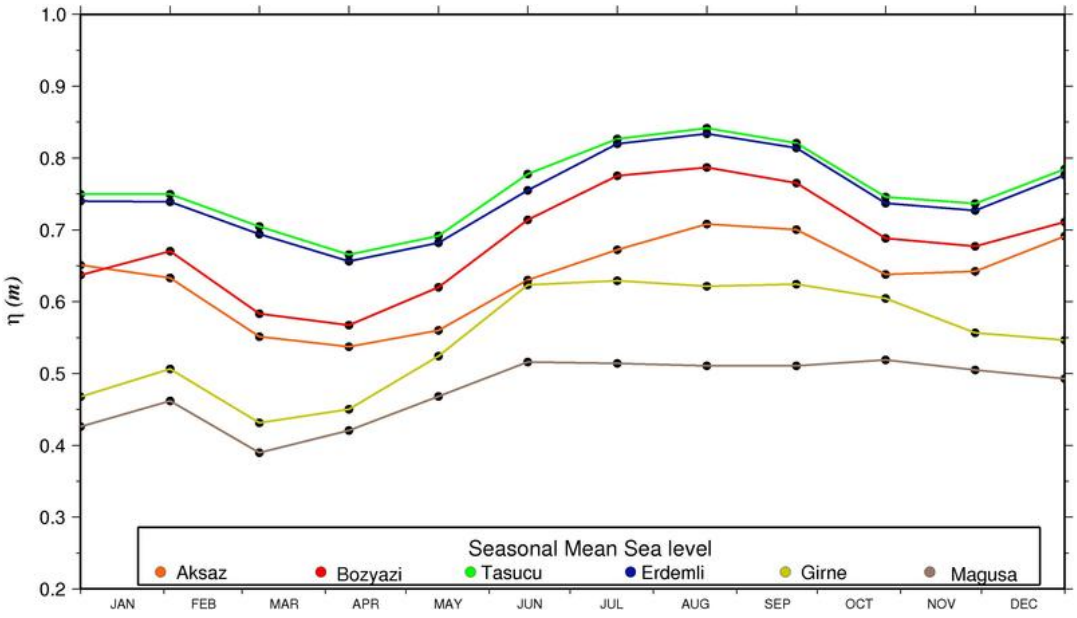

Figure 3.11: Monthly mean sea level from 2008 to 2011 in the Mediterranean

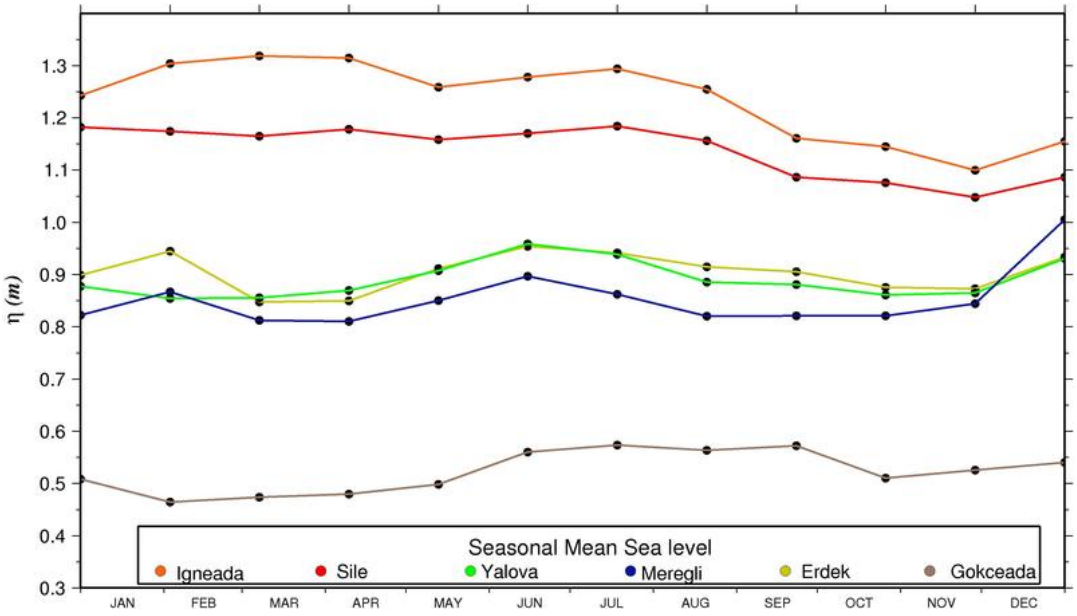

Figure 3.12: Monthly mean sea level from 2008 to 2011 in the Mediterranean

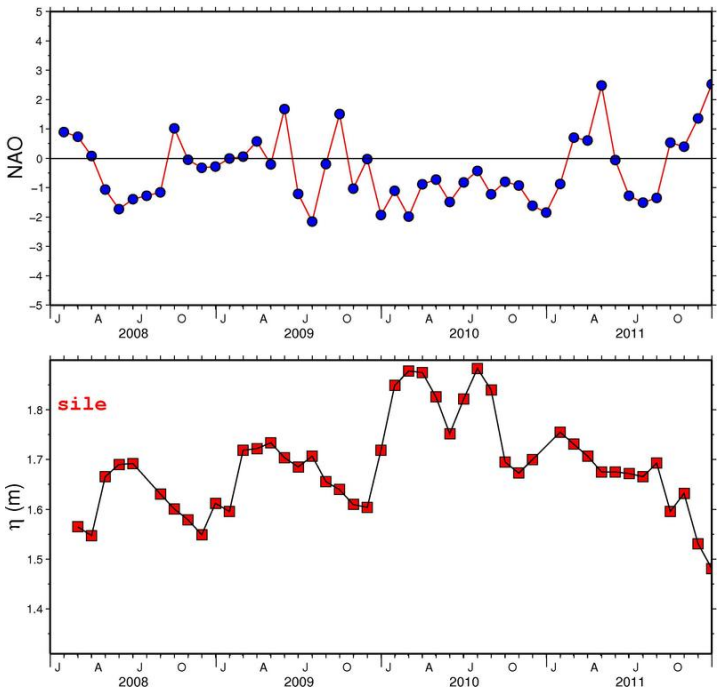

Figure 3.13: North Atlantic Oscillation monthly index (upper panel); Sile monthly sea level from 2008 to 2012 (lower panel)

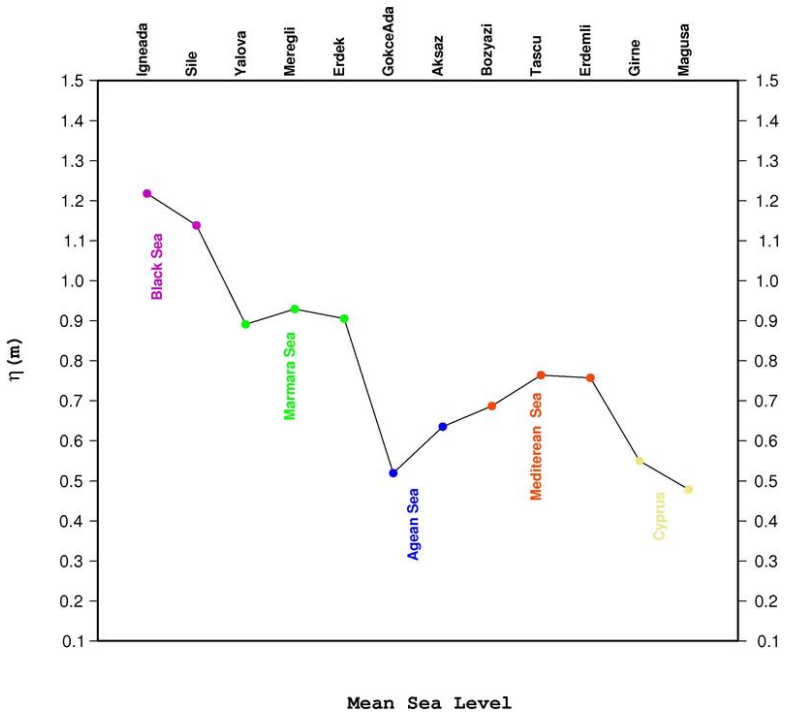

Figure 3.14: Local mean sea level differences between sampling areas

Event Base Analysis:

In the Mediterranean, sea level is variable during cyclone passages. As it is seen in Fig. 3.3, the depression between 490 and 492 days accompanied with a 20 cm increase of sea level. A similar case was observed between 1076 and 1079 days at Tasucu Station (Fig. 3.9)and the response to this cyclone in Bozyazi station was greater,almost 30 cm (Fig. 3.15).

In the Marmara Sea, there is approximately 50 cm increase in the sea level between 325 day and 327 day due to the atmospheric pressure and wind effect (Fig. 3.16). The atmospheric pressure dropped from 1015 m/bar to 982 m/bar and southwest wind with a 8 m/s velocity prevailed during this time. A similar example is also can be seen in Fig. 3.17 that a 30 cm increase of sea level between 652 day and 653 day which accompanied with a 5 m/s southwest wind and 10 m/bar atmospheric pressure decrease. An different case is also observed in Fig. 3.18. Northeast winds prevailed persistently during 46 and 49 days. The wind velocity reached 17 m/s and the atmospheric pressure is around 1030 m/bar during this time. This northeast wind resulted in 50 cm decrease in the sea level. In the Marmara, the onshore winds can directly push water towards the shore and vice versa. Cross-correlation analysis at Yalova station between sea level and its forcings; atmospheric pressure and wind components are given in Fig. 3.19. East-West wind component shows strong positive correlation with sea level since it is onshore component for Yalova station. On the other hand , there is no correlation between North-South wind component. It can be also suggested than sea level simultaneously responses to wind forcing. Additionally, there is almost perfect negative correlation between the sea level and atmospheric pressure due to inverse barometer effect in time lag of 0.5 day.

In the Black Sea, dominant factor causing the sea level changes is wind forcing. In Figure 3.20 demonstrates that there is 50 cm sudden increase in sea level between 269 day and 270 day. A similar cases are given in Figure 3.21 that sea level increased sharply of 30 cm and 40 cm on 750 day and 754 day, respectively. In order to see the relation with sea level and wind forcing clearly, 10 meter north-south wind obtained from ECMWF(Era-Interim) was averaged over western Black Sea and compared with the sea level. It can be clearly seen that in Figure 3.22 and 3.23, the sharp sea level rises in Black Sea mentioned above is due to the wind over the western basin.

In addition to these, there was an rare event occurred on February 2008. A high pressure system hovered over Marmara Sea during this month. The monthly mean atmospheric pressure is 1025 m/bar (max=1016,min=1032), whereas the monthly sea level mean of November is 27 cm less than the usual mean of November and the following month. Possibly, the sea

level responded to the high pressure system through the Dardanelle Strait since Dardanelle Strait hasn't a maximal exchange regime and the Mediterranean Sea can exhibit easily as inverted barometer response.

This kind of temporal sea level increases mentioned above are important when the atmospheric pressure systems;especially low pressure systems settled in since they are signs of extreme events. The combined effect of the atmospheric pressure, wind setup, tides and high waves can lead to hazards for coastal areas and should be studied in detail.

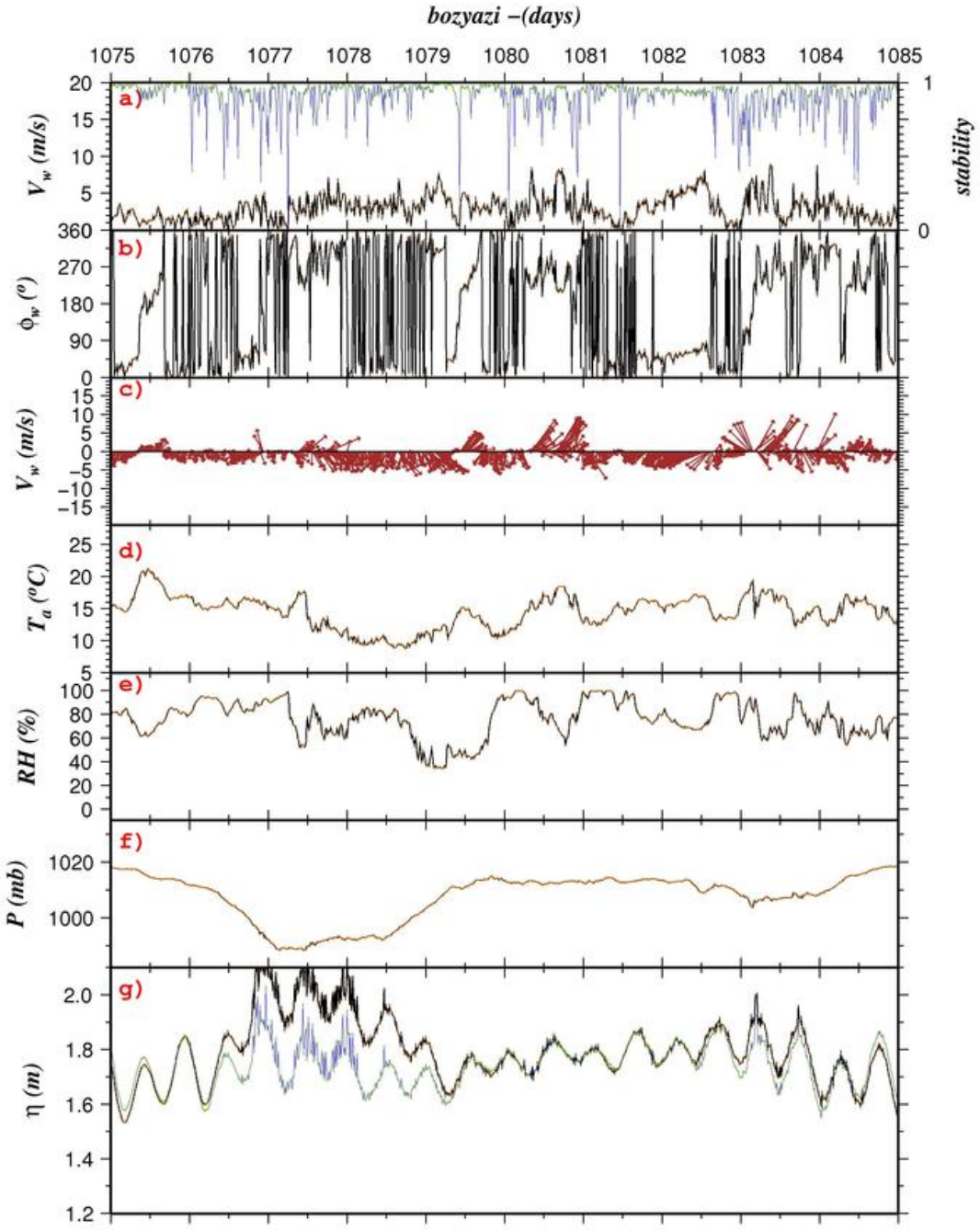

Figure 3.15: Bozyazi station time-series between 1075 day and 1085 day; a)Wind speed, b)wind direction, c)downwind vector diagram, d)air temperature, e)relative humidity, f)atmospheric pressure and g)sea level

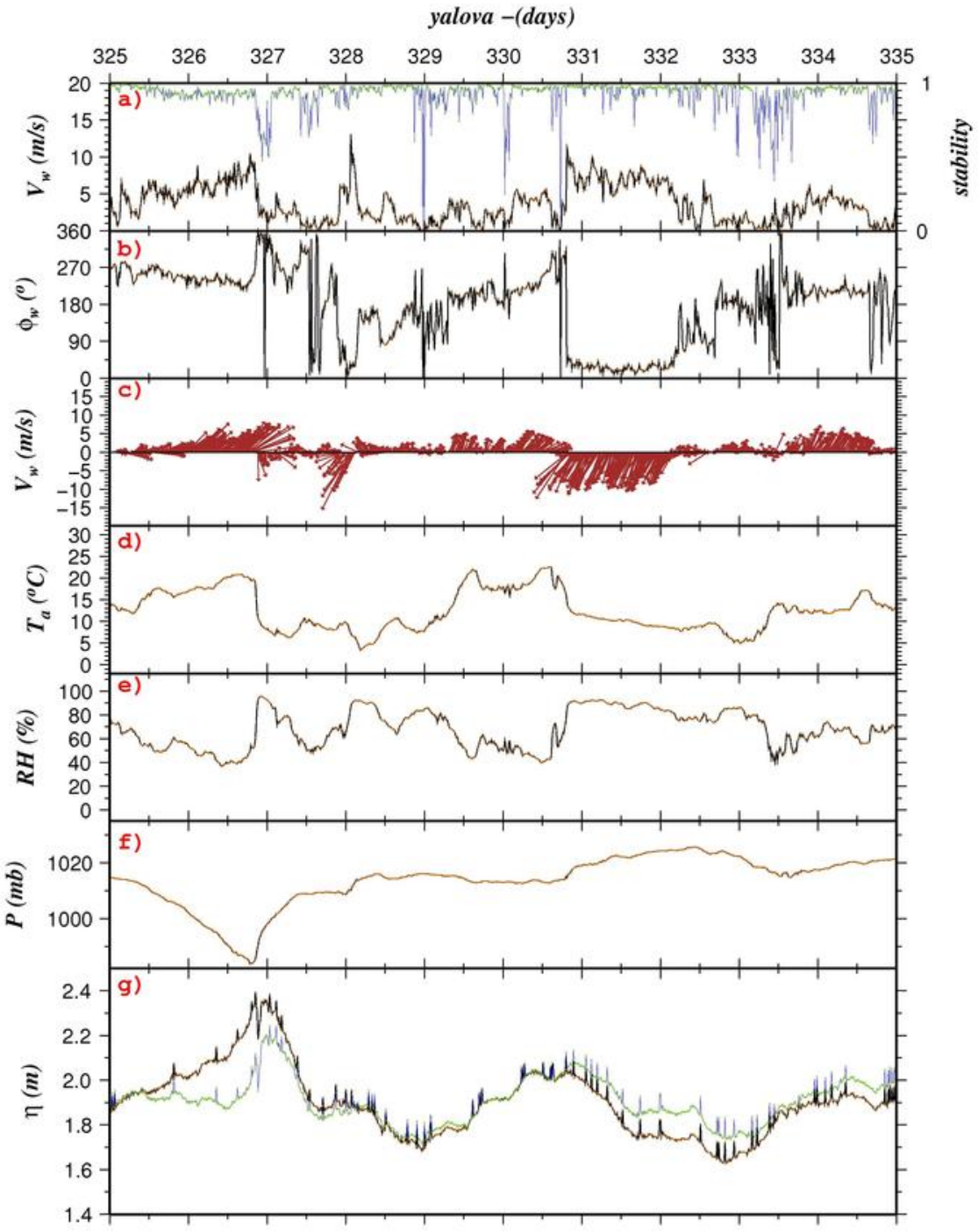

Figure 3.16: Yalova station Time-series between 325 day and 335 day; a)Wind speed, b)wind direction, c)downwind vector diagram, d)air temperature, e)relative humidity, f)atmospheric pressure and g)sea level

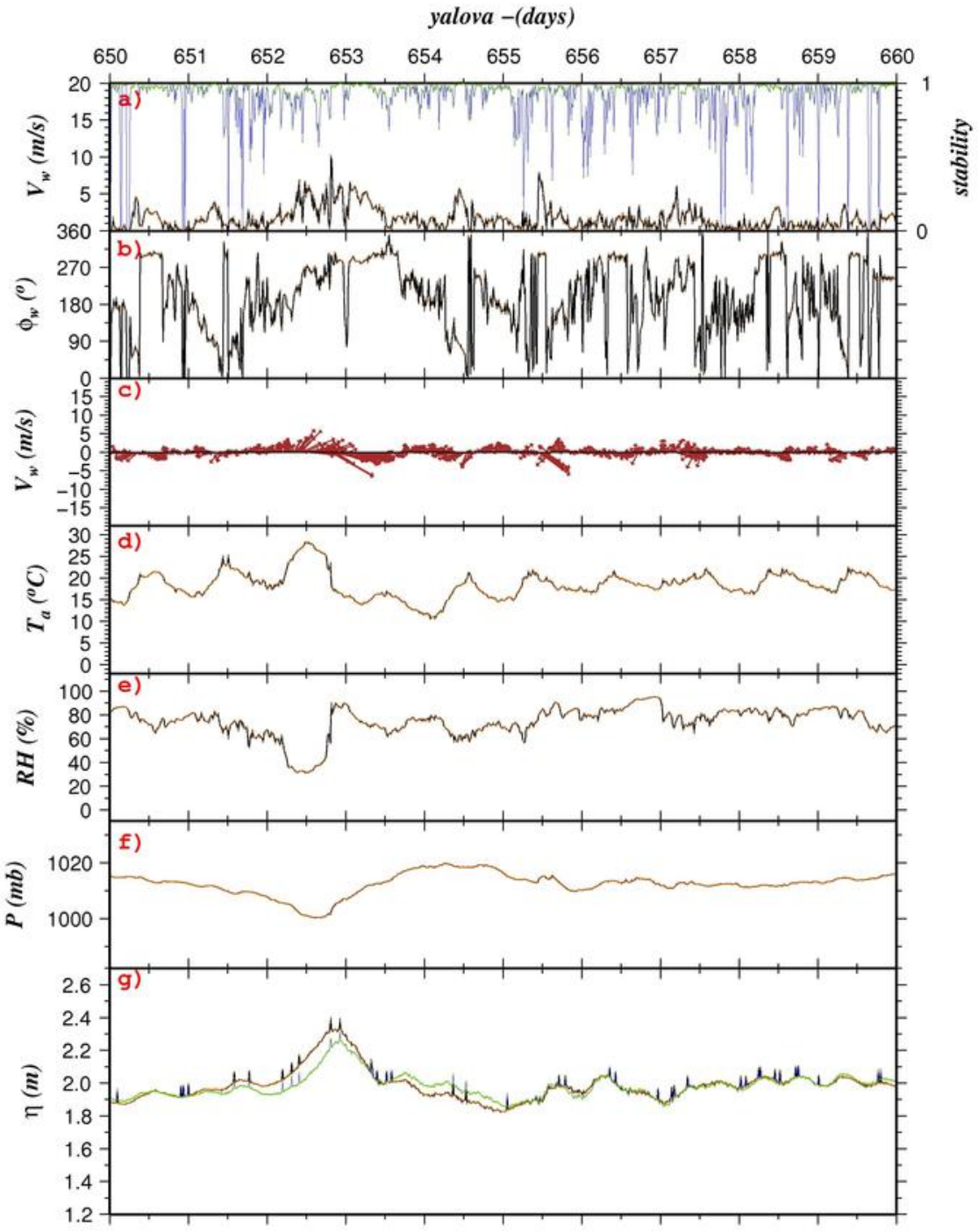

Figure 3.17: Yalova station time-series between 650 day and 660 day; a)Wind speed,b)wind direction, c)downwind vector diagram, d)air temperature, e)relative humidity, f)atmospheric pressure and g)sea level

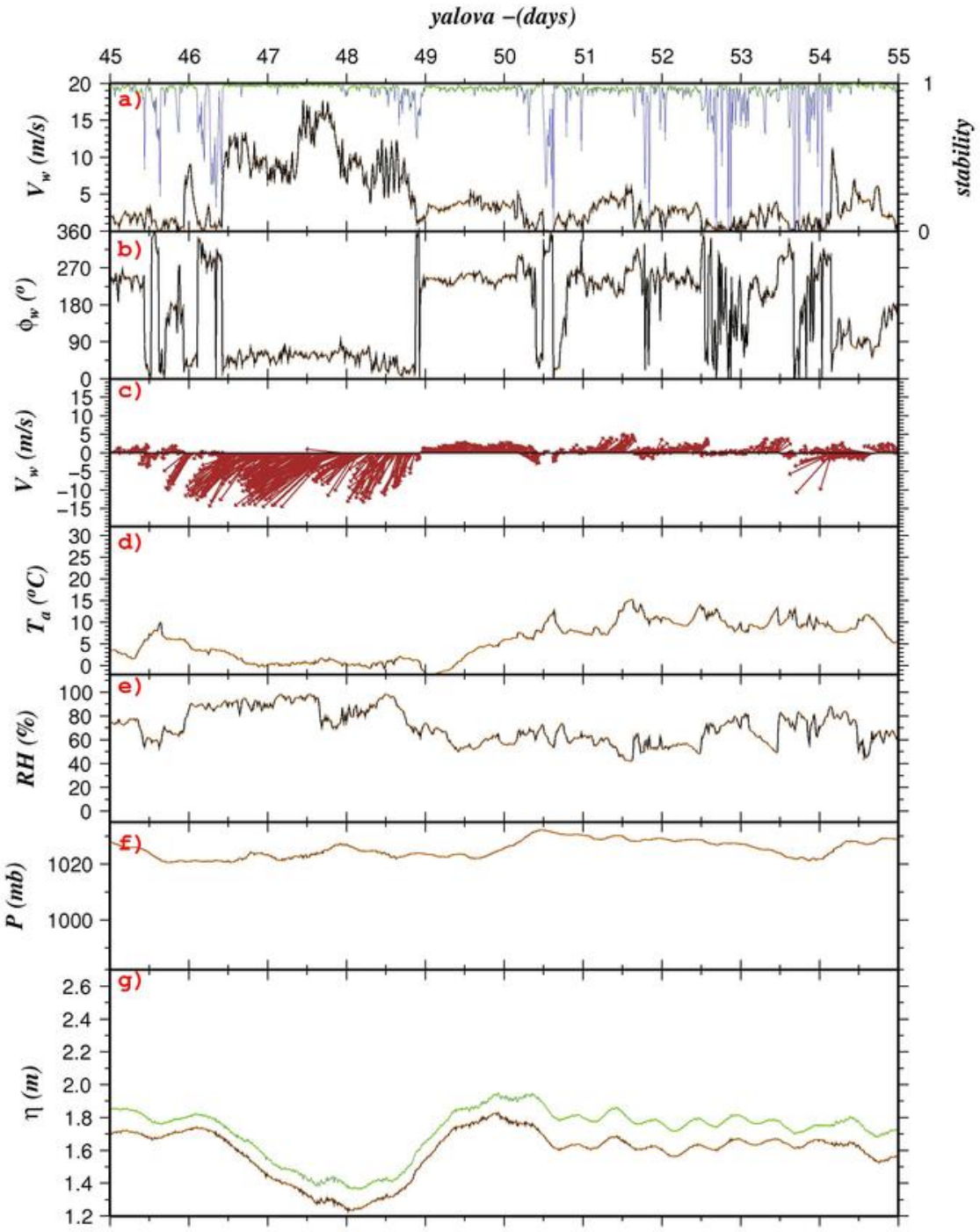

Figure 3.18: Yalova station time-series between 45 day and 55 day; a)Wind speed, b)wind direction, c)downwind vector diagram, d)air temperature, e)relative humidity, f)atmospheric pressure and g)sea level

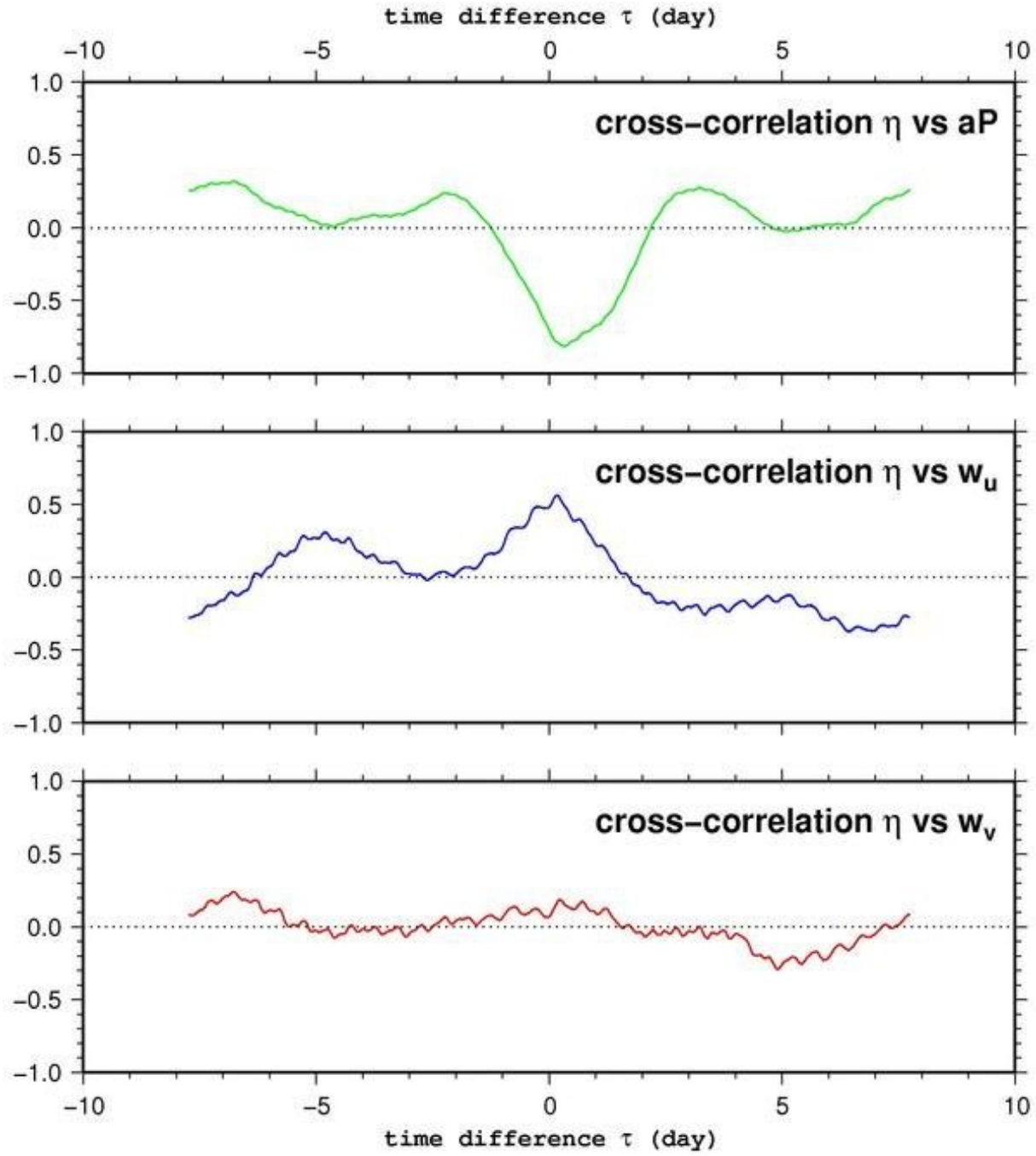

Figure 3.19: Cross-correlation between sea level and atmospheric Pressure (upper panel) ; sea level and east-west wind component (middle panel); sea level and north-south wind component (lower panel) at Yalova Station

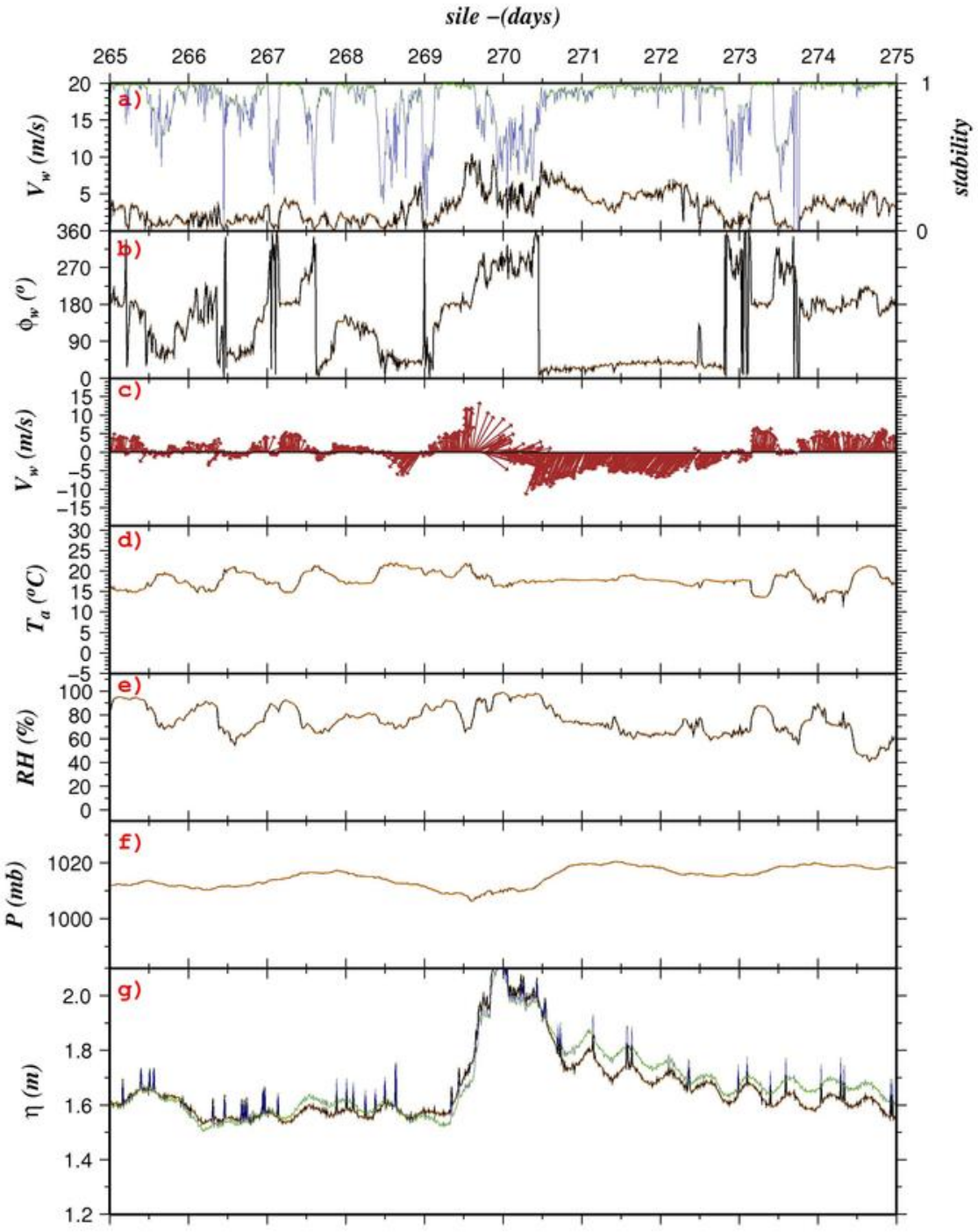

Figure 3.20: Sile station Time-series between 265 days and 275 days; a)Wind speed,b)wind direction, c)downwind vector diagram, d)air temperature, e)relative humidity, f)atmospheric pressure and g)sea level

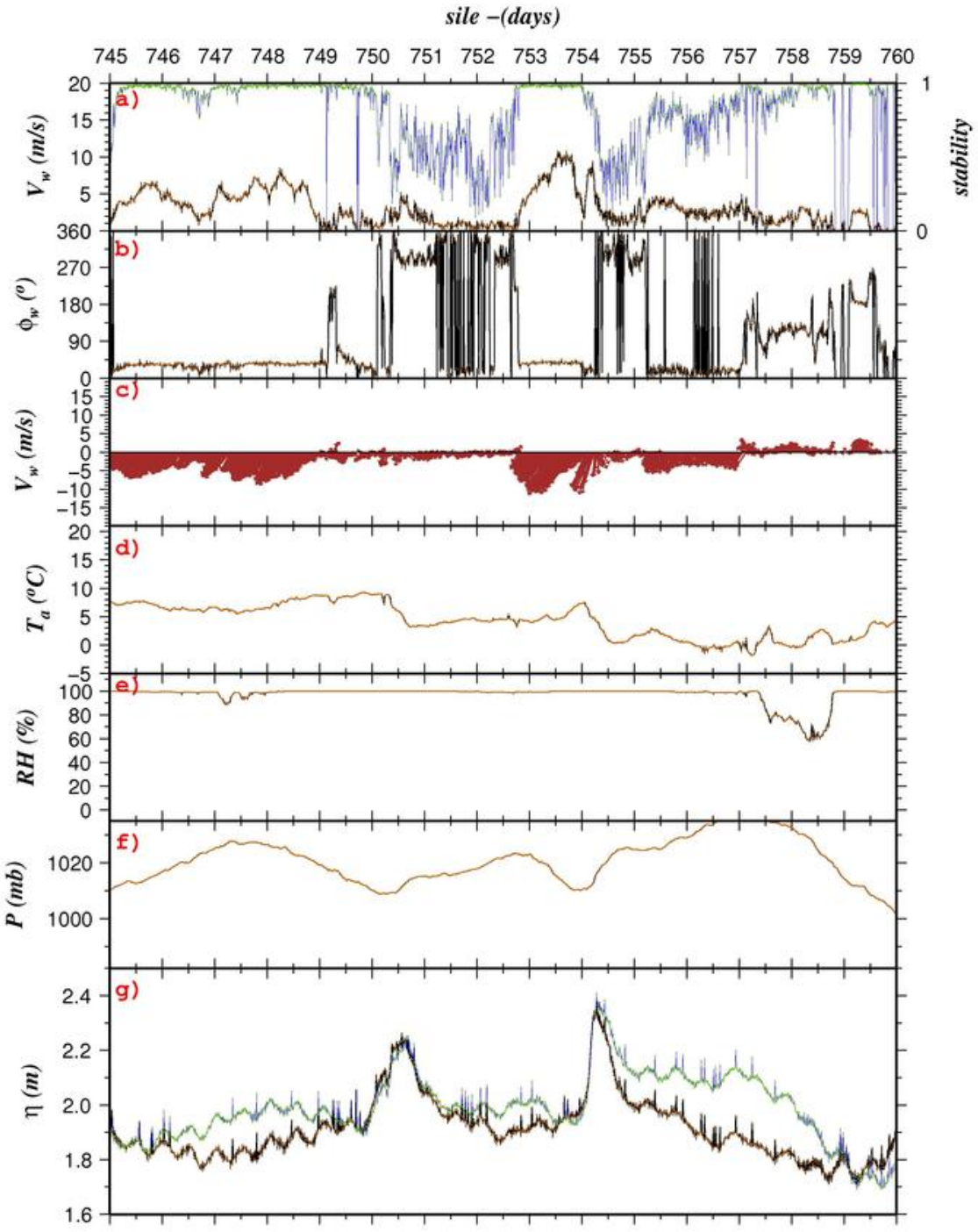

Figure 3.21: Sile station time-series between 745 day and 760 day; a)Wind speed, b)wind direction, c)downwind vector diagram, d)air temperature, e)relative humidity, f)atmospheric pressure and g)sea level

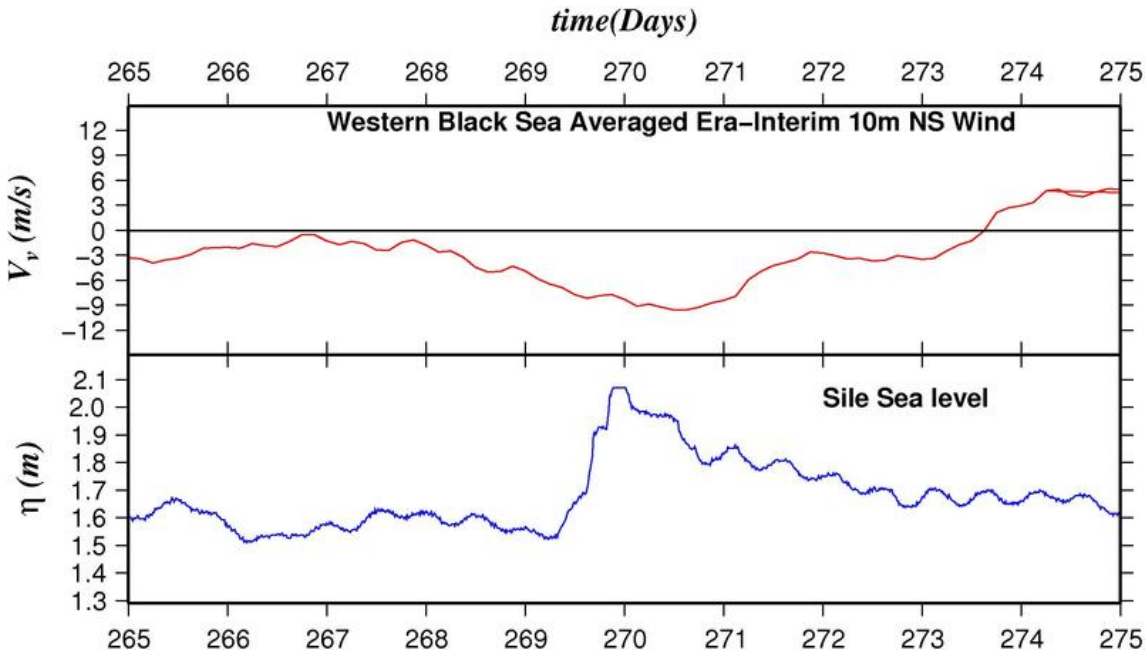

Figure 3.22: ECMWF 10 meter vector field average over Western Black Sea (upper panel) and Sile sea level between 265 day and 275 day (lower panel)

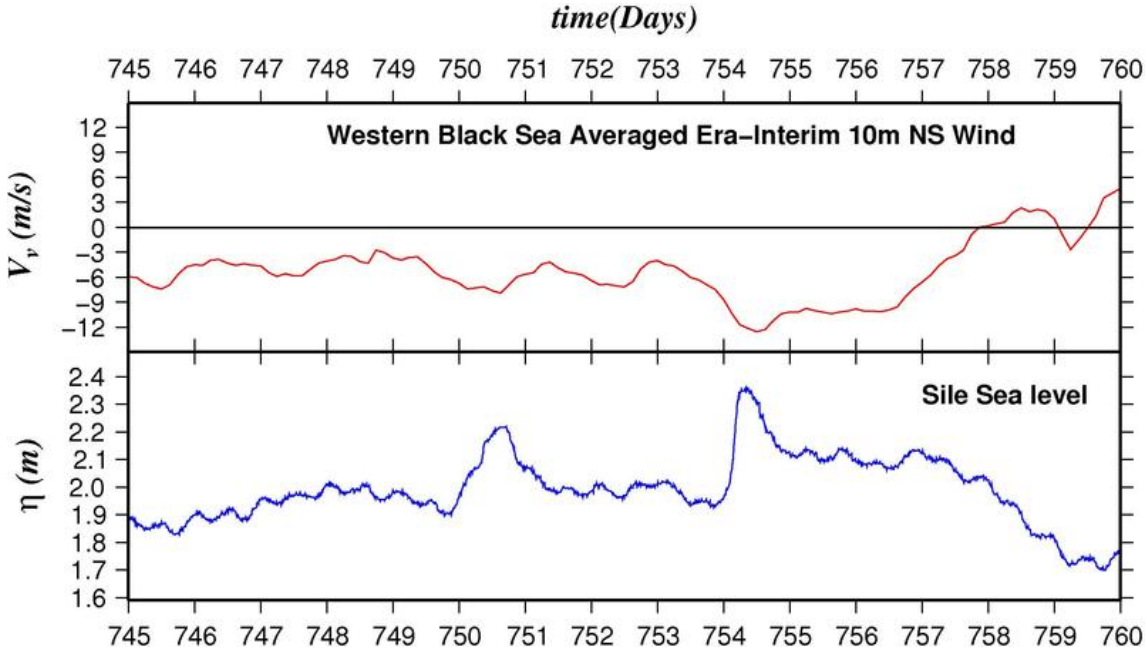

Figure 3.23: ECMWF 10 meter vector field average over Western Black Sea (upper panel) and Sile sea level between 745 day and 760 day (lower panel)

3.1.3 Current Data

The whole dataset obtained by the ADCP moored in the BOS are given in Figure 3.24-58. The lower layer current isn't properly examined in this study because the geometric shape of the area where the ADCP is deployed forms an eddy in the observed lower layer.Therefore the lower layer current data from the ADCP is not representative in terms of the general flow characteristic of the lower layer on thalweg of the Bosphourus(BOS).

The static summary of depth and monthly averaged upper layer is given in Table 3.4 using the whole dataset. The positive numbers for current velocity represent a current towards the Black Sea, whereas the negative values represent a flow to the Marmara Sea and this sign representation is also valid for volume flux which is discussed in a later section. In March and April, the highest means of upper layer current are found, with a range of 0.1 to 0.2 m/s greater than the other monthly means (Table 3.4). The maximum velocity in upper layer occurs during winter and early spring. The standard deviations of means indicate high temporal variability of the upper layer flow.

The annual mean of the upper layer flow is -0.515 m/s, -0.507 m/s and -0.552 m/s for 2008, 2009 and 2010, respectively. The annual mean of 2011 isn't mentioned due to the low data coverage. However, this low data coverage represent a mean of 0.483 m/s. The mean of -0.552 m/s for 2010 is remarkably high compared with the other years.

The Figures 3.24-58 demonstrate the two-layer exchange flow but it is clear that the system is not simple. The layers thickness vary with a short timescale in response to the atmospheric forcings like wind and atmospheric pressure which is discussed in more detail in following section.

Table 3.4: The depth and monthly averaged BOS upper layer from the whole dataset

Month	Number of Sampling	Mean	S.Deviation	Min	Max
January	16987	-0.46	0.3	-1.75	0.07
February	15738	-0.52	0.31	-1.75	0.07
March	12954	-0.68	0.23	-1.65	0.04
April	8938	-0.62	0.32	-1.5	0
May	9232	-0.47	0.27	-1.15	0.03
June	9598	-0.47	0.2	-1.17	0
July	7411	-0.56	0.17	-1.16	0.04
August	7504	-0.54	0.19	-1.13	0.05
September	5892	-0.51	0.18	-1.21	0.03
October	15364	-0.48	0.22	-1.23	0.1
November	15945	-0.49	0.24	-1.25	0.08
December	12886	-0.41	0.3	-1.65	0.11

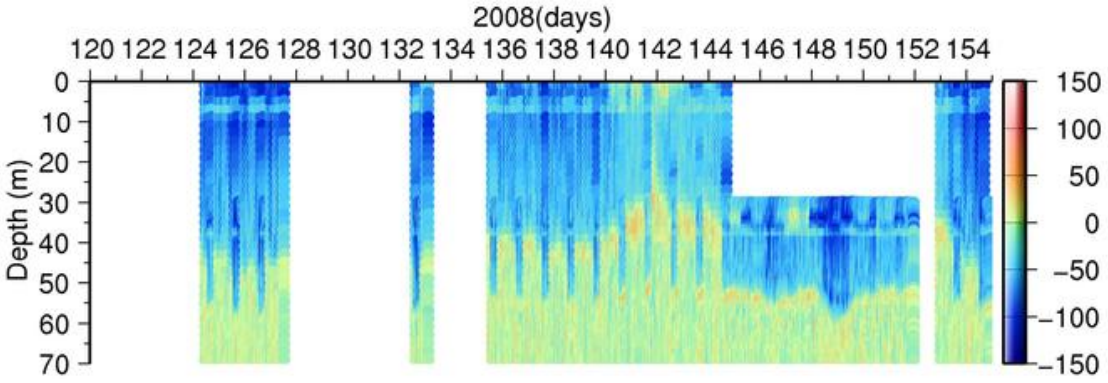

Figure 3.24: ADCP Current Profile on May 2008

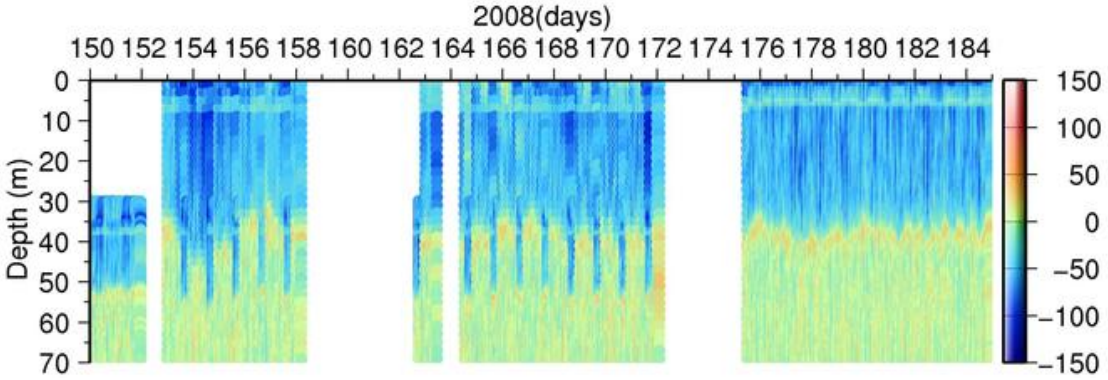

Figure 3.25: ADCP Current Profile on June 2008

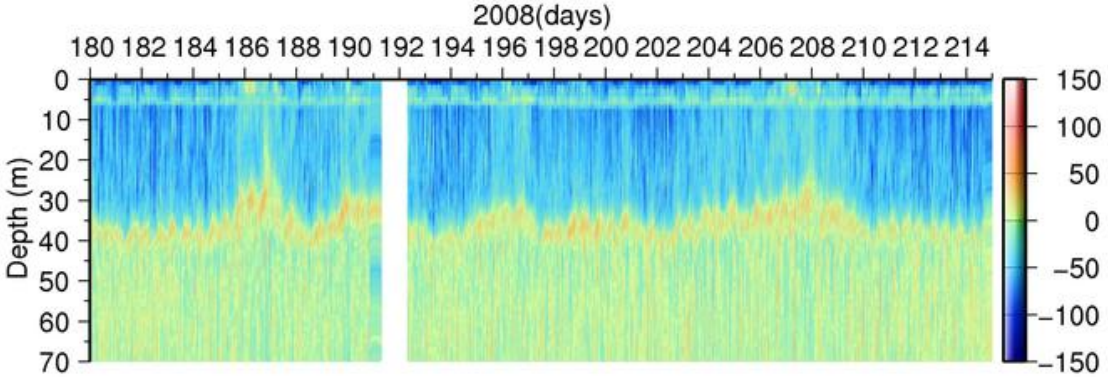

Figure 3.26: ADCP Current Profile on July 2008

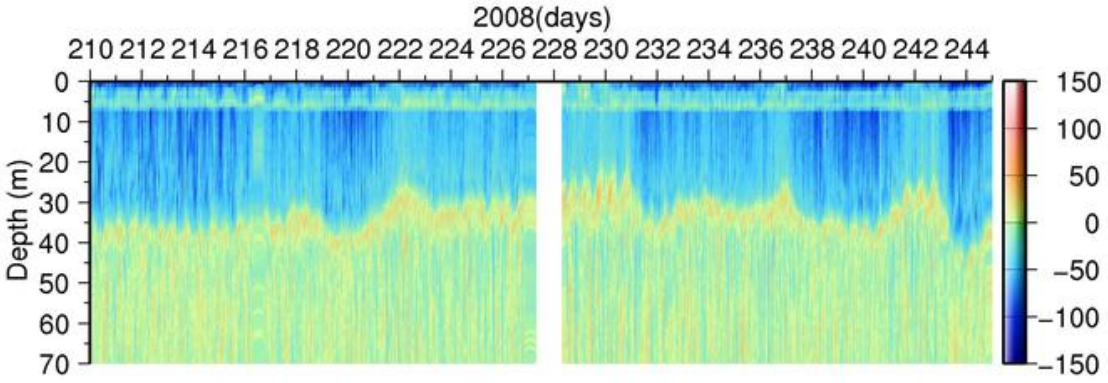

Figure 3.27: ADCP Current Profile on August 2008

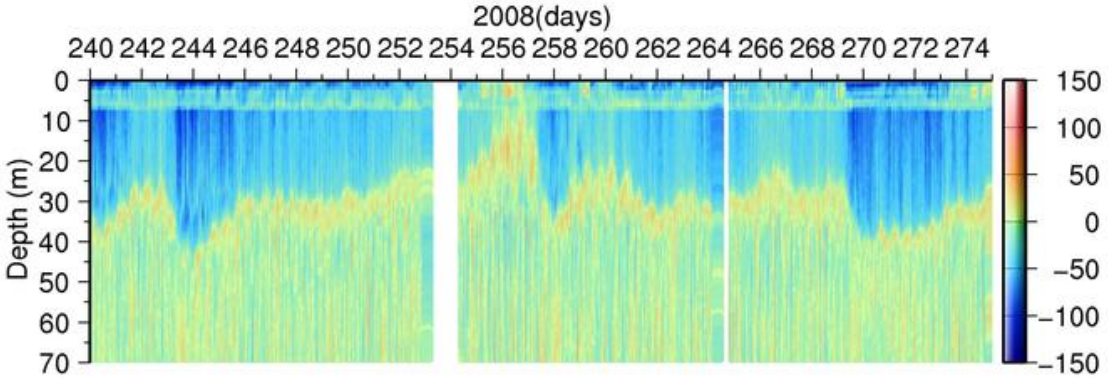

Figure 3.28: ADCP Current Profile on September 2008

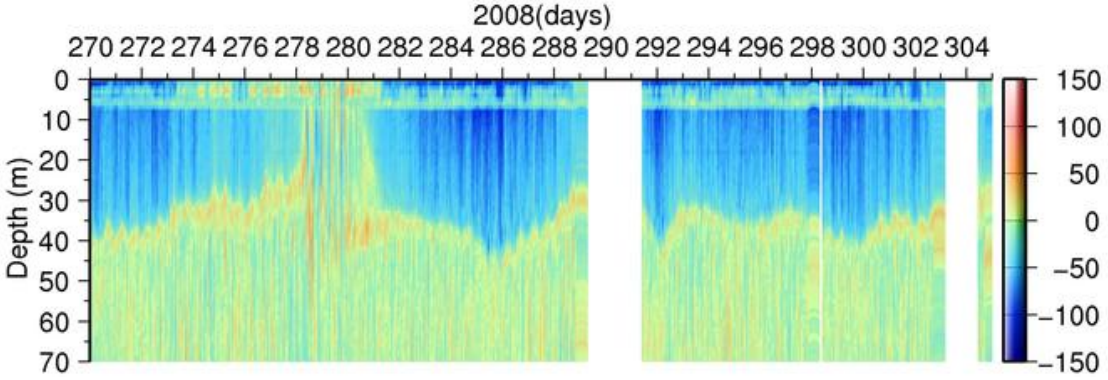

Figure 3.29: ADCP Current Profile on October 2008

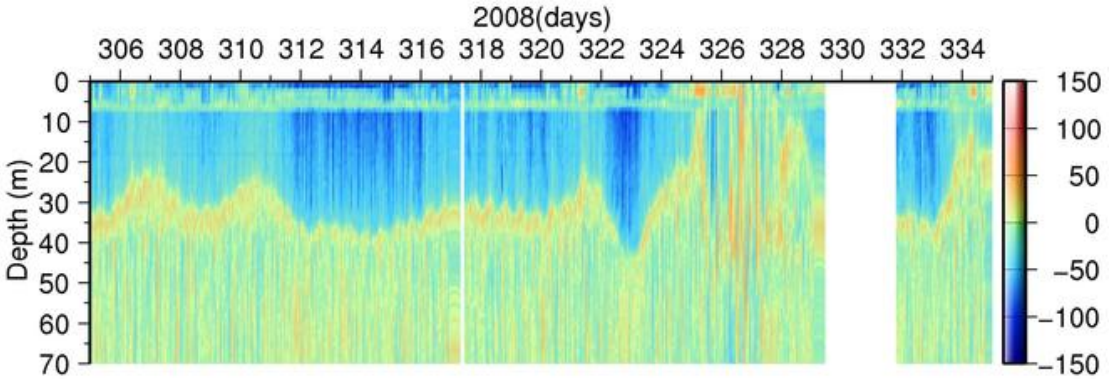

Figure 3.30: ADCP Current Profile on November 2008

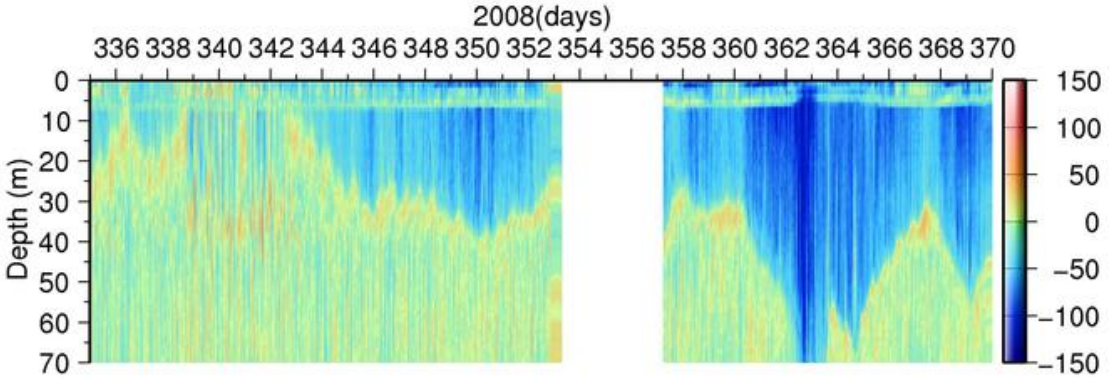

Figure 3.31: ADCP Current Profile on December 2008

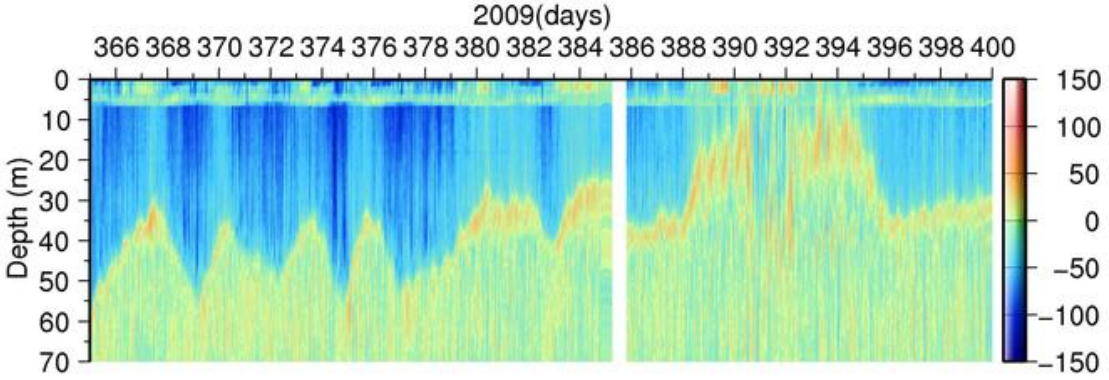

Figure 3.32: ADCP Current Profile on January 2009

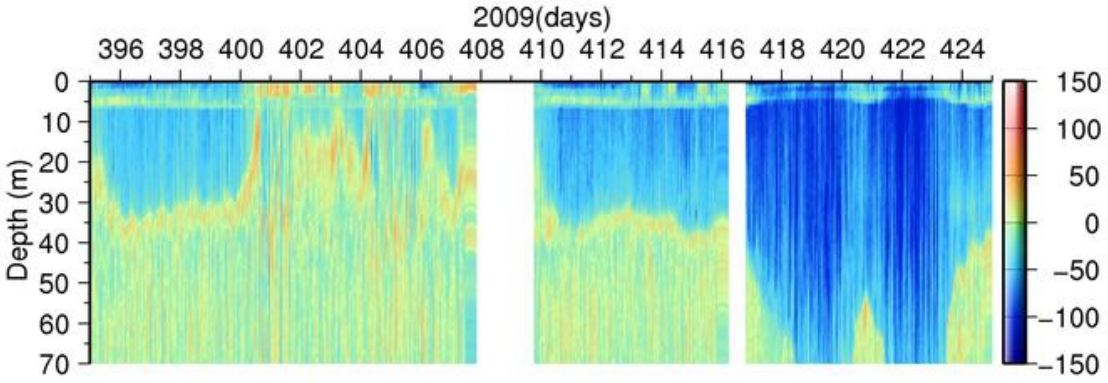

Figure 3.33: ADCP Current Profile on February 2009

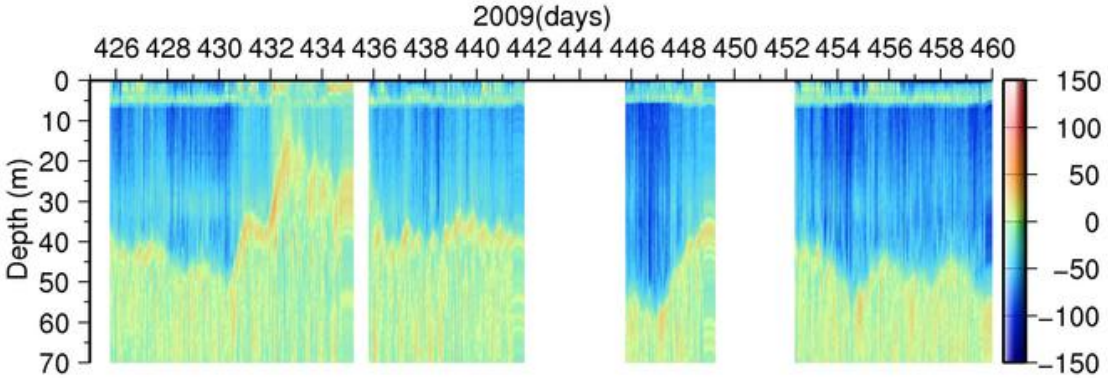

Figure 3.34: ADCP Current Profile on March 2009

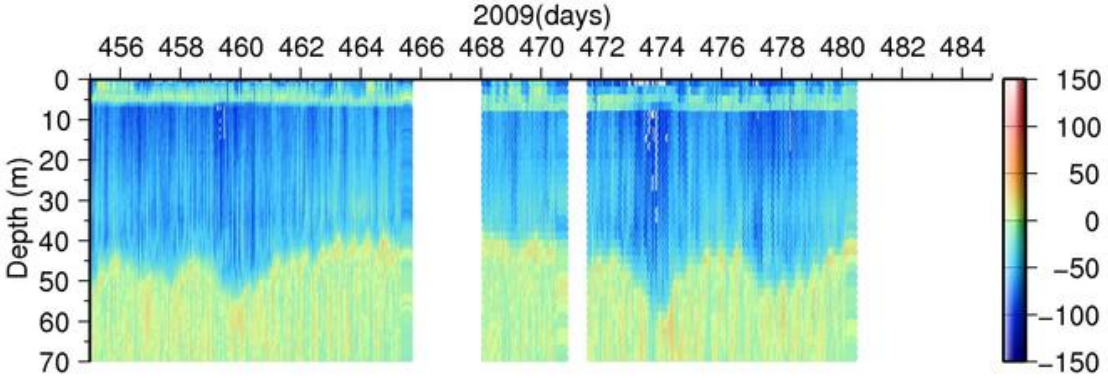

Figure 3.35: ADCP Current Profile on April 2009

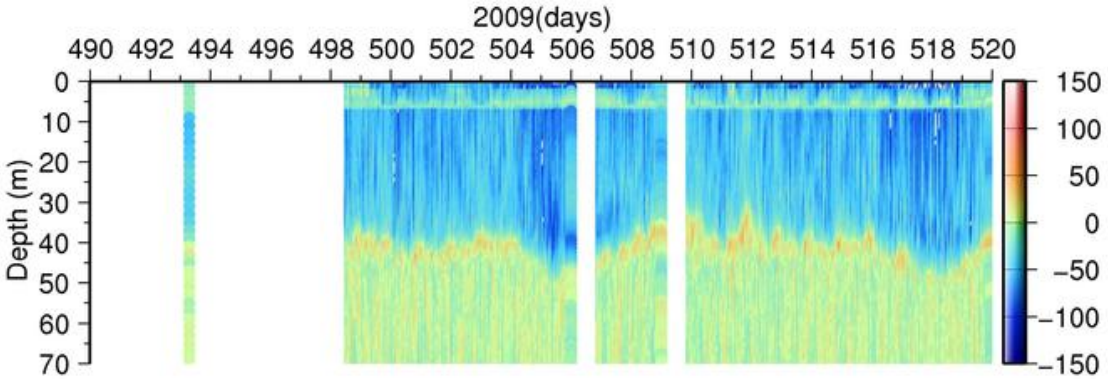

Figure 3.36: ADCP Current Profile on May 2009

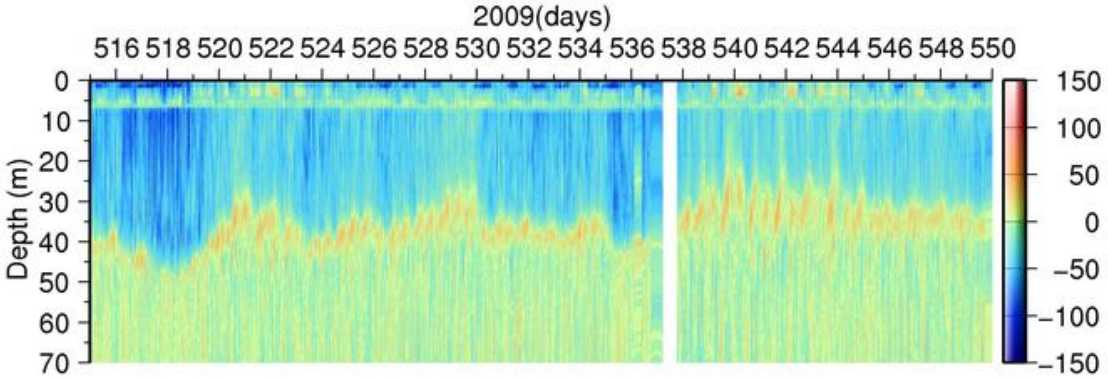

Figure 3.37: ADCP Current Profile on June 2009

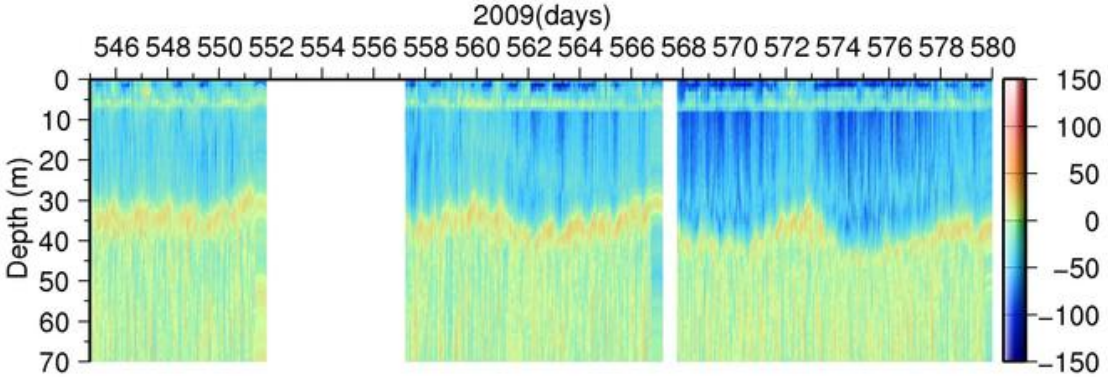

Figure 3.38: ADCP Current Profile on July 2009

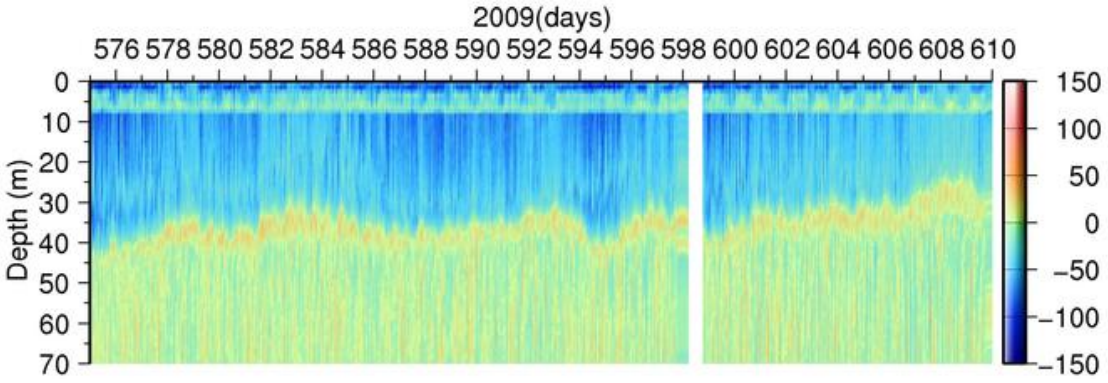

Figure 3.39: ADCP Current Profile on August 2009

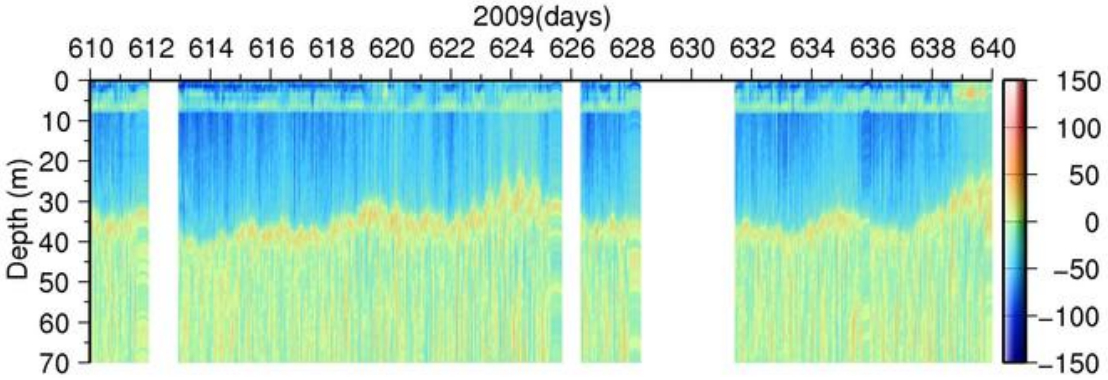

Figure 3.40: ADCP Current Profile on September 2009

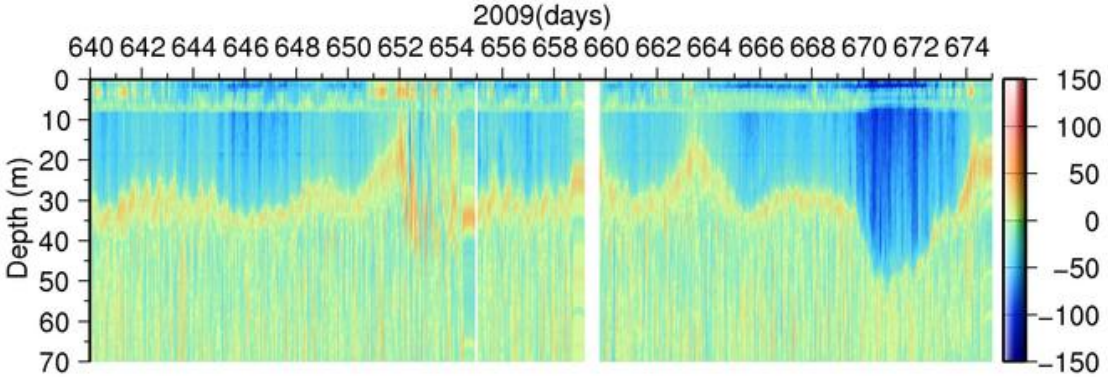

Figure 3.41: ADCP Current Profile on October 2009

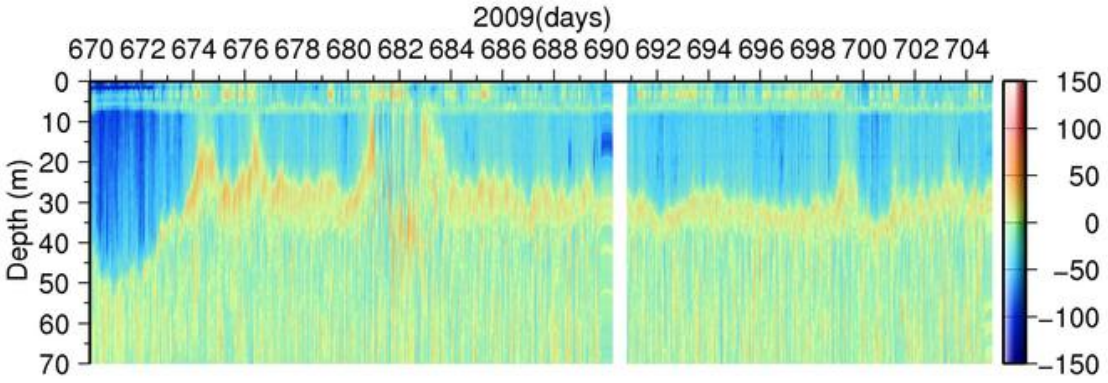

Figure 3.42: ADCP Current Profile on November 2009

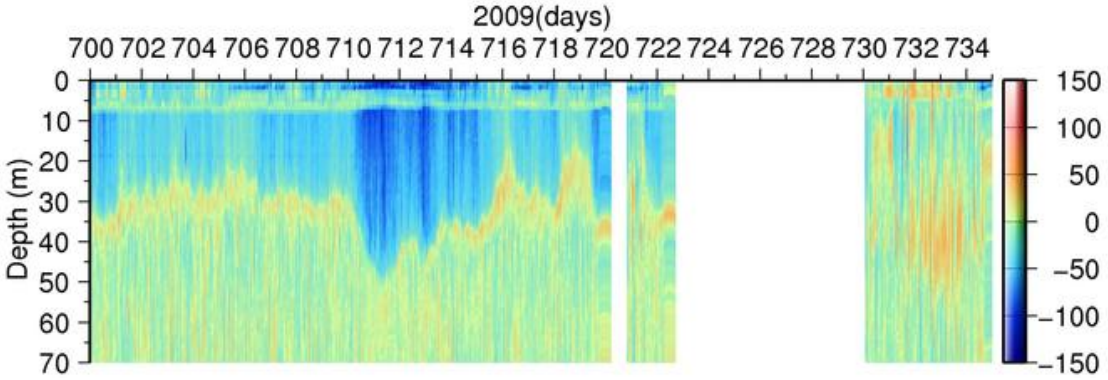

Figure 3.43: ADCP Current Profile on December 2009

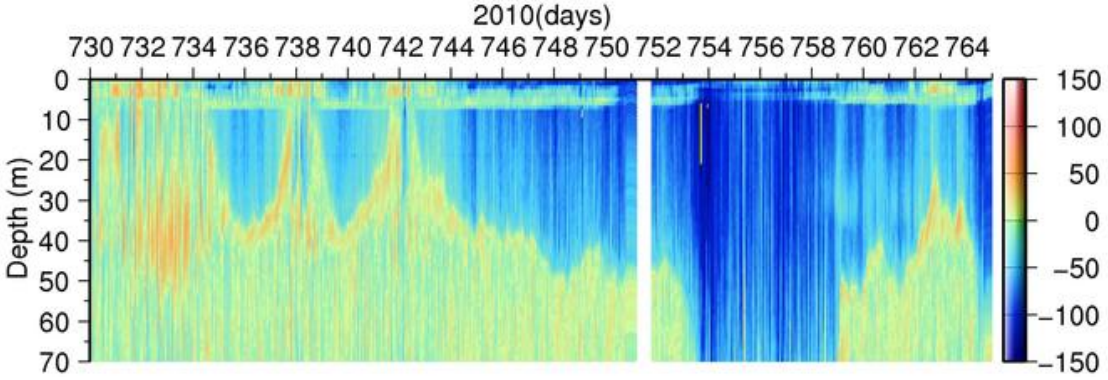

Figure 3.44: ADCP Current Profile on January 2010

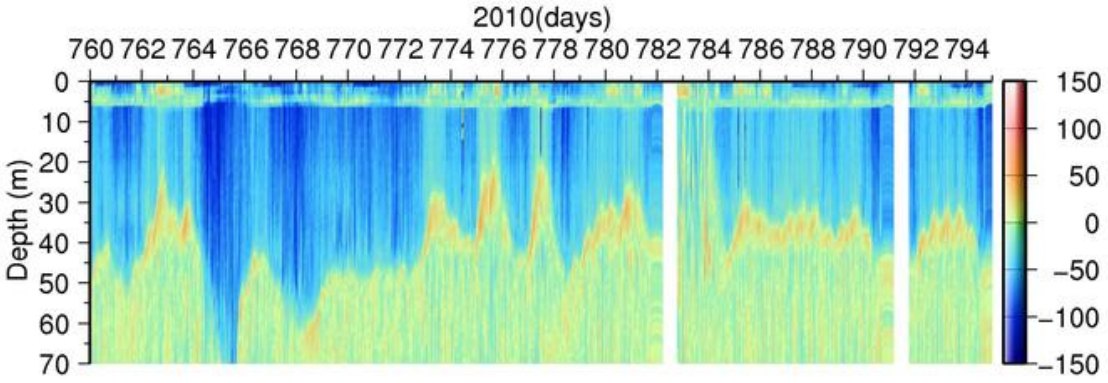

Figure 3.45: ADCP Current Profile on February 2010

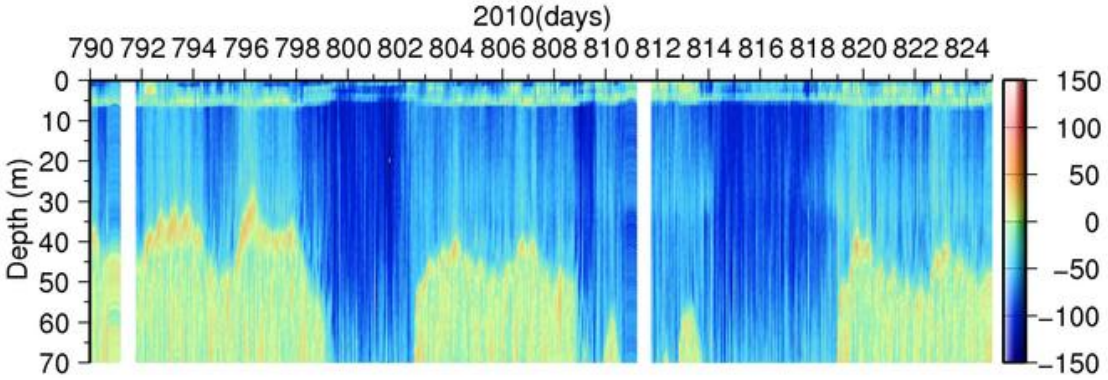

Figure 3.46: ADCP Current Profile on March 2010

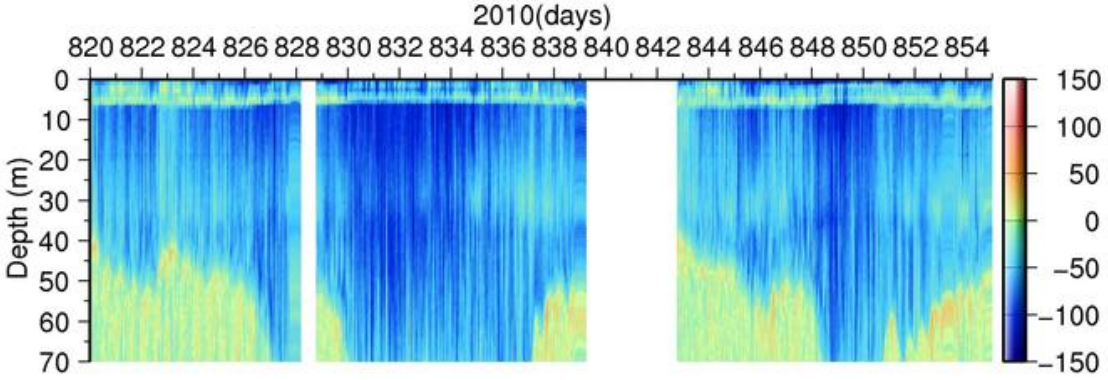

Figure 3.47: ADCP Current Profile on April 2010

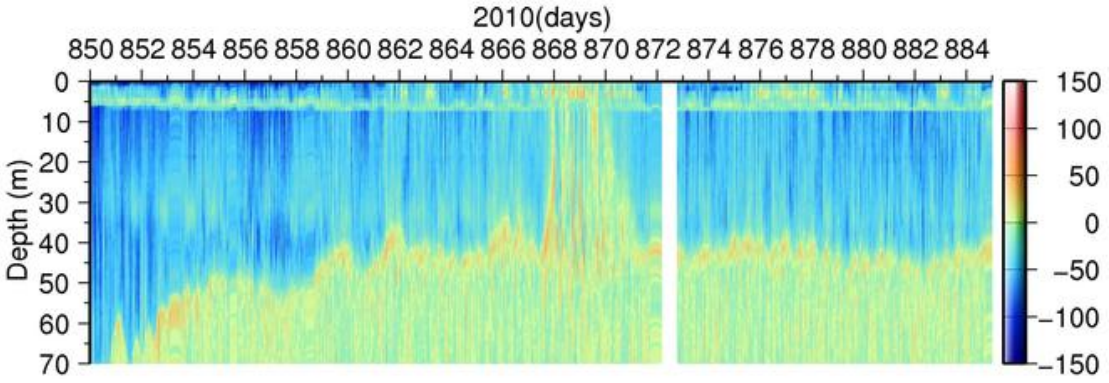

Figure 3.48: ADCP Current Profile on May 2010

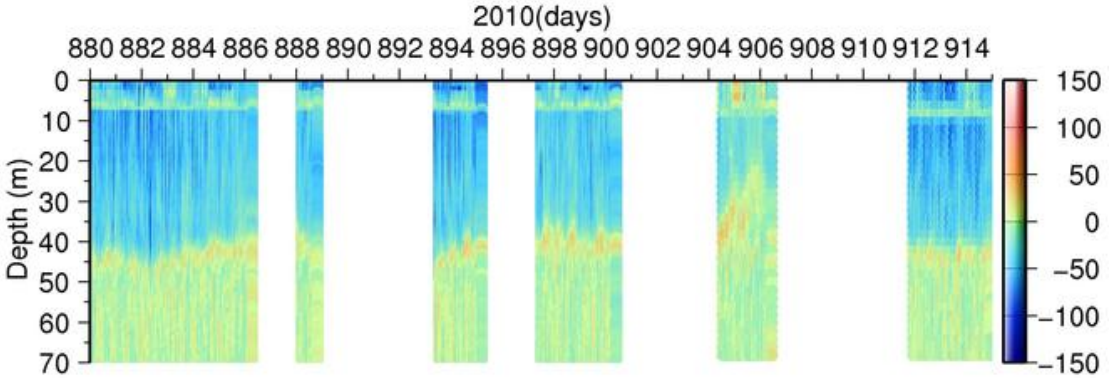

Figure 3.49: ADCP Current Profile on June 2010

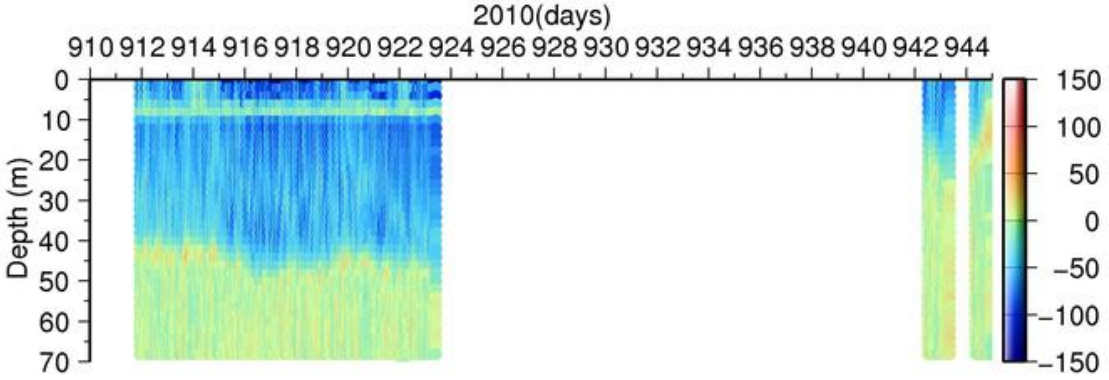

Figure 3.50: ADCP Current Profile on July 2010

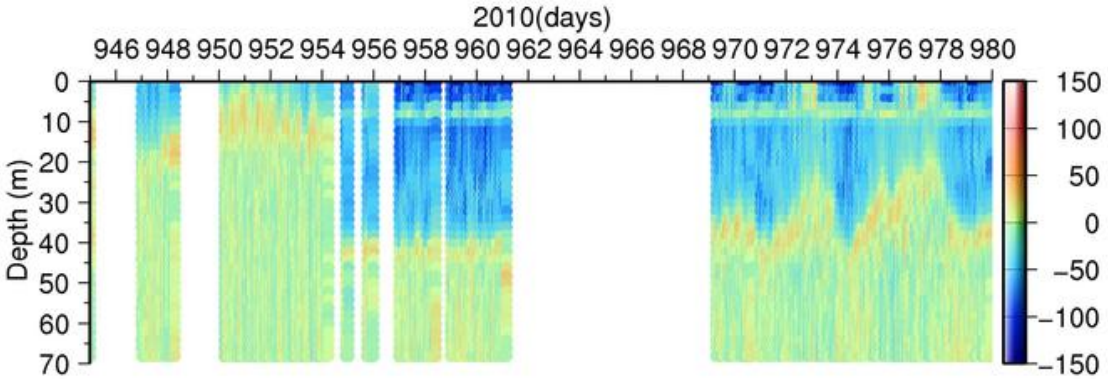

Figure 3.51: ADCP Current Profile on August 2010

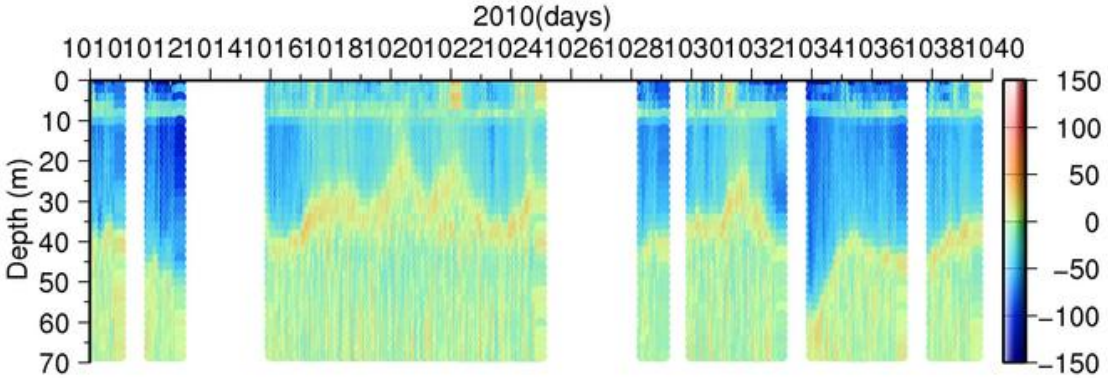

Figure 3.52: ADCP Current Profile on October 2010

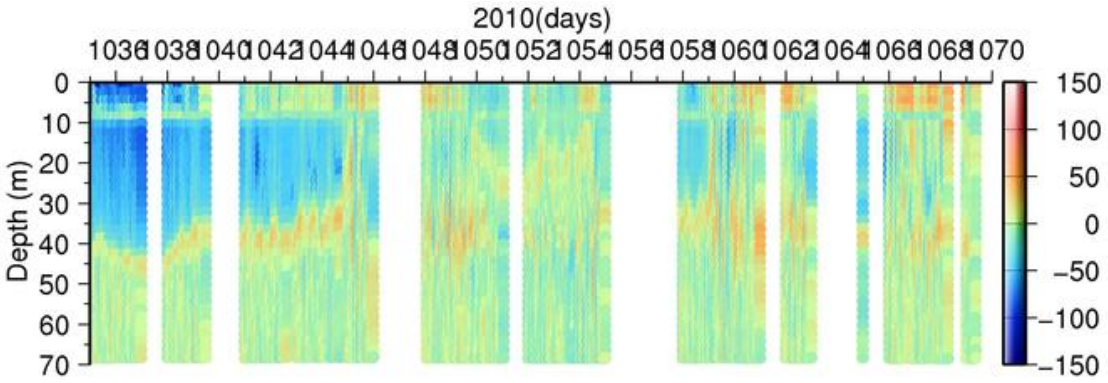

Figure 3.53: ADCP Current Profile on November 2010

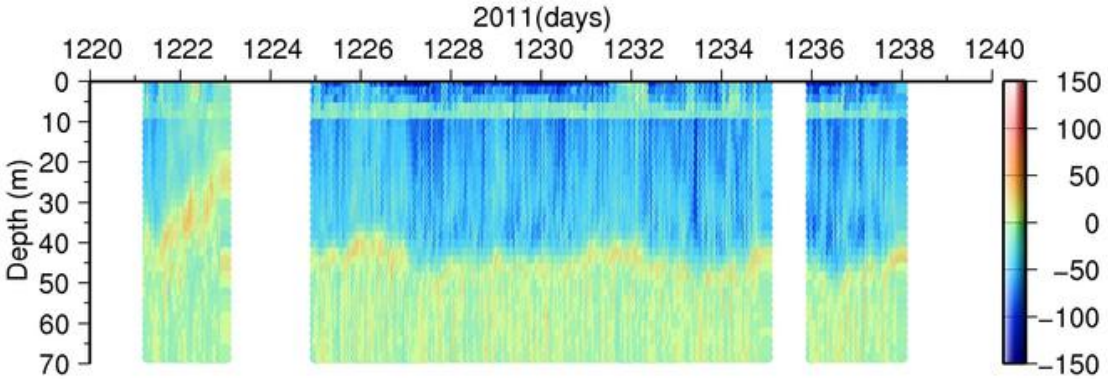

Figure 3.54: ADCP Current Profile on May 2011

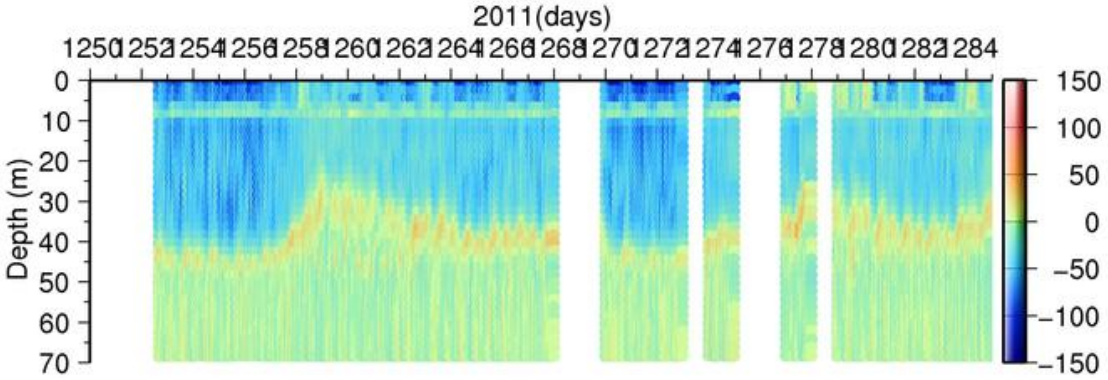

Figure 3.55: ADCP Current Profile on June 2011

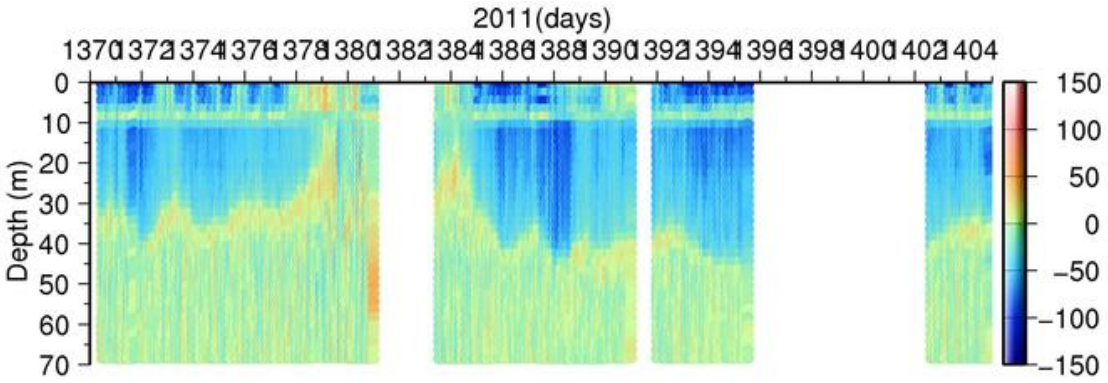

Figure 3.56: ADCP Current Profile on September 2011

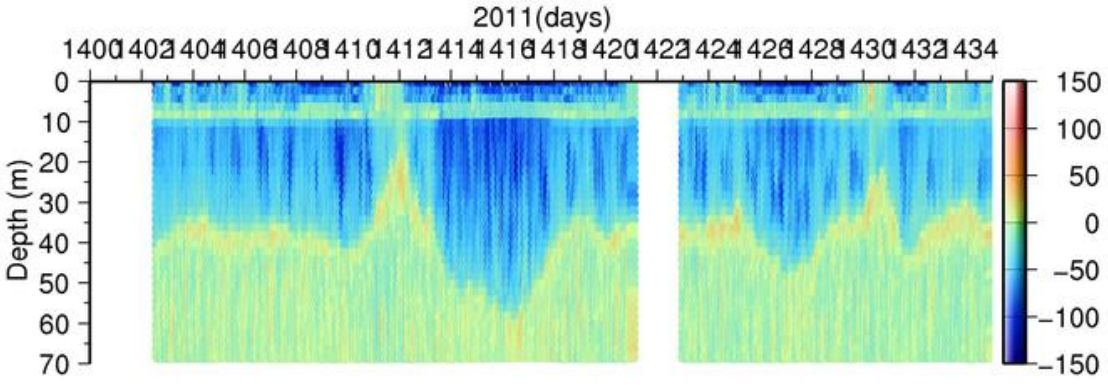

Figure 3.57: ADCP Current Profile on November 2011

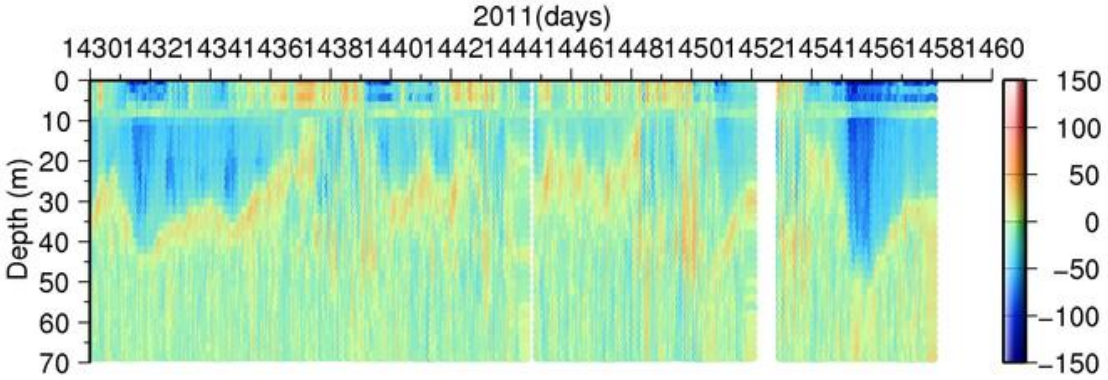

Figure 3.58: ADCP Current Profile on December 2011

3.1.3.1 Sea Level Difference Between The Marmara Sea and The Black Sea and its Intreaction with The Bosphorous Current

The sea level difference between the Black Sea and the Marmara Sea with ancillary data such as atmospheric pressure, atmospheric pressure difference and wind vector azimuth are given in Figure 3.59 using data from Yalova and Sile coastal stations. The sea level difference between the Black Sea and The Marmara Sea based on the data obtained from Yalova and Sile coastal stations over 2 years ranges from -14 cm to 71 cm with a mean of 26 cm. The sea level difference between the Black Sea and the Marmara is directly related to the winds over the region (Fig. 3.59), that is, the northerly winds increases the sea level at the north of Bosphorus,while the southerly increases the sea level at the south of the Bosphorus.The

theoretical ground suggests that the sea level due to the wind setup increases inversely with the water depth. it is observed that the sea level change due to the wind setup in the south of the Bosphorus is relatively greater than in the north of Bosphorus since the Marmara sea is shallower than the Black Sea. The barometric pressure difference varies between about ± 3 mbar (Fig. 3.59), which is not enough big to create the observed total changes in sea level differences.

When compared the calculated sea level difference between the Marmara Sea and the Black Sea with the previous observations made by other people , it appeals that results from this study are dissimilar with the formers . the average annual sea level differences are estimated between the ends of Bosphorus by Gunnerson and Ozturgut (1974) as 35 cm; by Cecen et al.(1981) as 33 cm and by Buyukay(1899) as 28 cm in 1985, as 29 in 1896, as 13 cm in 1987. The previous observations suggest that the average mean sea level difference is typically about 30 cm. The results obtained in this study only coincide with the Buyukay's results. This disagreement with previous observations may be caused by an offset measurement error.

Time series of Bosphorus averaged upper layer current and sea level differences (Fig. 3.60) indicate that upper current of Bosphrus responds simultaneously to the sea level differences. Increasing of the sea level difference results in accelerating the upper layer current and vice verse. The relationship between the sea level differences and the upper current is fitted to the linear equation below using the least squares approach.(Fig. 3.61)

$$U_v = -1.397794\Delta\eta - 15.39550$$

where, $U_v, \Delta\eta$ are upper current north-south component and sea level difference ,respectively.

The Bosphorus current exhibits two layer exchange flow layer with the exception of blockage events. blockage event occurs when the strong southerly winds diminishing sea level differences blow. Sometimes, the upper layer current can be reversed depending on the decreasing sea level differences. This phenomena is called "orkoz". The upper layer blockage events occur frequently in winter and autumn (Fig. 3.60). According to the ADCP data, blockages event lasting in one or two days are seen on 13 September (256 day,Figure 3.28) ,5 October (278 day,Figure 3.29) ,22 November (326 day,Figure 3.30) ,December 5 (339 day,Figure 3.31) of 2008, 25 January (390.day ,Figure 3.32), 5 February(401 day, Figure 3.33), 13 October(652 day,Figure 3.41),12 November(682.day,Figure 3.42) of 2009, 01 January (732 day,Figure 3.43),07 January (738 day,Figure 3.44), 11 January (742 day,Figure 3.44),17 May (869 day, Figure 3.48), 30 November(1066 day,Figure 3.53) of 2010 and 7 October (1378

day,Figure 3.56), 4 December (1436 day,Figure 3.58) and 10 December (1442 day,Figure 3.58) of 2011. There are a few other situations where the sea level difference diminish. But, the upper layer current couldn't be observed since there exists gaps in the ADCP data on that periods due to the instrumental problems. The upper current on 13 September,2009 is picked as an illustration to represent the upper layer blockage event. the figures related to this day are given in Figure 3.65 and 3.66. The Figure 3.65 shows the effect of southly winds on blockage events clearly. Sometimes different local wind can be observed simultaneously at both of ends of Bosphorus. In such case, the differences between wind setups at each end of BOS govern the exchange flow. According to this study, the blockage events are seen when the sea difference between two ends drops below -3 cm and the Figure 3.65 demonstrates that the upper layer flow returns to the usual state as soon as blocking conditions vanish, The water column profile (Fig. 3.66) indicates that the upper layer current speed can vary between 0.2 m/s and 0.5 m/s at the water column during orkoz. In summer and spring the blockage events aren't observed. This is possibly caused by the weak southerly winds and the Black sea sea level increasing due to the river input during that period. Figure 3.67 and 3.68 shows typical situation in the upper layer during the summer and autumn.

The lower layer blockage is also observed on 29 December (363 day, Figure 3.31) of 2008, 22 February (418 day, Figure 3.33) of 2009 and 22 January (753 day,Figure 3.44), 3 February (765 day, Figure 3.45), 8 March (799 day, Figure 3.46),8 April (830 days, Figure 3.47), 27 April (849 day, Figure 3.47). In terms of duration of events, the lower layer blockages typically last longer than the upper layer blockages, but it can be noted that the lower layer blockages occurs less than upper layer blockages during this study. In addition,lower layer blockage events accompany the sea level differences greater than 60 cm.

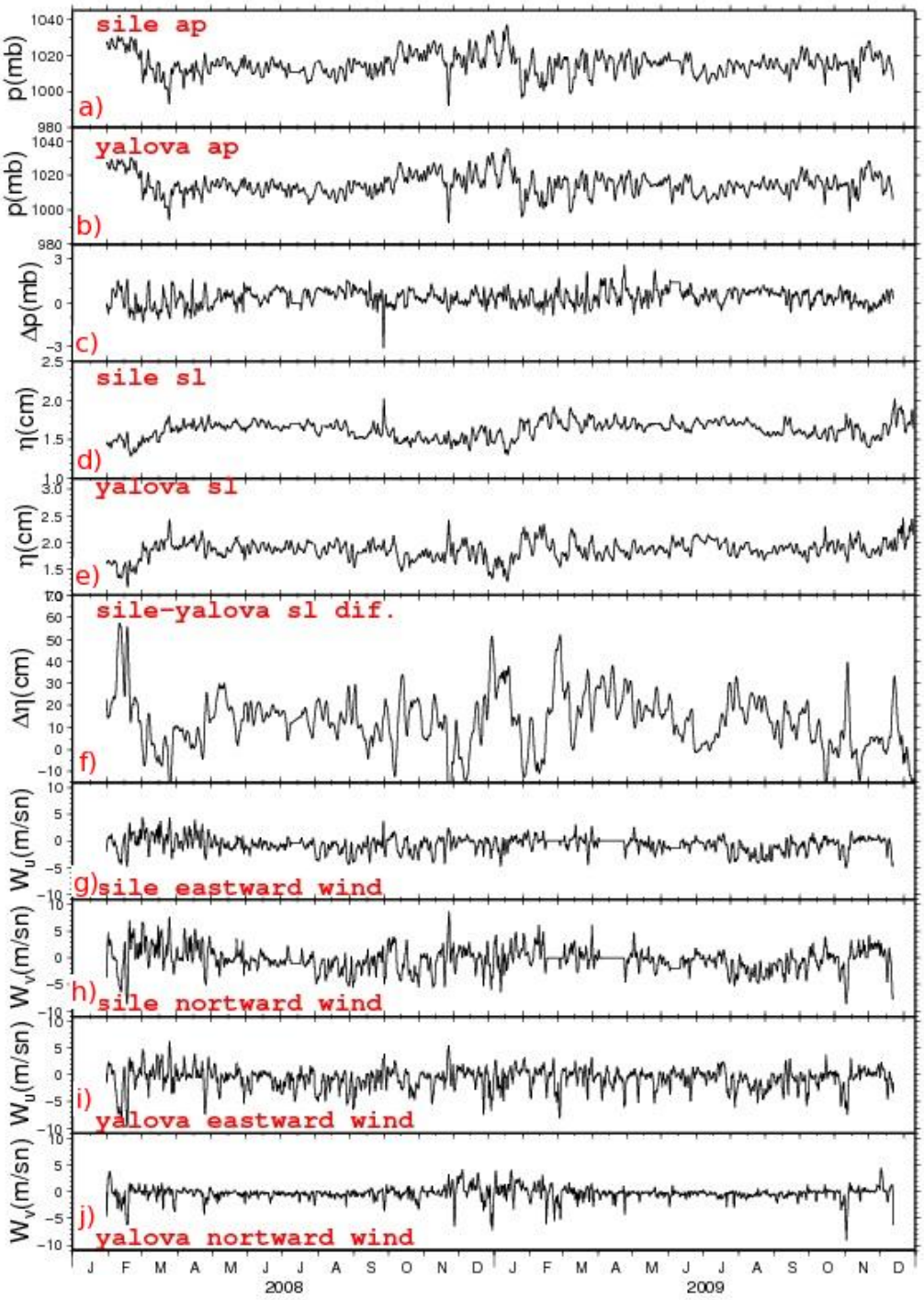

Figure 3.59: Atmospheric pressure in a) Sile and b) Yalova stations, Atmospheric pressure differences between c) Sile and Yalova, Sea level in d) Sile and e) Yalova stations, sea level difference between f) Sile and Yalova station, g) eastward and h) northward wind at sile and i) eastward and j) northward Yalova during the study period

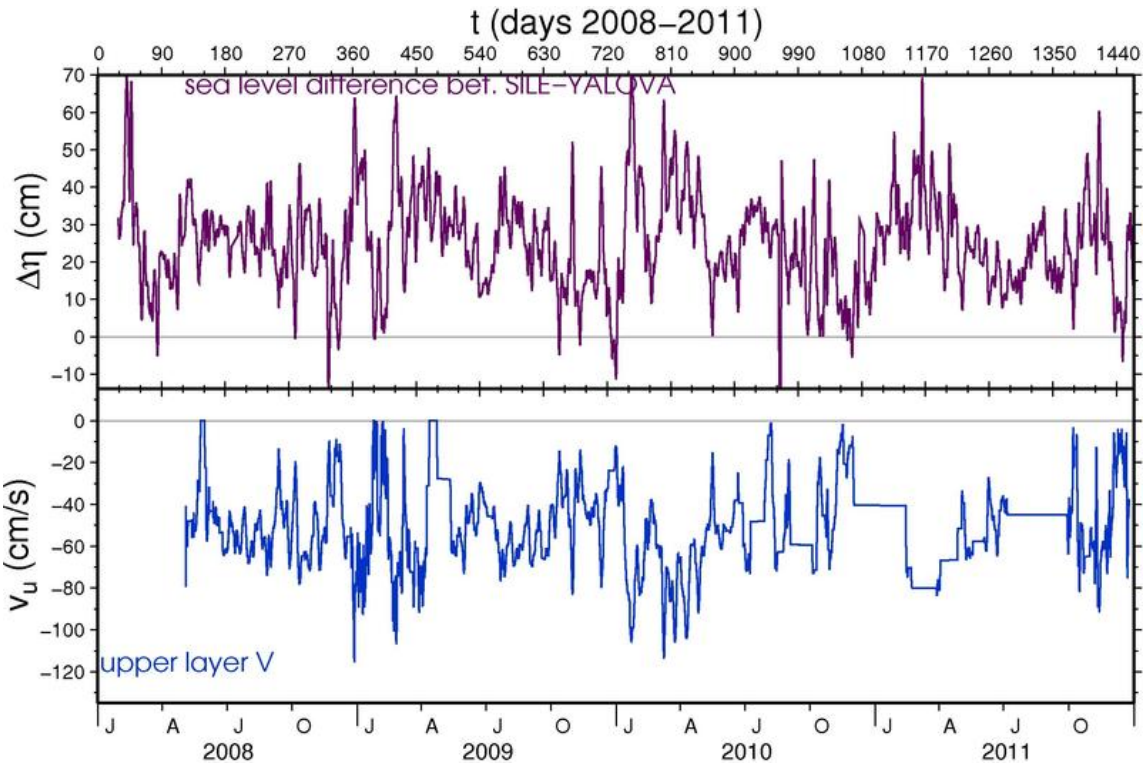

Figure 3.60: Time series of sea level differences (upper panel) and Upper layer velocity (lower panel)

3.1.3.2 Upper layer Volume flux

Quantifying the volume flux properly with a bottom-mounted ADCP in the Bosphorus is a challenging work due to the lack of the measurement along the cross section on where the calculations is done . It is assumed that the upper layer velocity and the upper layer thickness is the same along the cross-section,therefore it may cause underestimation or overestimation of upper layer flux. Nonetheless, the Figure 3.63 shows the upper layer flux calculations based on ADCP data show almost same pattern with calculations based on the Bosphorus model developed by Sozer(2012).

The static summary of monthly mean upper layer flux is tabulated in the Table 3.3. It indicates that the largest transport in the upper layer occurs in spring, especially March whereas the lowest transport in the upper layer takes place in the fall and winter. Taking into account the maximal exchange, it can be emphasized that the lower layer transport exhibit the opposite characteristics during the periods mentioned above.

The annual mean of upper layer volume flux is -9028 m^3/s, -8549 m^3/s and -10341 m^3/s

Table 3.5: The upper layer flux

Month	Number of Sampling	Mean	S.Deviation	Min	Max
January	16987	-7608	5208	-49407	3373
February	15738	-8894	5603	-46887	1884
March	12954	-11605	4478	-51175	1081
April	8938	-10931	6006	-41491	0
May	9232	-9306	5626	-28457	680
June	9598	-9525	4439	-28960	0
July	7411	-10413	3712	-28241	792
August	7504	-9577	3715	-24496	1689
September	5892	-8900	3258	-26492	849
October	15364	-9641	4979	-29761	4014
November	15945	-10234	5611	-32640	3076
December	12886	-7570	5527	-41441	2314

for 2008, 2009 and 2010, respectively. Similar to the case of flow velocity, the upper layer volume flux for 2010 is larger compared with other years. The Figure 3.64 demonstrate that the flux in the upper layer is so variable in short term scale and fluctuation in volume transport can be often two or there times larger than the mean of whole dataset.

As it is done before, the relationship between the sea level differences and the upper layer transport is fitted to linear equation using the least squares approach (Fig. 3.62). The equation is

$$Q_1 = 0.2387796\Delta\eta + 2.503935$$

where, $Q_1, \Delta\eta$ are upper layer volume flux and sea level difference ,respectively.

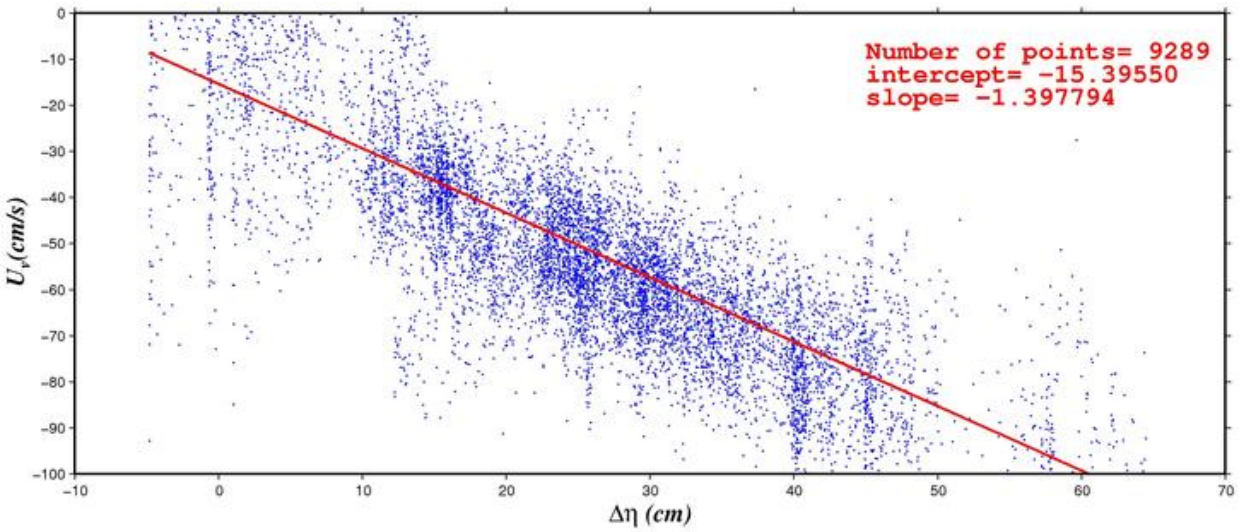

Figure 3.61: Least Square Estimation between Upper Layer velocity and Sea level Differences

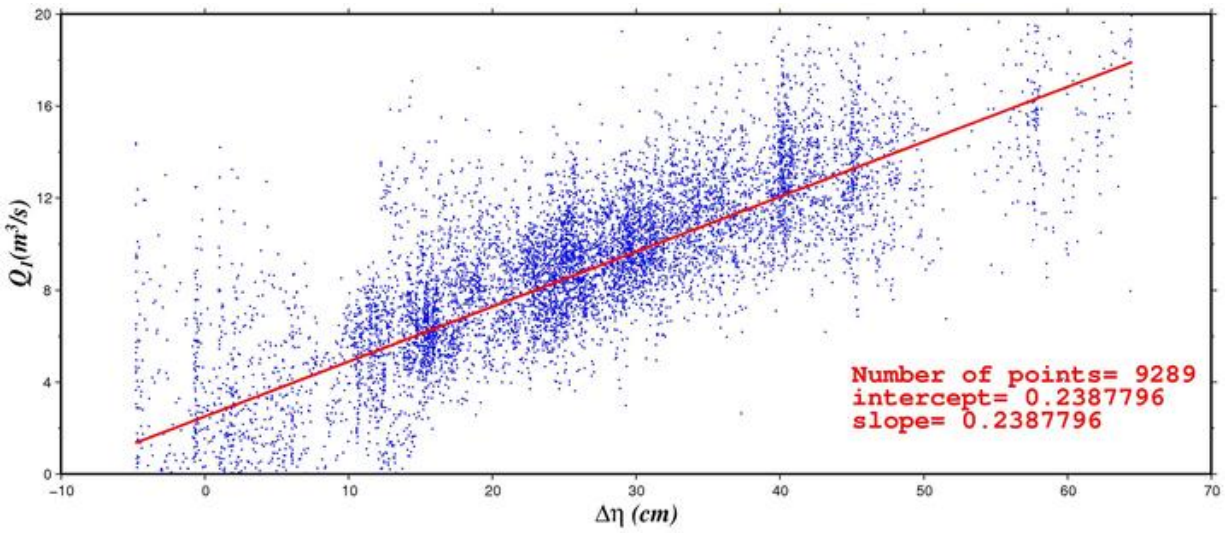

Figure 3.62: Least Square Estimation between Upper Layer Volume flux and Sea level Differences

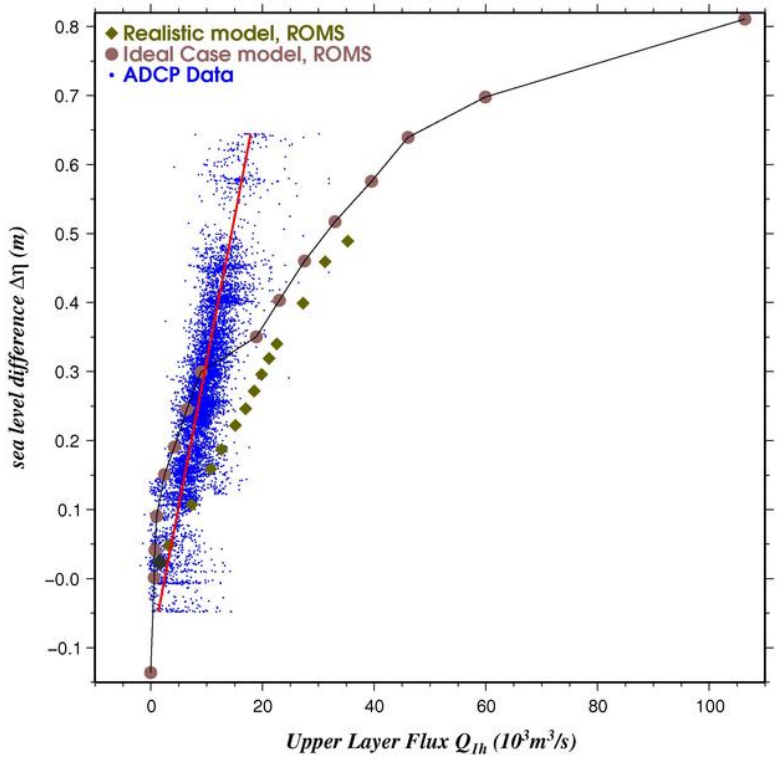

Figure 3.63: Comparison of upper layer flux calculated from ADCP with the upper layer flux calculated from the model

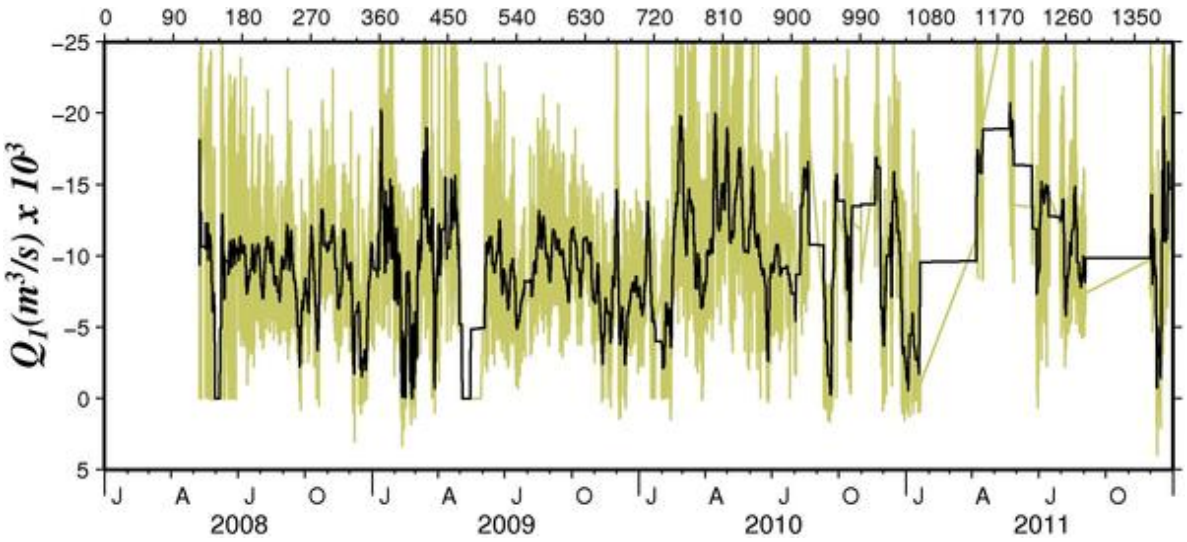

Figure 3.64: Time series of the upper layer volume flux during the study period (yellow=15 minutes data, black= 3-day low pass filtered data)

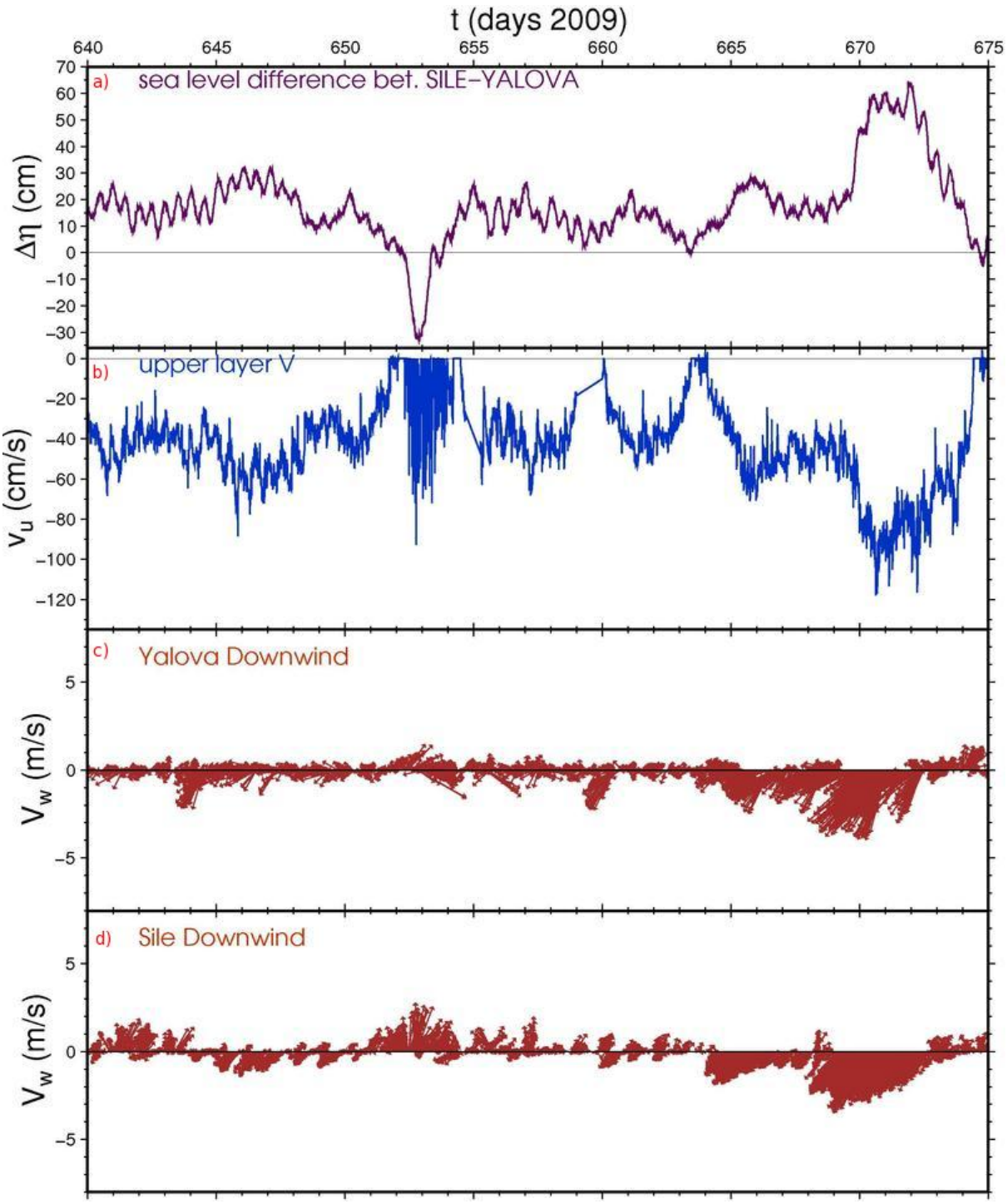

Figure 3.65: Time-series of a) sea level differences between Sile and Yalova , b) upper layer velocity u and c) v components, downwind at d) Yalova and e) Sile stations on November,2009.

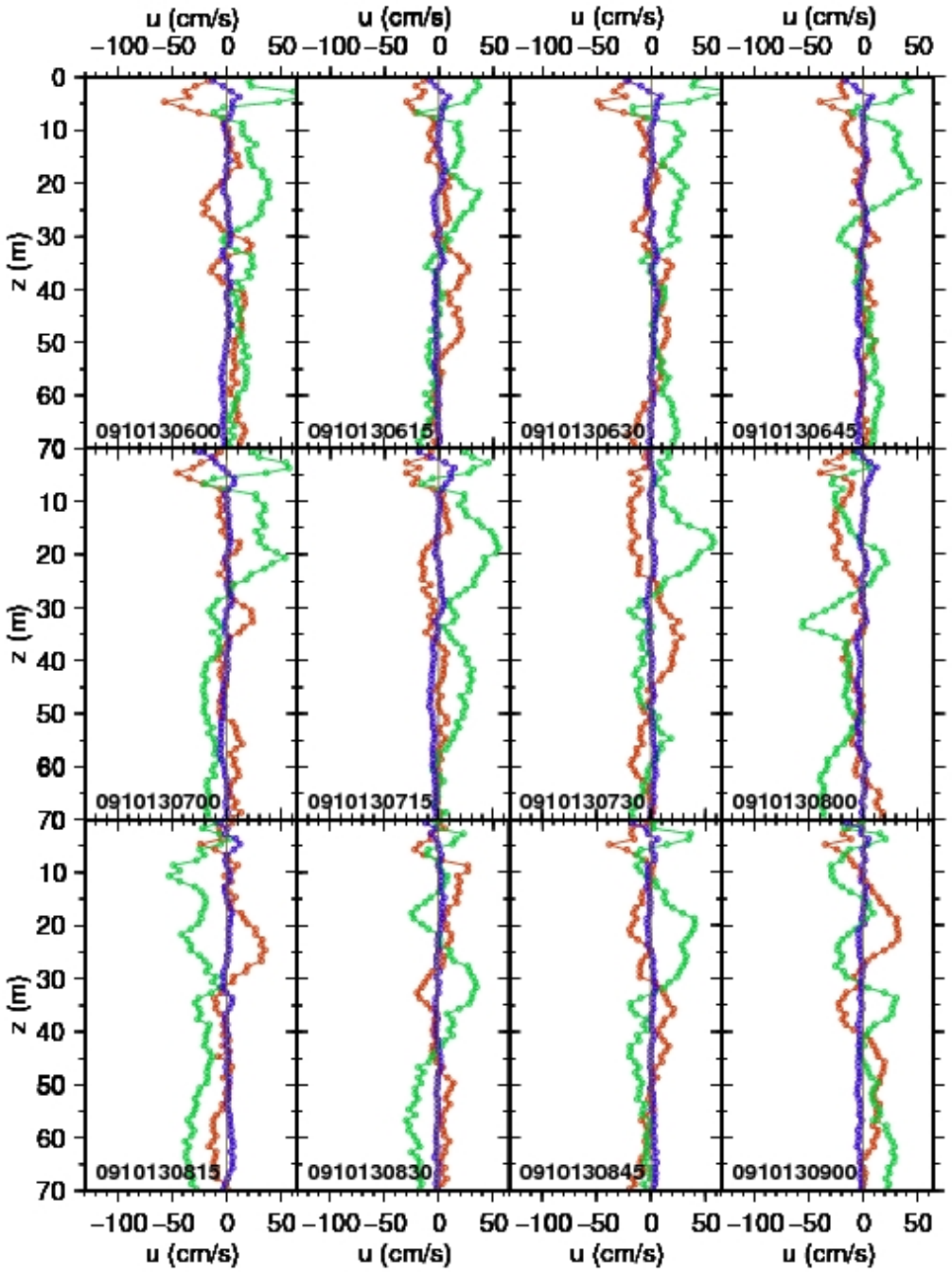

Figure 3.66: The Bosphorous current profiles on 13 October,2009 (starting at 6 a.m and every 15 minutes profile green=northward component, brown= eastward component, purple=upward component)

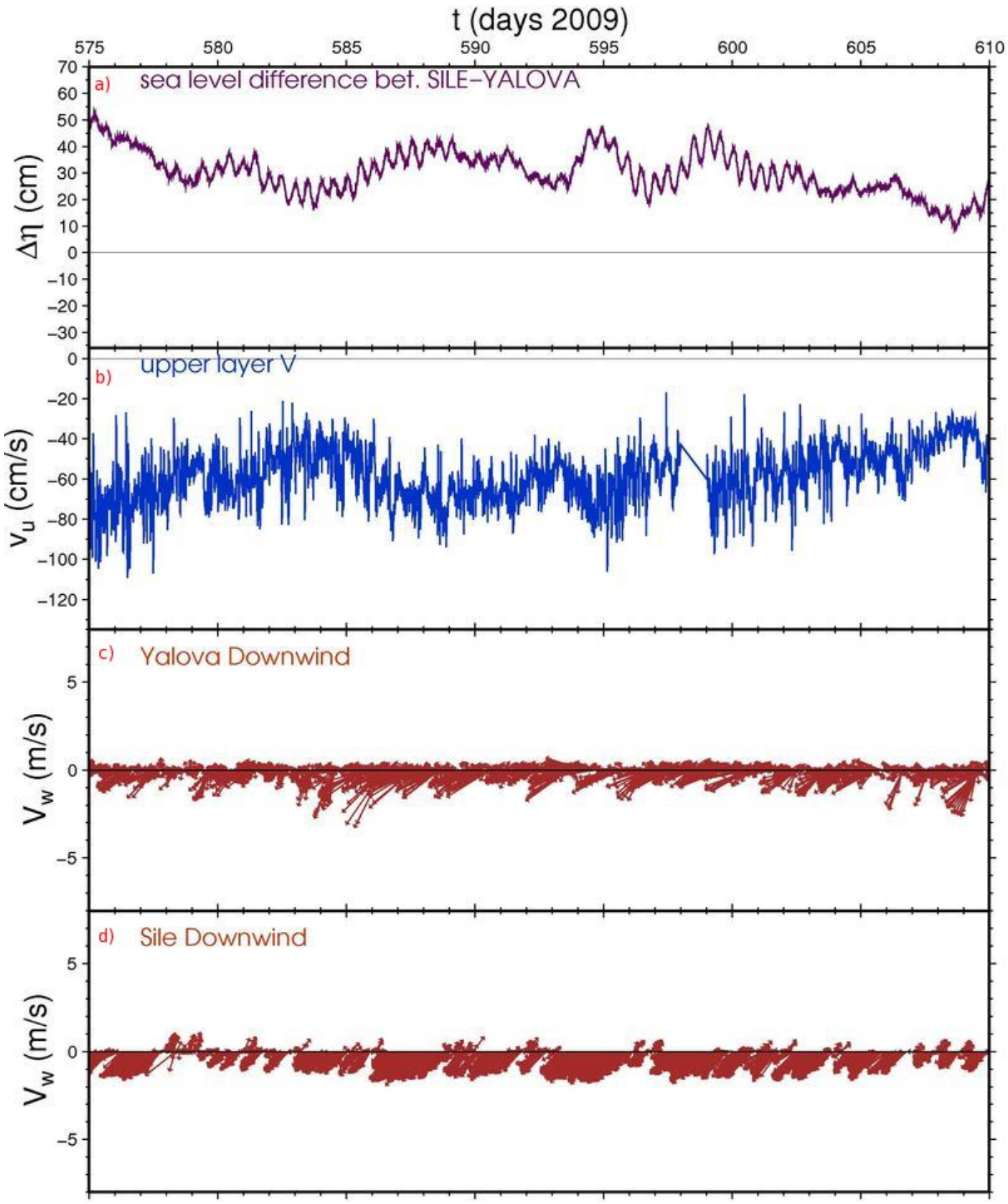

Figure 3.67: Time-series a) sea level differences between Sile and Yalova , upper layer velocity b) u and c) v components and downwind at d) Yalova and e) Sile stations on Agust,2009.

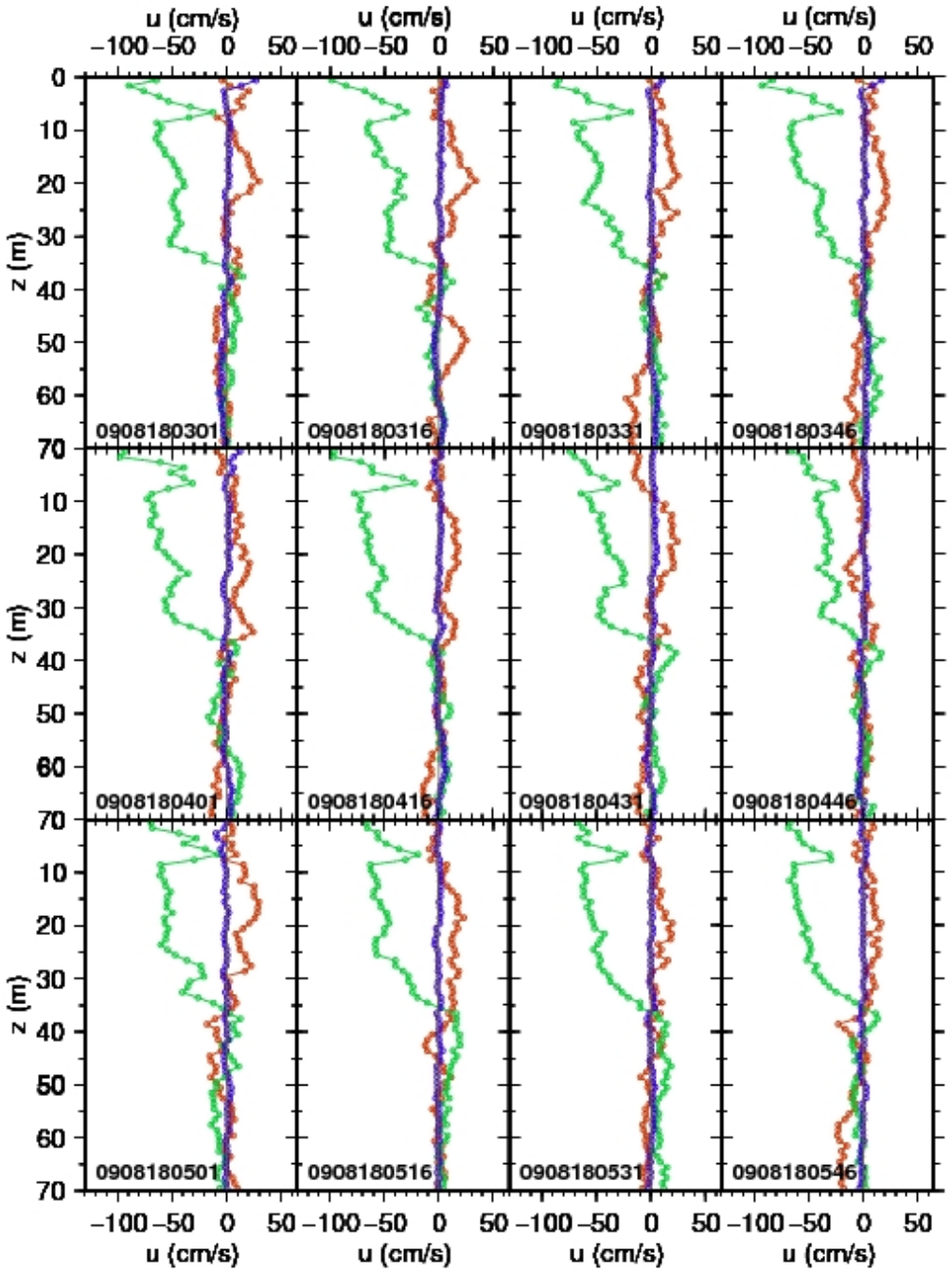

Figure 3.68: The Bosphorous current profiles on 18 August,2009 (starting at 3 a.m and every 15 minutes profile green=northward component, brown= eastward component, purple=upward component)

3.2 Spectral Analysis

The main aim of this section to apply spectral analysis to better understand sea level responds to the forcings that affect the sea level and resolve time scales of these forcings.

3.2.1 Tides

Tides are periodic signals with well known period of semi-diurnal and diurnal. Although dynamic of tides is difficult to understand, it is easy to determine the tides in a fixed point and easily can be averaged out using harmonics analysis or be reduced in the sea level signal using low-pass filtering. In this study, low-pass filters are used to remove the tidal components out of the sea level signal, as needed.

The spectral analysis results in the Figure 3.69 show that the Eastern Mediterranean tidal amplitudes is greater than Black Sea and Marmara. In the Marmara Sea the power in the tidal frequencies are too low, especially in the middle part Of Marmara Sea. The tides in Turkish Seas are mixed, but mainly dominated by the semi-diurnal oscillation, expect in the Marmara Sea that is partly effected by diurnal oscillation.

In order to interpret tides in more detail, harmonic tidal analysis may be conducted using sea level data. However,the results agree with previous works. Yuce (1993a,1993b,1994) mentioned that The Marmara Sea isn't affected by the adjacent seas tidal oscillations due the geometric features of Turkish straits and the presence of the two-layer exchange system and not enough big to generate its own tides.

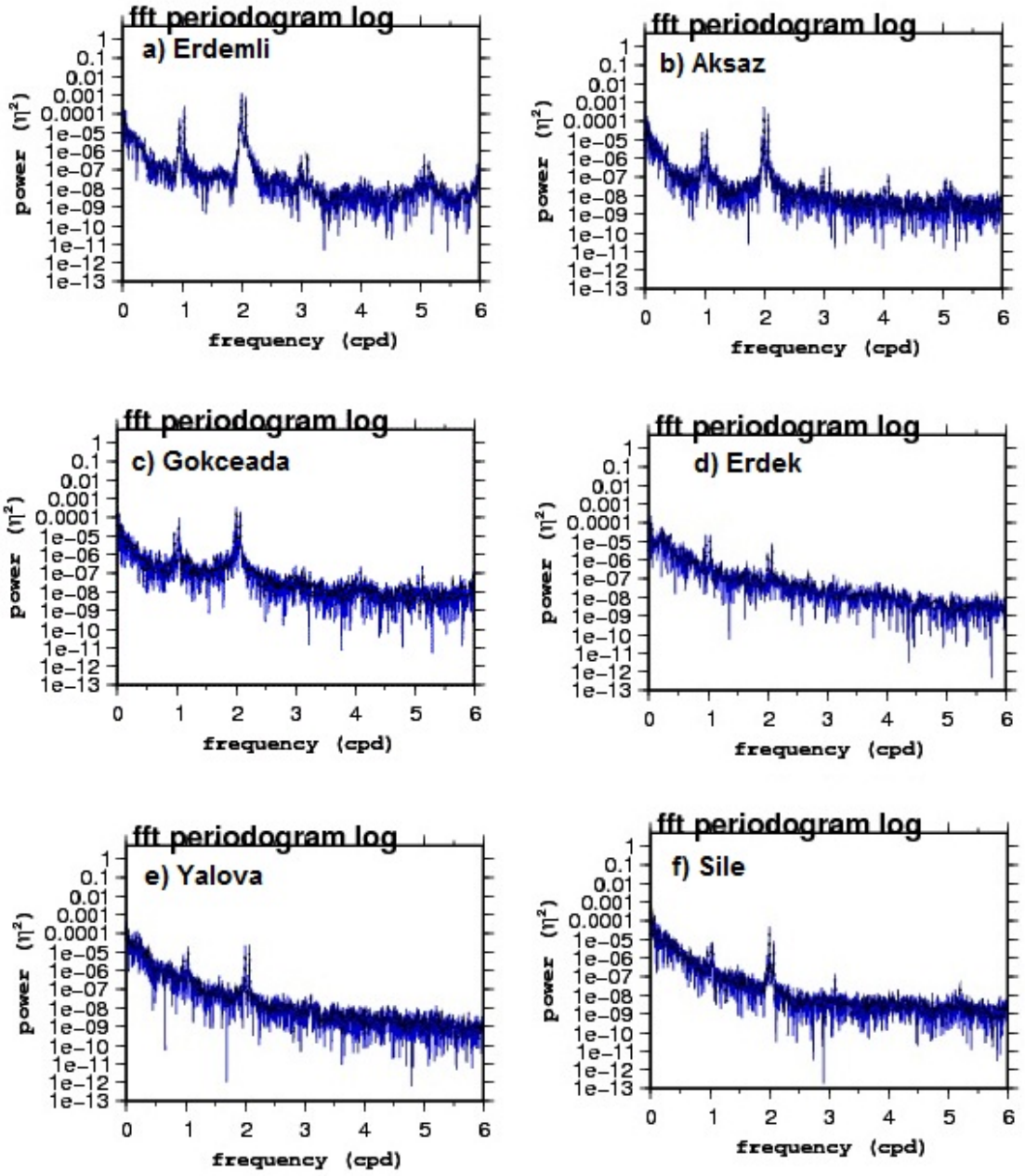

Figure 3.69: Spectral Analysis of Sea level stations in high frequency

3.2.2 Some Calculations for Surface and Internal Oscillations in Turkish Strait System

Since the sampling interval is 15 minutes, the shortest period of oscillation that can be resolved is theoretically 30 minutes. Short periodic oscillations of sea level in a basin is possibly caused by the standing waves. Standing waves can be generated by direct external forcing (atmospheric pressure, wind, and seismic activity), as well as by long waves entering through the open boundary from the open sea. The period of free standing wave (seiches) is calculated using Merian Formula below for a closed basin

$$T = \frac{2L}{(k+1)\sqrt{gd}} \tag{5.1}$$

where l,d and g are length, depth and gravitational acceleration, respectively and k depends on the oscillation mode.

In addition to the standing waves modes of oscillation determined by using 5.1, a basin open to the sea through a channel or inlet can resonate in a mode called Helmhothz oscillation. The Helmhothz oscillation can be calculated by using 5.2 and 5.3 (LeBlond and Mysak,1978 qutoed in Buyukay,1983)

$$w^2 = g.W.H/Q.D \tag{5.2}$$

$$T = 2\Pi/\omega \tag{5.3}$$

where , w is the angular frequency g is the gravitational acceleration W is the mean width of the channel Q is the total area of the Basin. D is the channel length.

Using equations 5.1, 5.2 and 5.3, the natural period of free standing waves and the Helmothz mode for both Marmara Sea and Black sea was calculated substituting the values in table 3.6. The natural period along the basin and cross the basin was found 3.1 hours and 55.8 min ,respectively. The Helmothz mode period for the Black Sea and Marmara 13 day and 2.1 day, respectively.

Moreover, Similar calculations are made in 3D dimensional condition. In the Marmara Sea, the barotropic Rossby radius is bigger than the basin so that the Coriolis force can be neglected even though the internal motions are affected by the Coriolis and also the surface and bottom stress can be neglected for patterns of oscillations. Finally, a simply combined form of equations of motions and continuity equation is obtained for the two horizontal di-

Table 3.6: Physical Values used in calculations

	Marmara	BlackSea	Bosphorous
W(m)	*	*	1000
Q(km^3)	11.500x10^3	420.325x10^3	*
D(km)	*	*	30
H(m)	1000	*	35

rection, which is given in equation 5.4.

$$gd(\frac{\partial \eta}{\partial x^2} + \frac{\partial \eta}{\partial y^2}) = \frac{\partial \eta}{\partial t^2} \tag{5.4}$$

where η , g ,d is free surface, gravity and basin depth,respectively.

Dividing the Marmara Sea to two basins as Deep(depth=1000 m, width=50 km, length=200 km) and Shelf (depth=100 m, width=40km, length=200 km), the equation 5.4 is analytically solved for both surface and internal oscillations.

The periods of surface and internal oscillations calculated from equation 5.4 are tabulated in Table 3.7 and Table 3.8, respectively. In tables, "n" means the mode in East-West direction whereas "m" indicates the mode in North-South direction. Shelf(k=1) and Deep(k=2) basins are numbered with k values and the resonant periods according to the modes are given in last six columns.

The results (Table 3.7) shows that the bigger surface oscillations periods are found as 2.508 hrs and 1.254 hrs. On the other hand, the greater internal oscillations periods are 3.414 days and 1.707 days (Table 3.8). Internal oscillations depends on the layers thickness and density gradients between the layers, therefore they can show seasonal variability. In this calculation, the upper layer thickness and $\frac{\Delta\rho}{\rho}$ is assumed 25 m and 0.5e-2, respectively.

When compared with this calculated values with spectral analysis results of high-pass filtered sea level, these periods couldn't be detected. This maybe due to the coupling of both of surface and internal oscillations or lack of enough sampling interval to resolve the oscillations in these periods.

Table 3.7: Surface Oscillation Periods

n	m	k	f(rad/s)	f(Hz)	T(ss)	T(mm)	T(hr)	T(day)
1	0	1	0.00069578	0.00011074	9030.473	150.508	2.508	0.105
2	0	1	0.00139155	0.00022147	4515.236	75.254	1.254	0.052
3	0	1	0.00208733	0.00033221	3010.158	50.169	0.836	0.035
0	1	1	0.00245994	0.00039151	2554.203	42.57	0.71	0.03
1	1	1	0.00255644	0.00040687	2457.783	40.963	0.683	0.028
2	1	1	0.00282626	0.00044981	2223.149	37.052	0.618	0.026
3	1	1	0.00322618	0.00051346	1947.562	32.459	0.541	0.023
0	2	1	0.00491988	0.00078302	1277.102	21.285	0.355	0.015
1	2	1	0.00496883	0.00079081	1264.519	21.075	0.351	0.015
2	2	1	0.00511289	0.00081374	1228.892	20.482	0.341	0.014
3	2	1	0.00534436	0.00085058	1175.667	19.594	0.327	0.014
0	3	1	0.00737982	0.00117453	851.401	14.19	0.237	0.01
1	3	1	0.00741254	0.00117974	847.642	14.127	0.235	0.01
2	3	1	0.00750987	0.00119523	836.657	13.944	0.232	0.01
3	3	1	0.00766933	0.00122061	819.261	13.654	0.228	0.009
0	1	2	0.00622321	0.00099045	1009.638	16.827	0.28	0.012
1	1	2	0.00660071	0.00105054	951.895	15.865	0.264	0.011
2	1	2	0.00762184	0.00121305	824.366	13.739	0.229	0.01
3	1	2	0.00907181	0.00144382	692.606	11.543	0.192	0.008
0	2	2	0.01244642	0.00198091	504.819	8.414	0.14	0.006
1	2	2	0.0126394	0.00201162	497.111	8.285	0.138	0.006
2	2	2	0.01320142	0.00210107	475.948	7.932	0.132	0.006
3	2	2	0.01408839	0.00224224	445.983	7.433	0.124	0.005
0	3	2	0.01866963	0.00297136	336.546	5.609	0.093	0.004
1	3	2	0.01879883	0.00299193	334.233	5.571	0.093	0.004
2	3	2	0.01918122	0.00305279	327.57	5.459	0.091	0.004
3	3	2	0.01980213	0.00315161	317.298	5.288	0.088	0.004

Table 3.8: Internal Oscillation Periods

n	m	k	f(rad/s)	f(Hz)	T(ss)	T(mm)	T(hr)	T(day)
1	0	1	0.0000213	0.00000339	294934.031	4915.567	81.926	3.414
2	0	1	0.00004261	0.00000678	147467.016	2457.784	40.963	1.707
3	0	1	0.00006391	0.00001017	98311.344	1638.522	27.309	1.138
0	1	1	0.00007532	0.00001199	83419.938	1390.332	23.172	0.966
1	1	1	0.00007827	0.00001246	80270.875	1337.848	22.297	0.929
2	1	1	0.00008654	0.00001377	72607.734	1210.129	20.169	0.84
3	1	1	0.00009878	0.00001572	63607.105	1060.118	17.669	0.736
0	2	1	0.00015064	0.00002398	41709.969	695.166	11.586	0.483
1	2	1	0.00015214	0.00002421	41299.02	688.317	11.472	0.478
2	2	1	0.00015655	0.00002492	40135.438	668.924	11.149	0.465
3	2	1	0.00016364	0.00002604	38397.141	639.952	10.666	0.444
0	3	1	0.00022596	0.00003596	27806.645	463.444	7.724	0.322
1	3	1	0.00022696	0.00003612	27683.879	461.398	7.69	0.32
2	3	1	0.00022994	0.0000366	27325.109	455.418	7.59	0.316
3	3	1	0.00023482	0.00003737	26756.957	445.949	7.432	0.31
0	1	2	0.0000687	0.00001093	91455.156	1524.253	25.404	1.059
1	1	2	0.00007287	0.0000116	86224.75	1437.079	23.951	0.998
2	1	2	0.00008414	0.00001339	74672.82	1244.547	20.742	0.864
3	1	2	0.00010015	0.00001594	62737.723	1045.629	17.427	0.726
0	2	2	0.0001374	0.00002187	45727.578	762.126	12.702	0.529
1	2	2	0.00013954	0.00002221	45029.406	750.49	12.508	0.521
2	2	2	0.00014574	0.0000232	43112.375	718.54	11.976	0.499
3	2	2	0.00015553	0.00002475	40398.129	673.302	11.222	0.468
0	3	2	0.00020611	0.0000328	30485.053	508.084	8.468	0.353
1	3	2	0.00020753	0.00003303	30275.531	504.592	8.41	0.35
2	3	2	0.00021175	0.0000337	29671.973	494.533	8.242	0.343
3	3	2	0.00021861	0.00003479	28741.584	479.026	7.984	0.333

3.2.3 Sub-tidal response to wind and atmospheric pressure

A great amount of variance in sea level is related directly to fluctuations in atmospheric pressure and surface wind. The effect of atmospheric pressure on sea level variability is usually estimated using so-called "inverse barometer effect", which is described by

$$\Delta n = \frac{-P_a - \overline{P_a}}{\rho g}, \tag{5.5}$$

where the overbar denotes a spatial average of atmospheric pressure(P_a) , ρ and g is the surface density and acceleration of gravity,respectively. The equation 5.5 states that an increase in 1 mbar of atmospheric pressure accompany with the an decrease in 1 cm of sea level so that subsurface pressure doesn't change. In open seas, the respond of sea level to atmospheric pressure is nearly isostatic (inverse barometer effect) (Hamon,1996; Wunsch,1972). But, in the semi-enclosed seas the respond exhibits the departure from the isostatic respond depending on the frequency of P_a owing to the adjustment through the straits.

In order to obtain dynamical component, the barometric correction is made to the sea level records. Ponte(1993) suggests that even if the response to P_a contains a dynamic component, applying an IB correction is always useful, as the gradients of inverse barometer signal merely balance out P_a gradients.

The variance of sea level records obtained from this study is calculated before and after atmospheric pressure correction. The results (Fig. 3.70) indicate that sea level response to atmospheric pressure in Black Sea is away from isostatic whereas the correction for Marmara and Mediterranean Seas reduces the variance of sea level records. This result supports the study conducted by Ducet *et al.* 1999. They suggested that Black Sea level doesn't the sea level respond at all to atmospheric pressure.

Sea level inverse-barometer-corrected sea level. In spectra analysis, the atmospheric pressure corrected sea level are used. Erdemli, Yalova and Sile station spectra are selected to illustrate below. It is considered that Erdemli, Yalova and Sile Station represent Mediterranean, Marmara Sea and Black Sea, respectively. Spectra analysis are applied annually and the results of 2009 and 2010 are given in Fig 3.71 - 94.

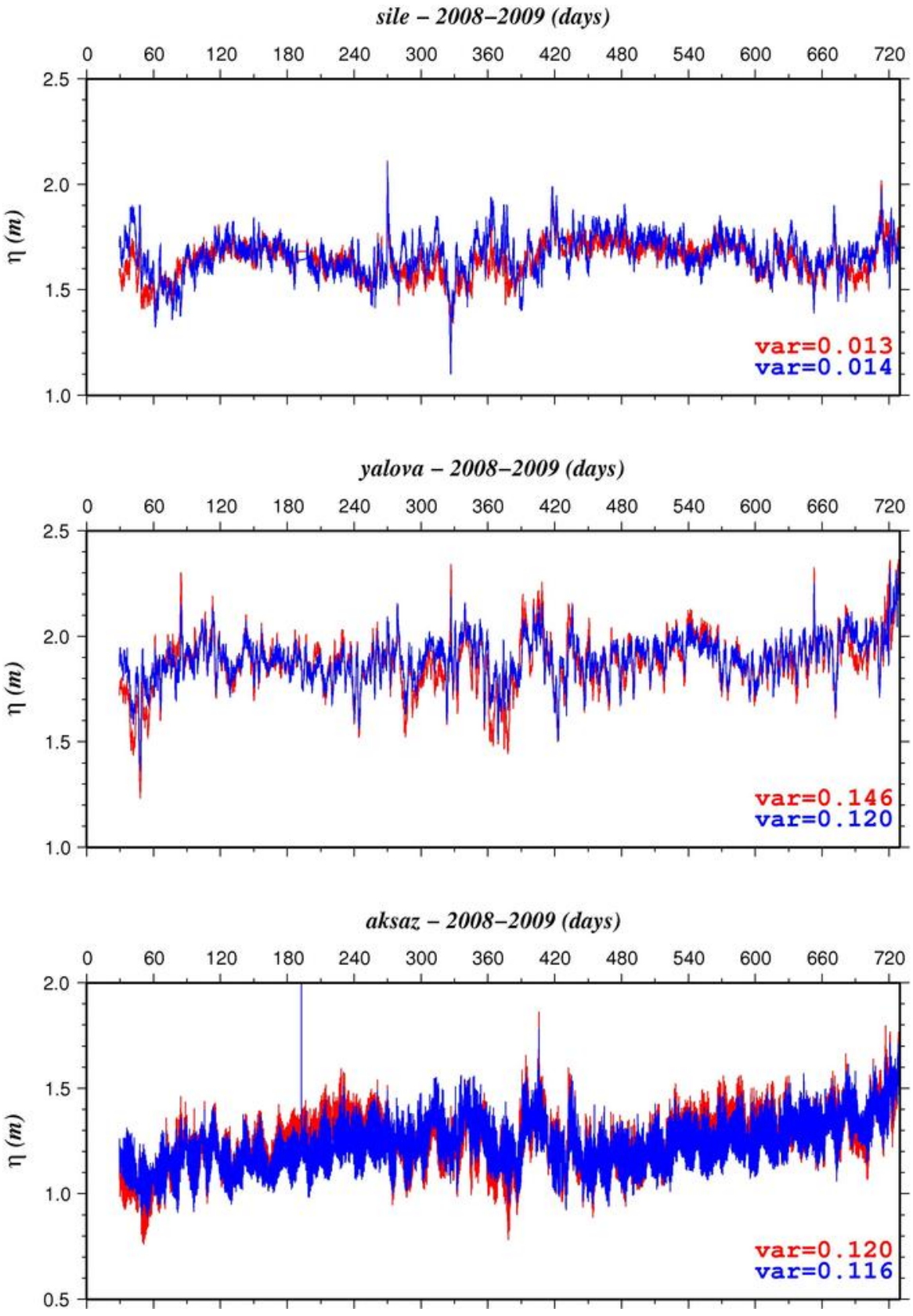

Figure 3.70: Variance of Sea level measurements (red line) and after inverse barometric corrected(blue line); Sile(upper panel), Yalova(middle panel), Aksaz(lower panel)

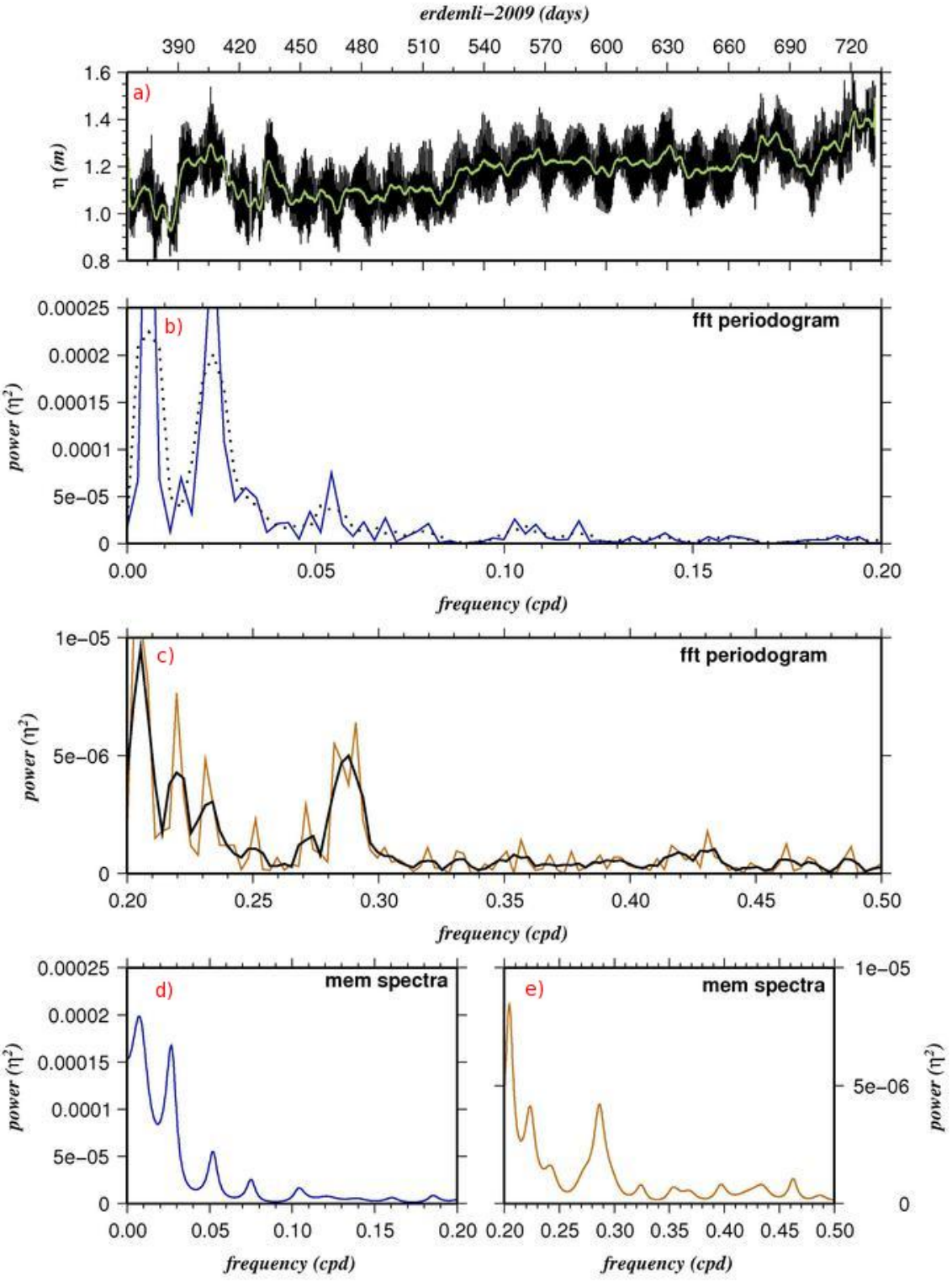

Figure 3.71: Erdemli sea level spectra in 2009; a) time series, FFT power spectrum between b) 0 - 0.2 cpd, c) 0.2 - 0.5 cpd , MEM power spectrum between d) 0 - 0.2 cpd, e) 0.2 - 0.5 cpd

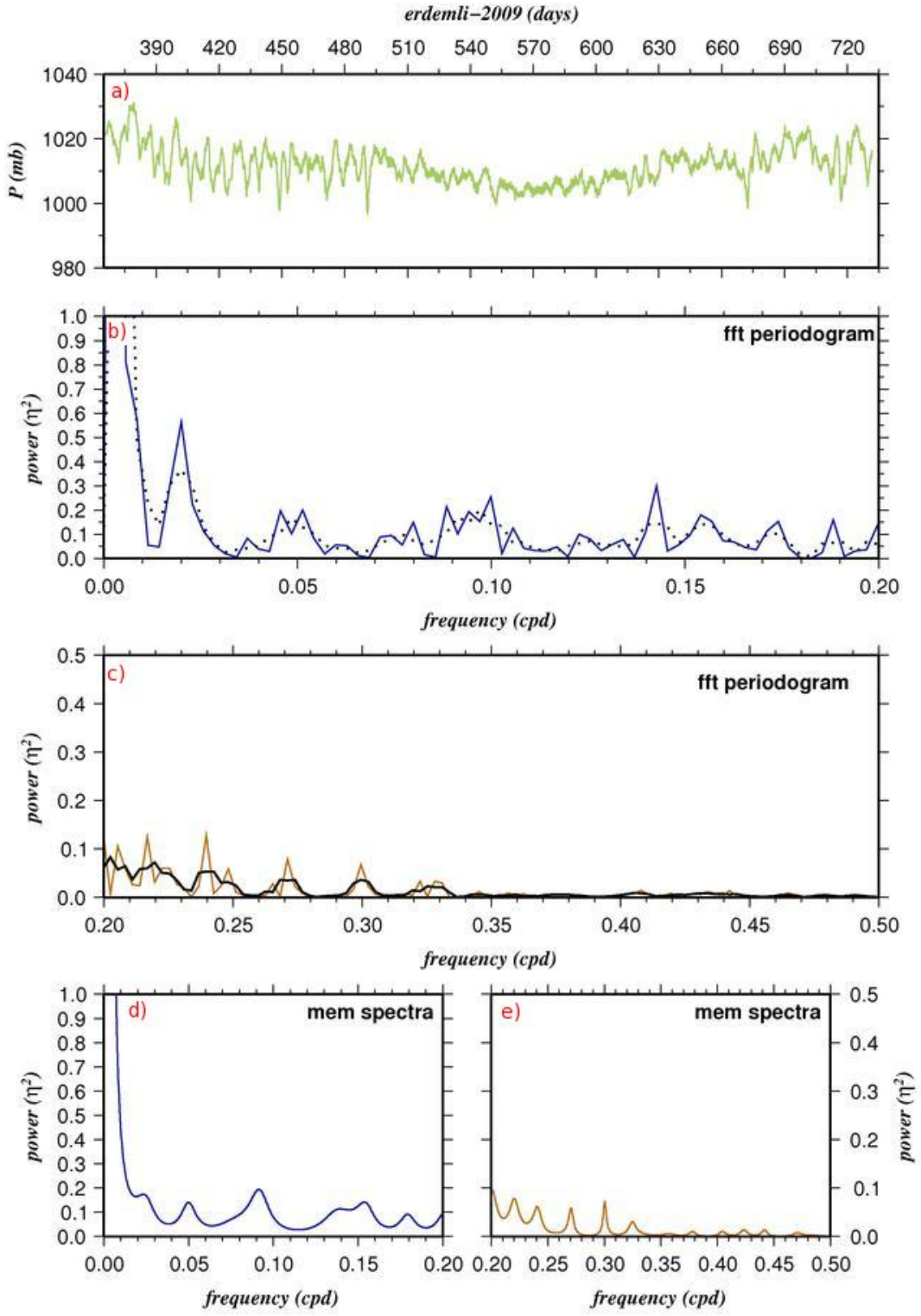

Figure 3.72: Erdemli atmospheric pressure spectra in 2009; a) time series, FFT power spectrum between b) 0 - 0.2 cpd, c) 0.2 - 0.5 cpd , MEM power spectrum between d) 0 - 0.2 cpd, e) 0.2 - 0.5 cpd

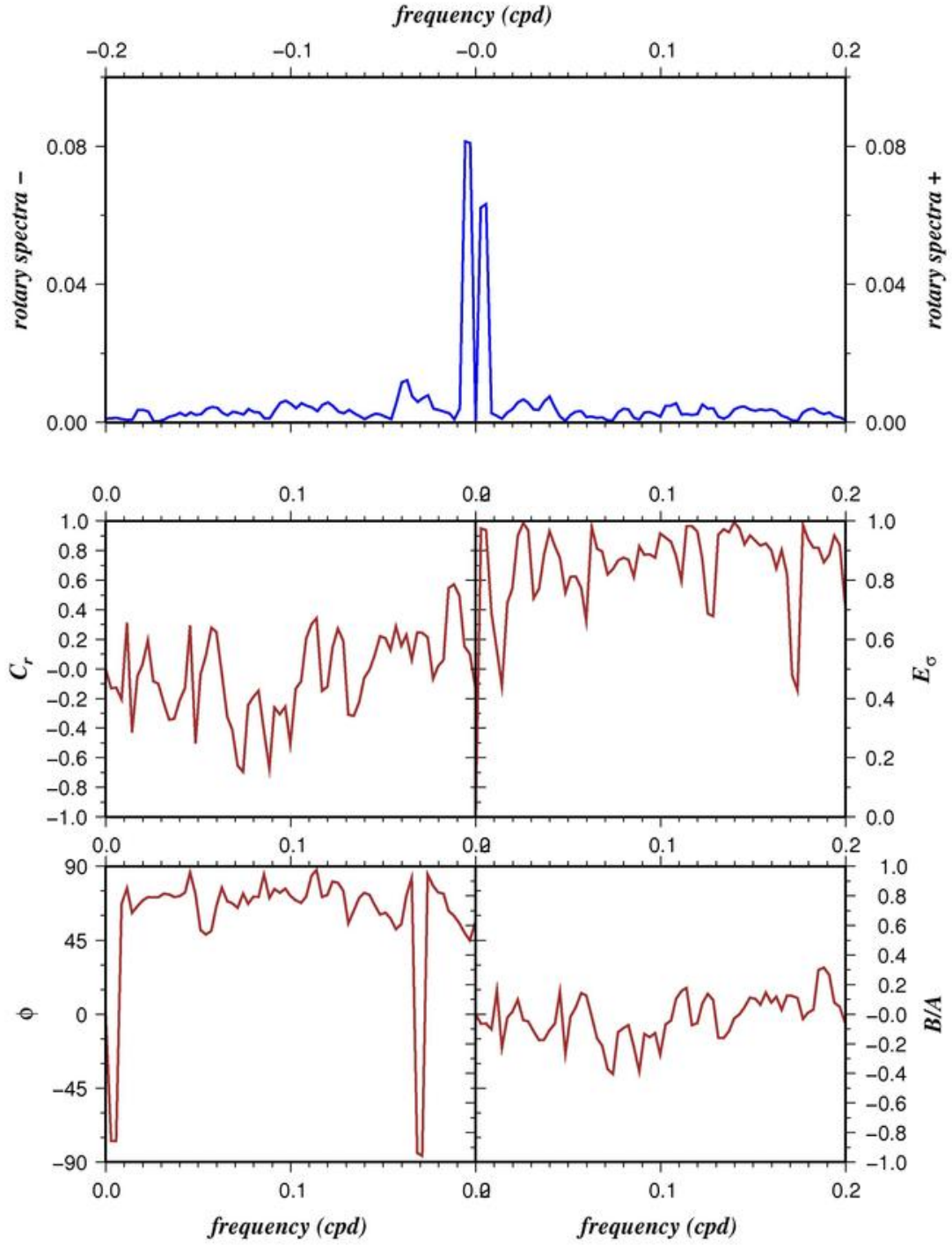

Figure 3.73: Erdemli wind rotary spectra in 2009; Power spectrum in 0-0.2 cpd range (upper panel), rotary coefficent (middle left), ellipse stability (middle right), orientation angle (lower left), the ratio of major axis to minor axis (lower right).

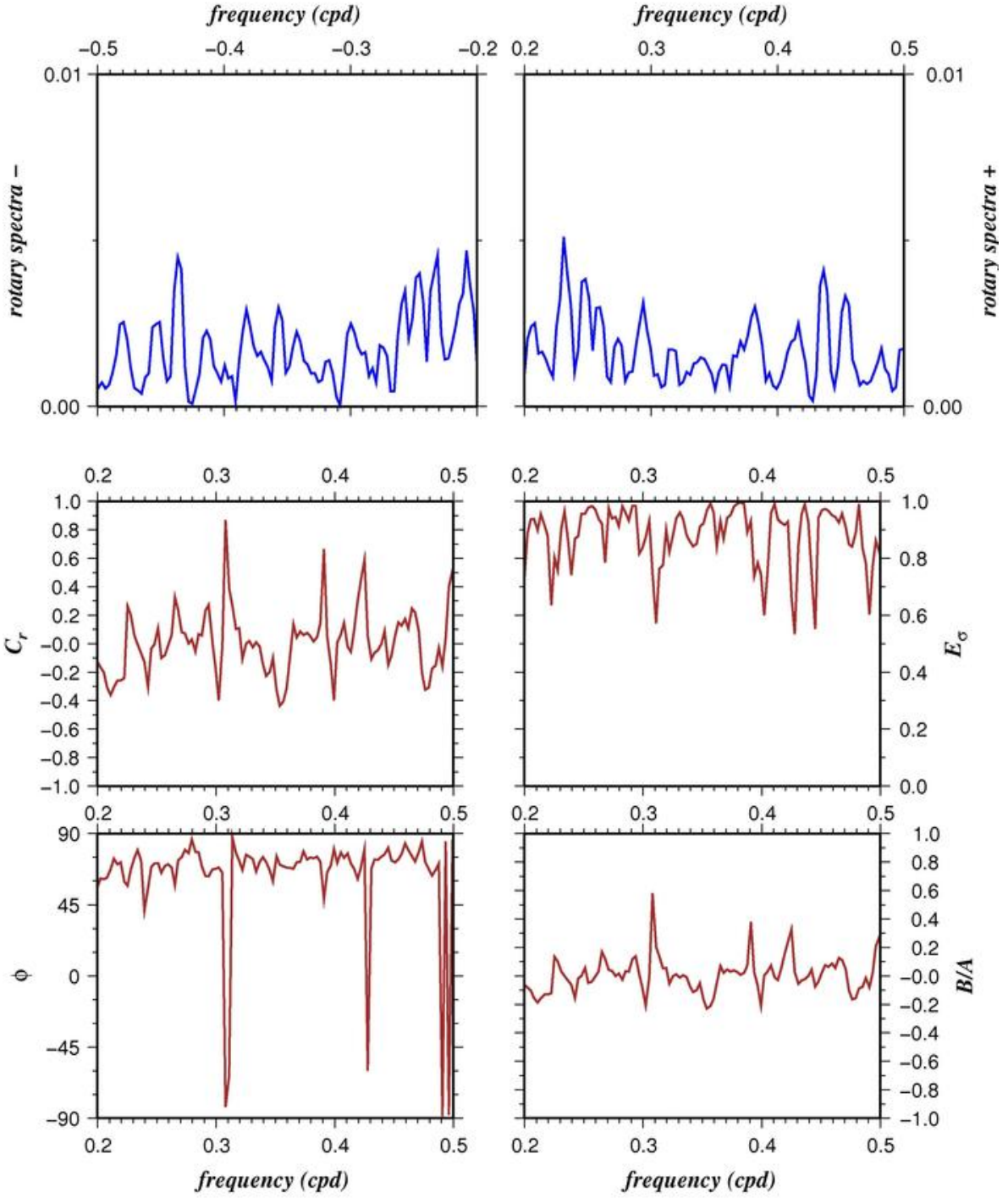

Figure 3.74: Erdemli wind rotary spectra in 0.2-0.5 cpd range in 2009

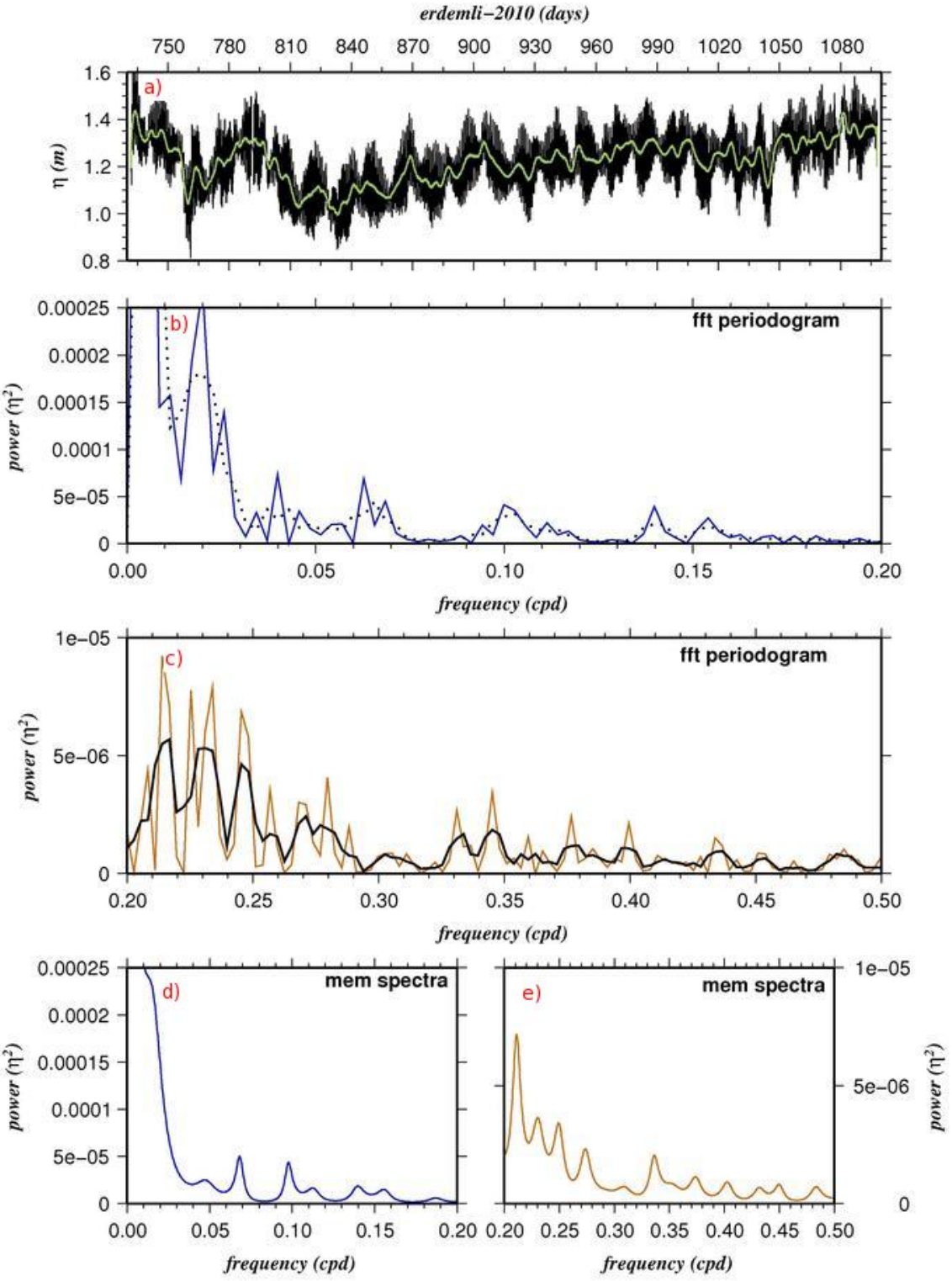

Figure 3.75: Erdemli sea level spectra in 2010; a) time series, FFT power spectrum between b) 0 - 0.2 cpd, c) 0.2 - 0.5 cpd , MEM power spectrum between d) 0 - 0.2 cpd, e) 0.2 - 0.5 cpd

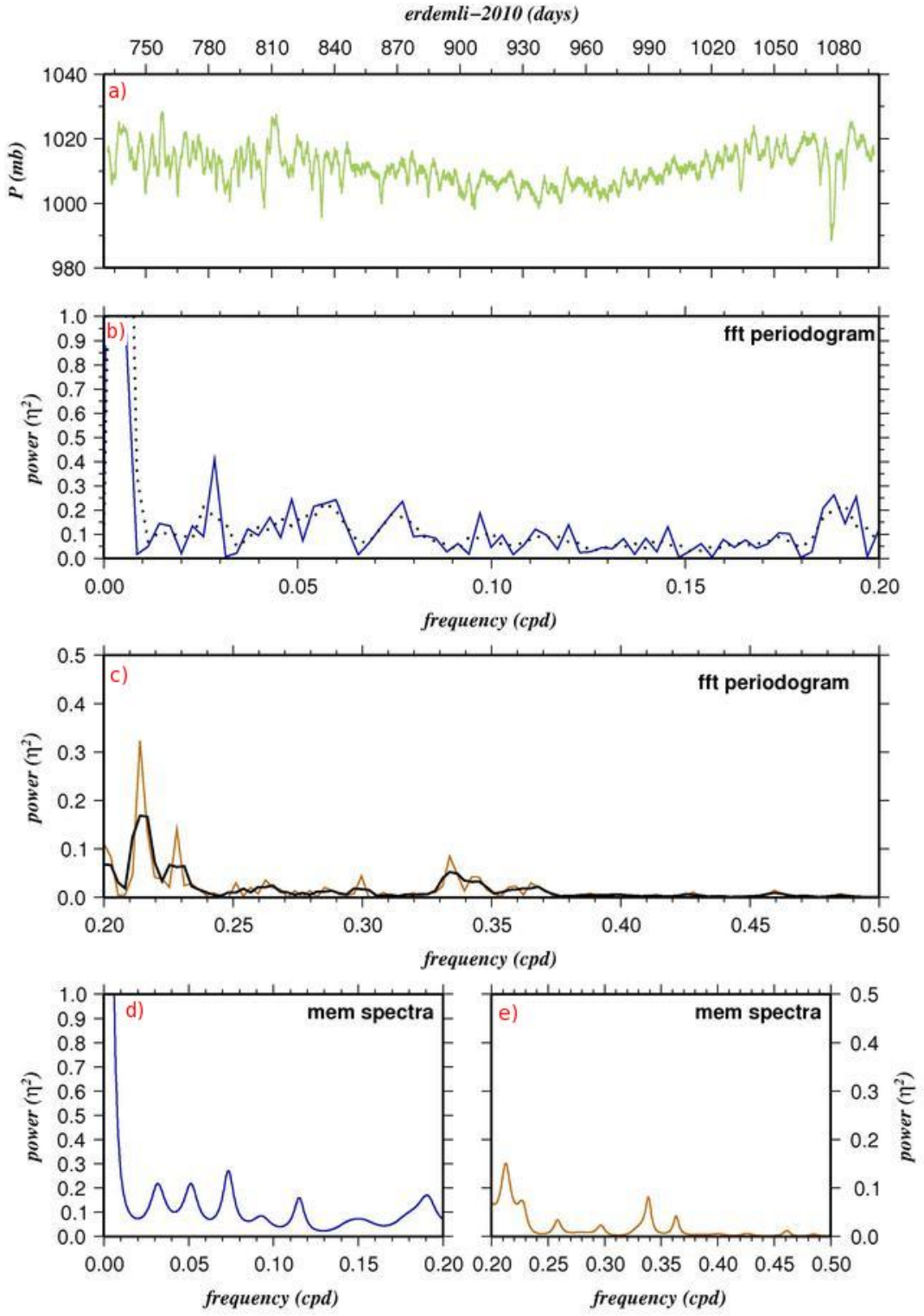

Figure 3.76: Erdemli atmospheric pressure spectra in 2010; a) time series, FFT power spectrum between b) 0 - 0.2 cpd, c) 0.2 - 0.5 cpd , MEM power spectrum between d) 0 - 0.2 cpd, e) 0.2 - 0.5 cpd

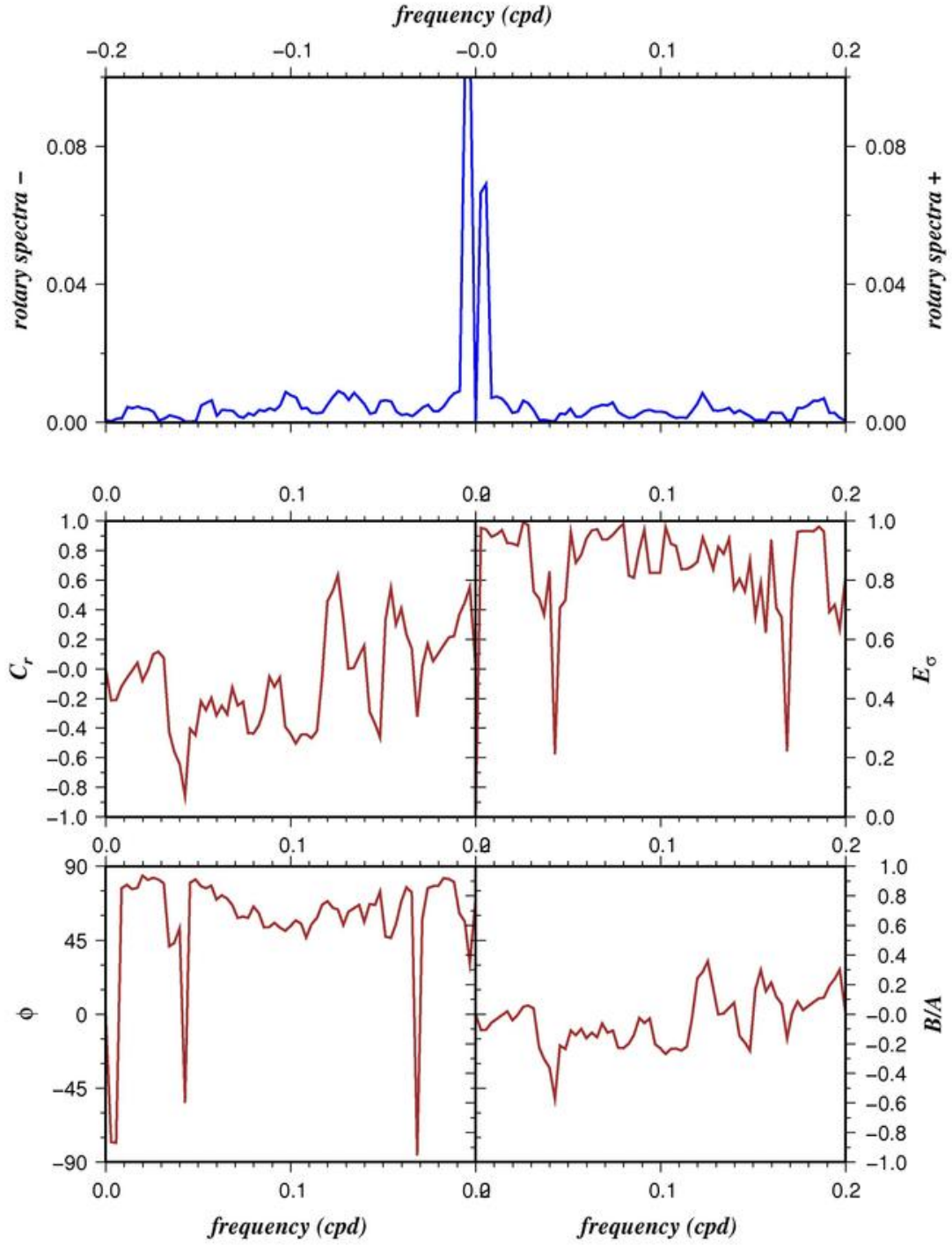

Figure 3.77: Erdemli wind rotary spectra in 2010; Power spectrum in 0 - 0.2 cpd range (upper panel), rotary coefficent (middle left), ellipse stability (middle right), orientation angle (lower left), the ratio of major axis to minor axis (lower right)

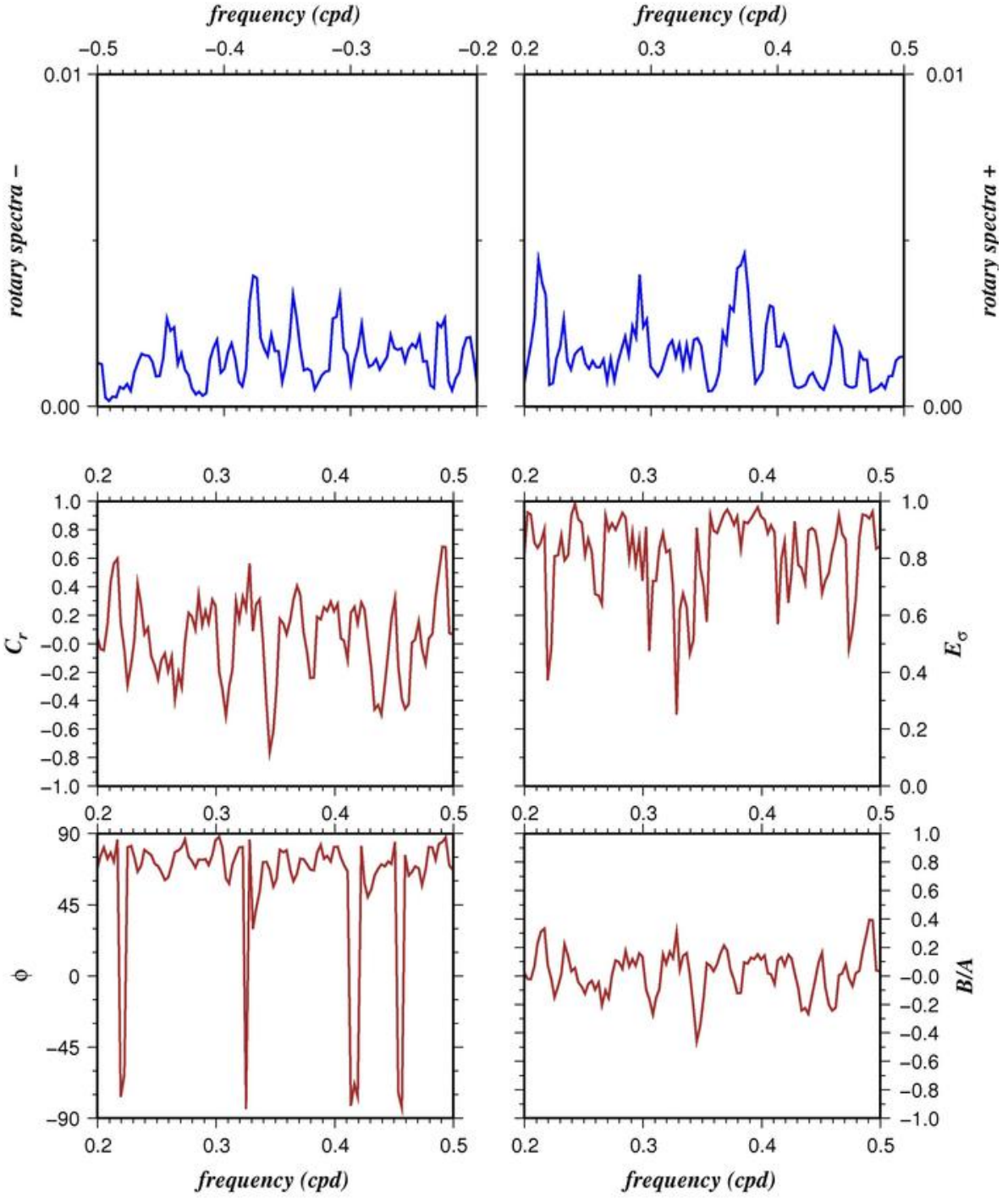

Figure 3.78: Erdemli wind rotary spectra in 2010; Power spectrum in 0.2 - 0.5 cpd range (upper left and right), rotary coefficent (middle left), ellipse stability (middle right), orientation angle (lower left), the ratio of major axis to minor axis (lower right)

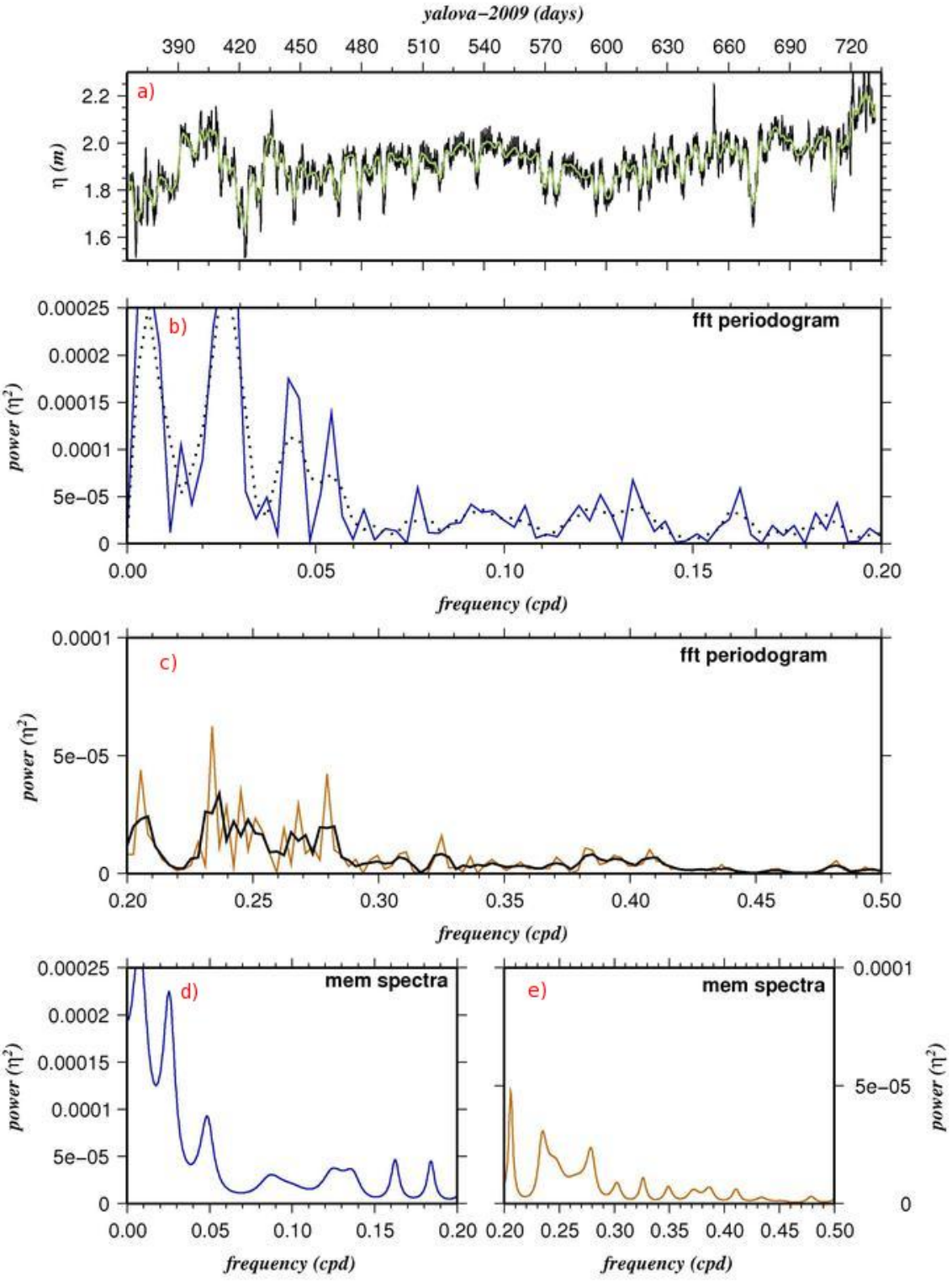

Figure 3.79: Yalova sea level spectra in 2009; a) time series, FFT power spectrum between b) 0 - 0.2 cpd, c) 0.2 - 0.5 cpd , MEM power spectrum between d) 0 - 0.2 cpd, e) 0.2 - 0.5 cpd

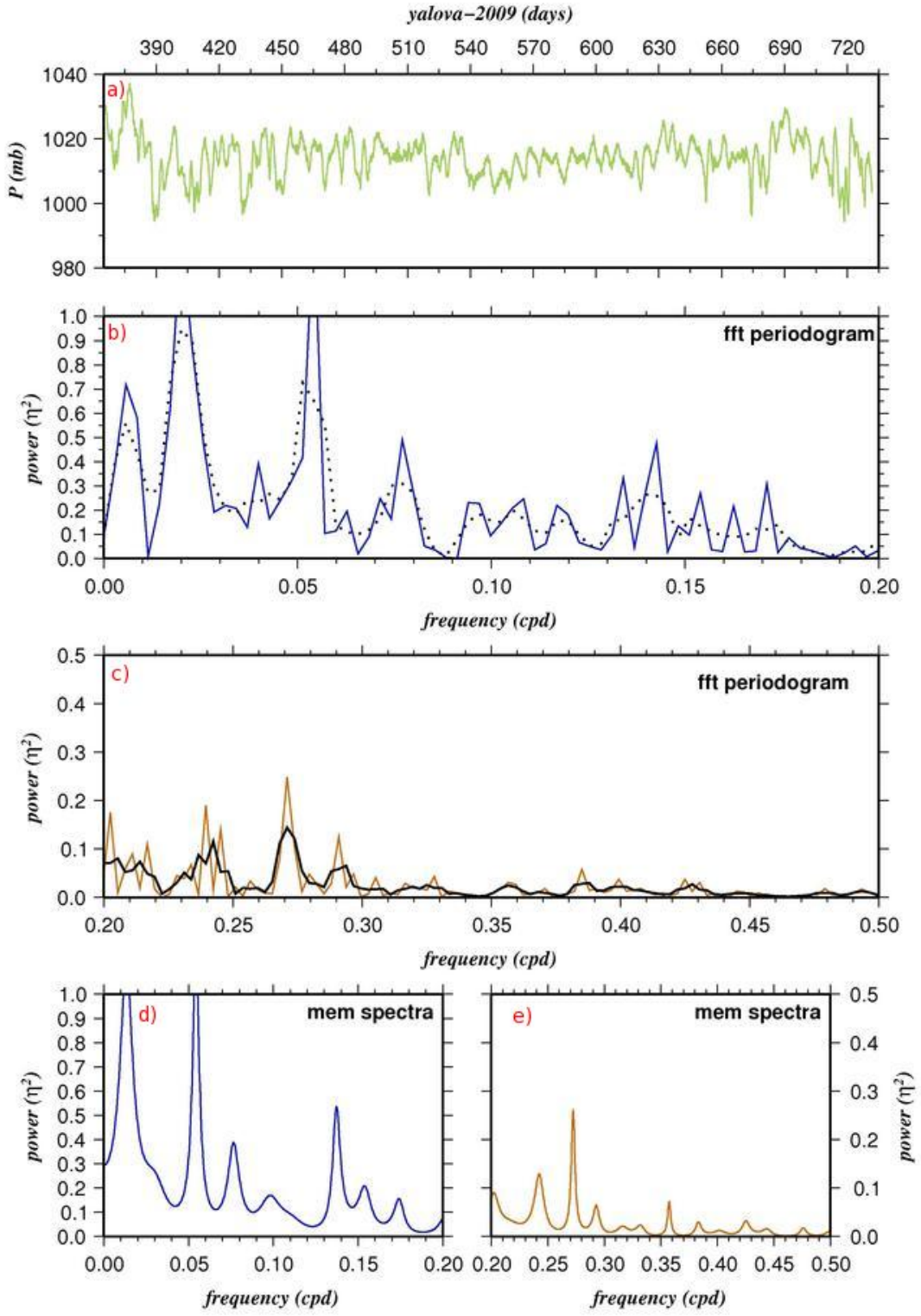

Figure 3.80: Yalova atmospheric pressure spectra in 2009; a) time series, FFT power spectrum between b) 0 - 0.2 cpd, c) 0.2 - 0.5 cpd , MEM power spectrum between d) 0 - 0.2 cpd, e) 0.2 - 0.5 cpd

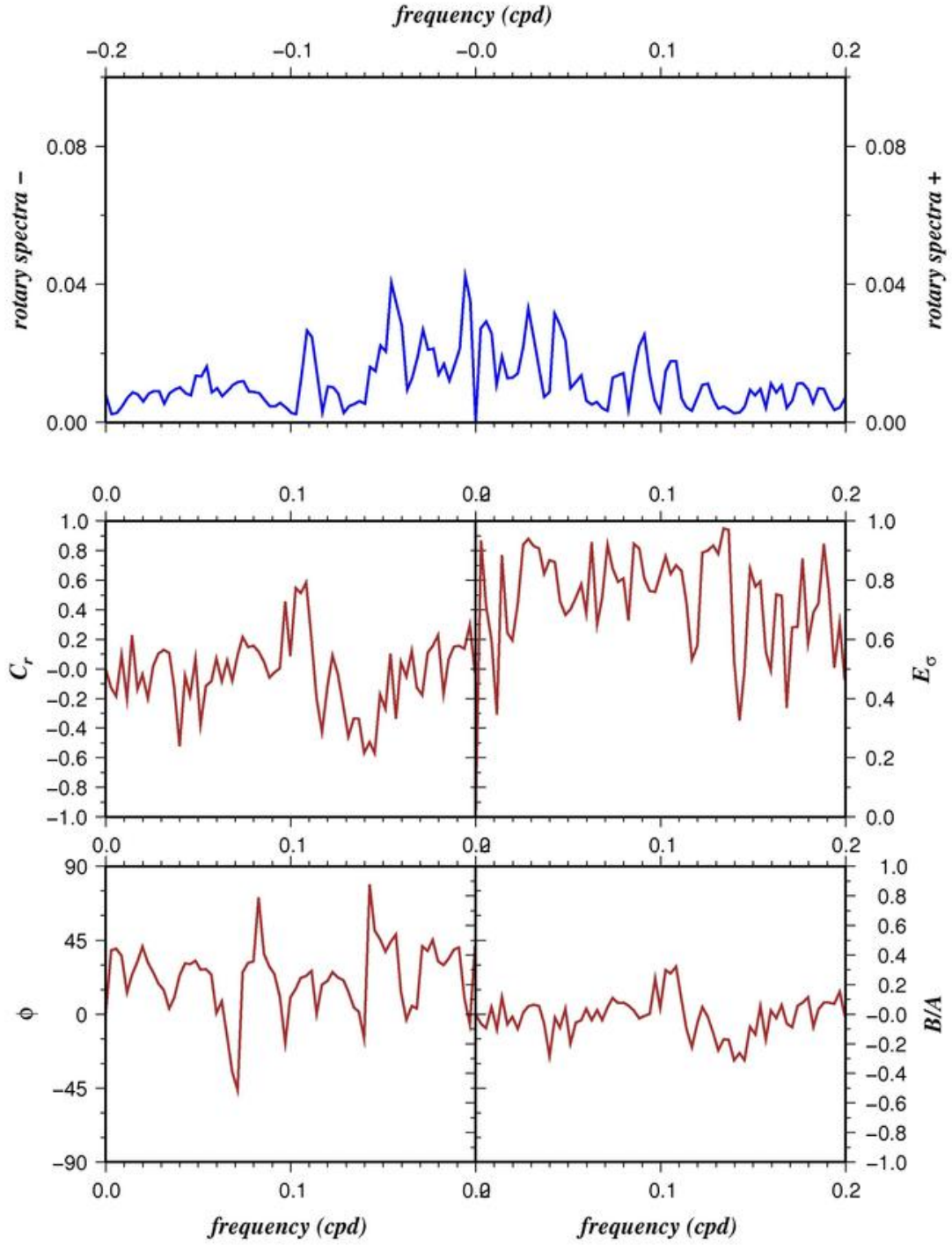

Figure 3.81: Yalova wind rotary spectra in 2009; Power spectrum in 0 - 0.2 cpd range (upper panel), rotary coefficent (middle left), ellipse stability (middle right), orientation angle (lower left), the ratio of major axis to minor axis (lower right)

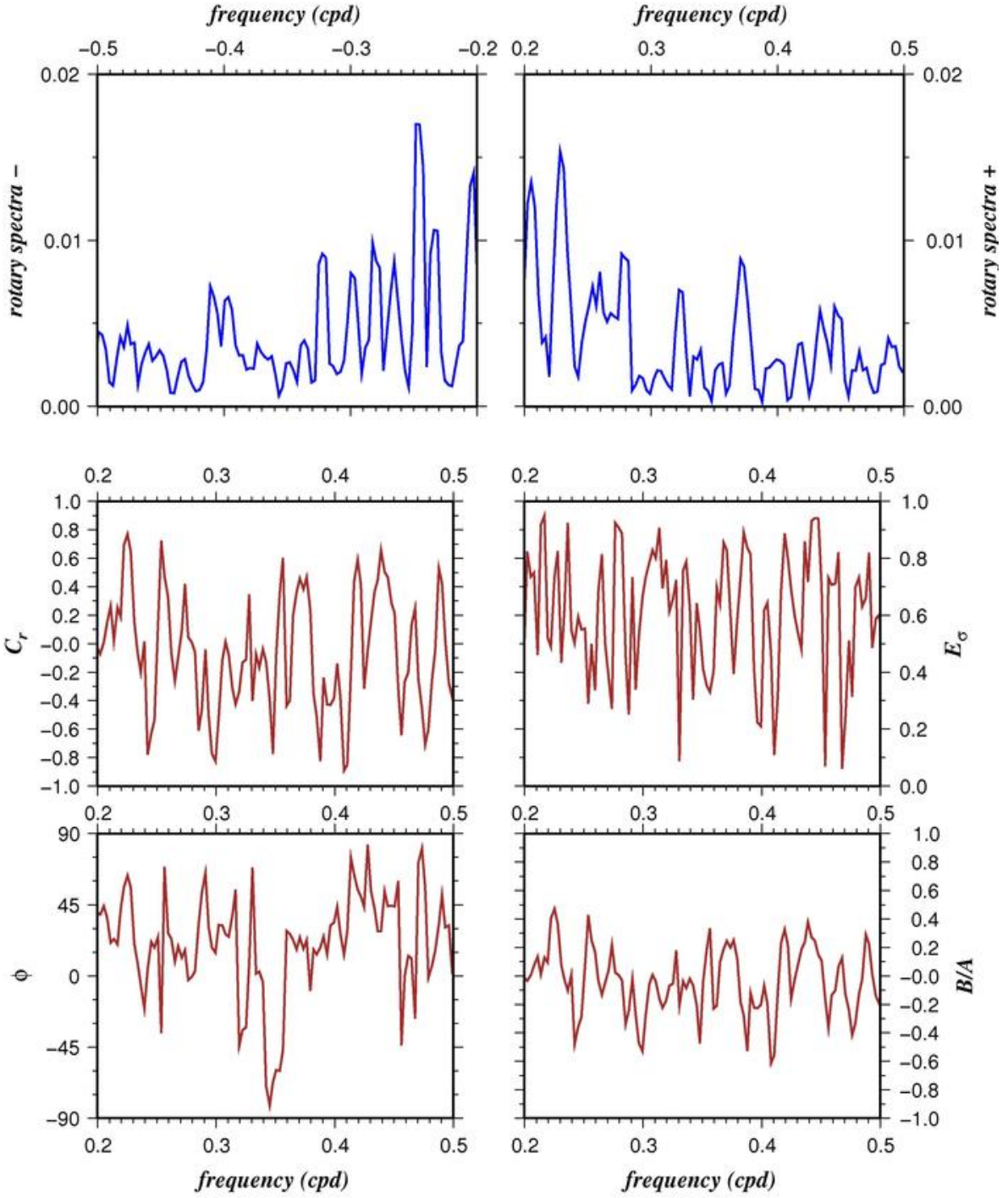

Figure 3.82: Yalova wind rotary spectra in 2009; Power spectrum in 0.2 - 0.5 cpd range (upper left and right), rotary coefficent (middle left), ellipse stability (middle right), orientation angle (lower left), the ratio of major axis to minor axis (lower right)

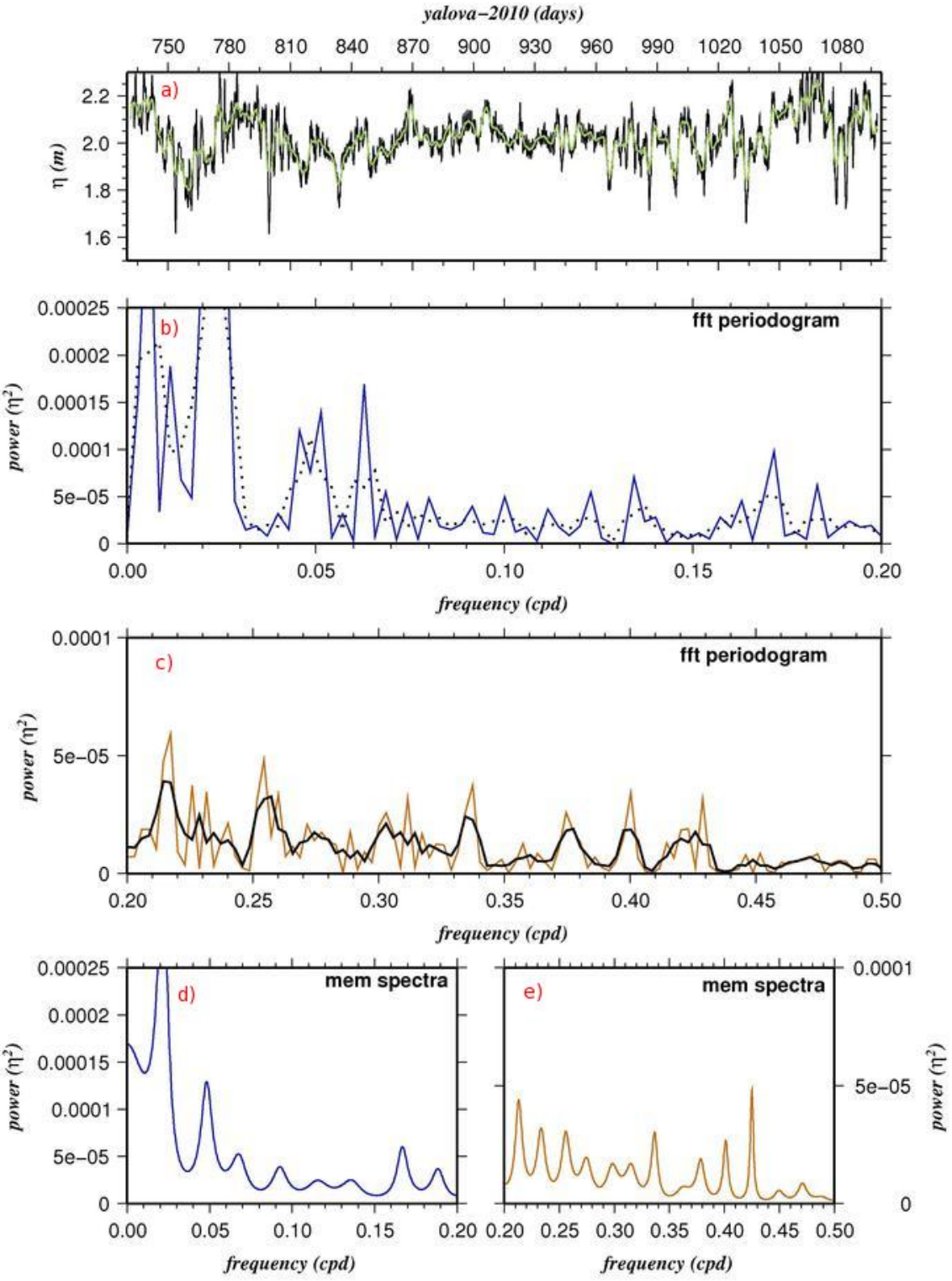

Figure 3.83: Yalova sea level spectra in 2010; a) time series, FFT power spectrum between b) 0 - 0.2 cpd, c) 0.2 - 0.5 cpd , MEM power spectrum between d) 0 - 0.2 cpd, e) 0.2 - 0.5 cpd

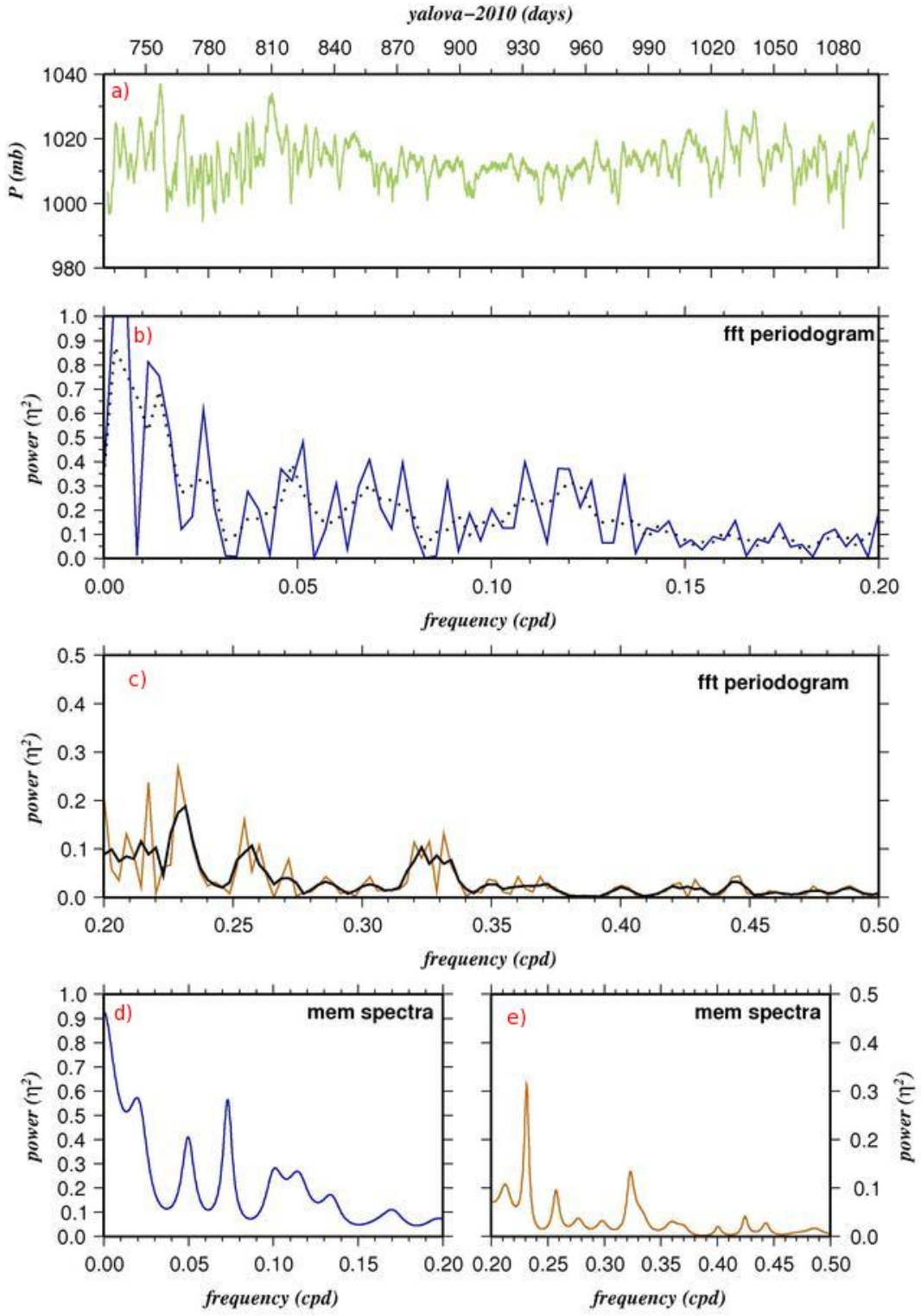

Figure 3.84: Yalova atmospheric pressure spectra in 2010; a) time series, FFT power spectrum between b) 0 - 0.2 cpd, c) 0.2 - 0.5 cpd , MEM power spectrum between d) 0 - 0.2 cpd, e) 0.2 - 0.5 cpd

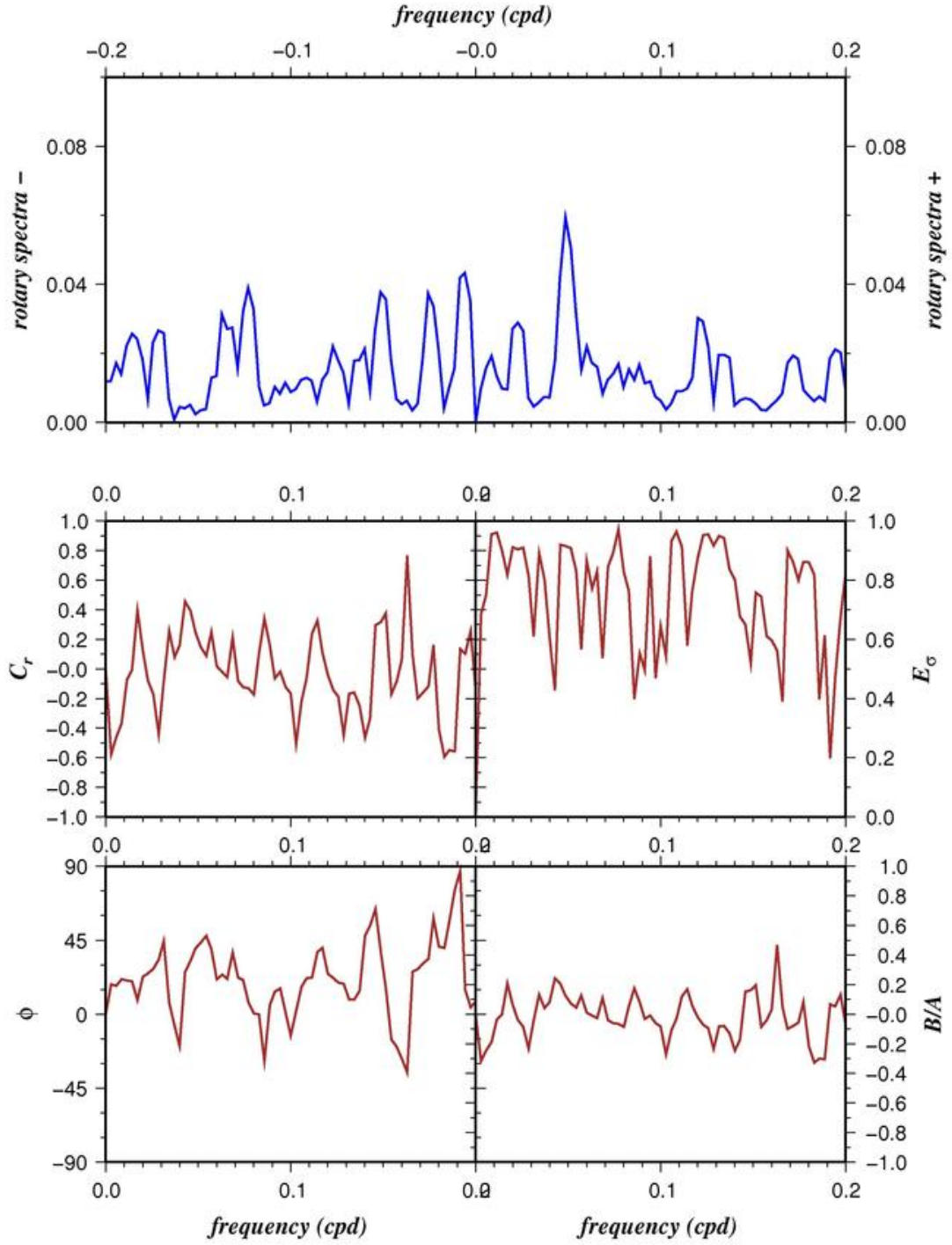

Figure 3.85: Yalova wind rotary spectra in 2010; Power spectrum in 0 - 0.2 cpd range (upper panel), rotary coefficent (middle left), ellipse stability (middle right), orientation angle (lower left), the ratio of major axis to minor axis (lower right)

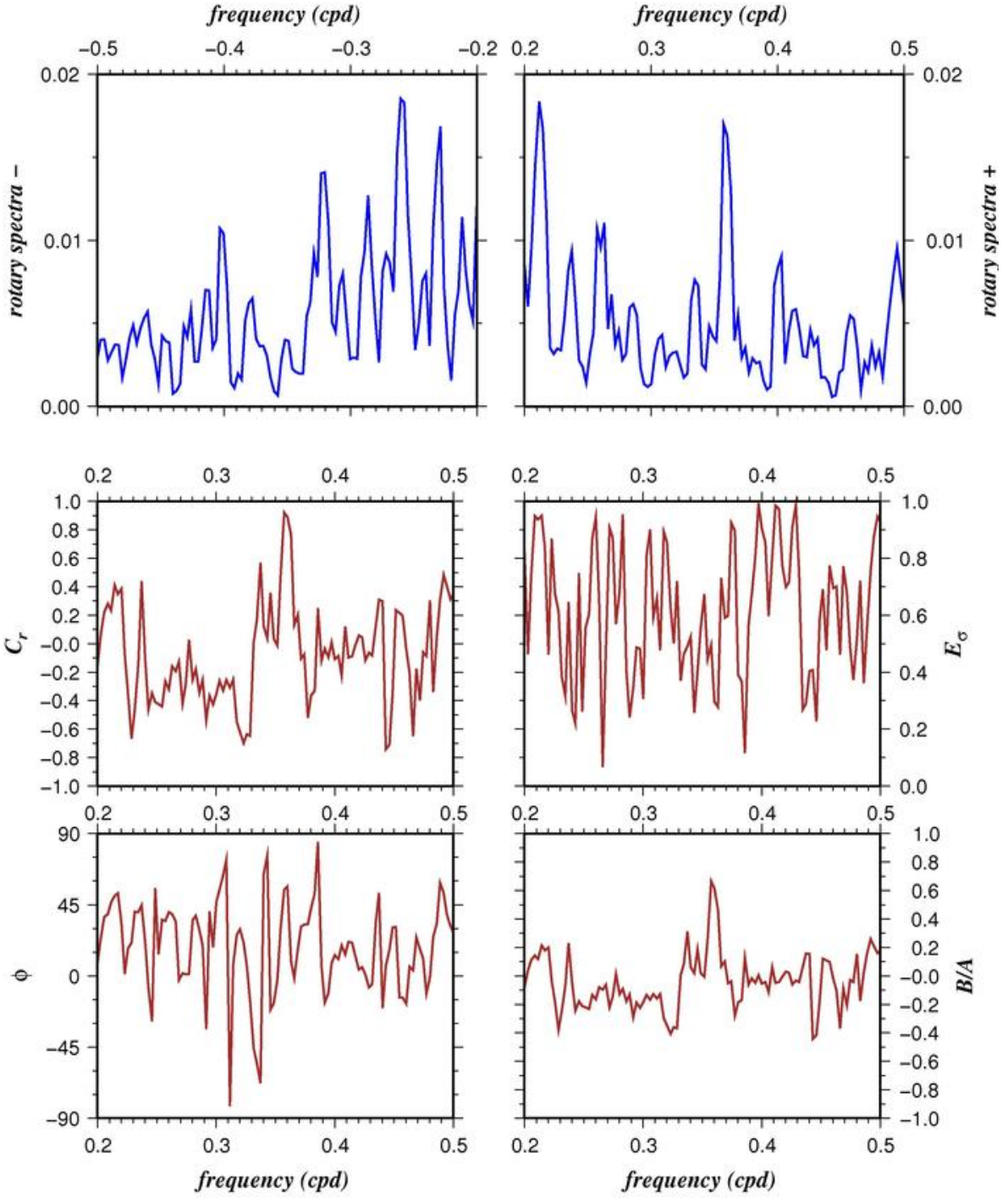

Figure 3.86: Yalova wind rotary spectra in 2010; Power spectrum in 0.2 - 0.5 cpd range (upper left and right), rotary coefficent (middle left), ellipse stability (middle right), orientation angle (lower left), the ratio of major axis to minor axis (lower right)

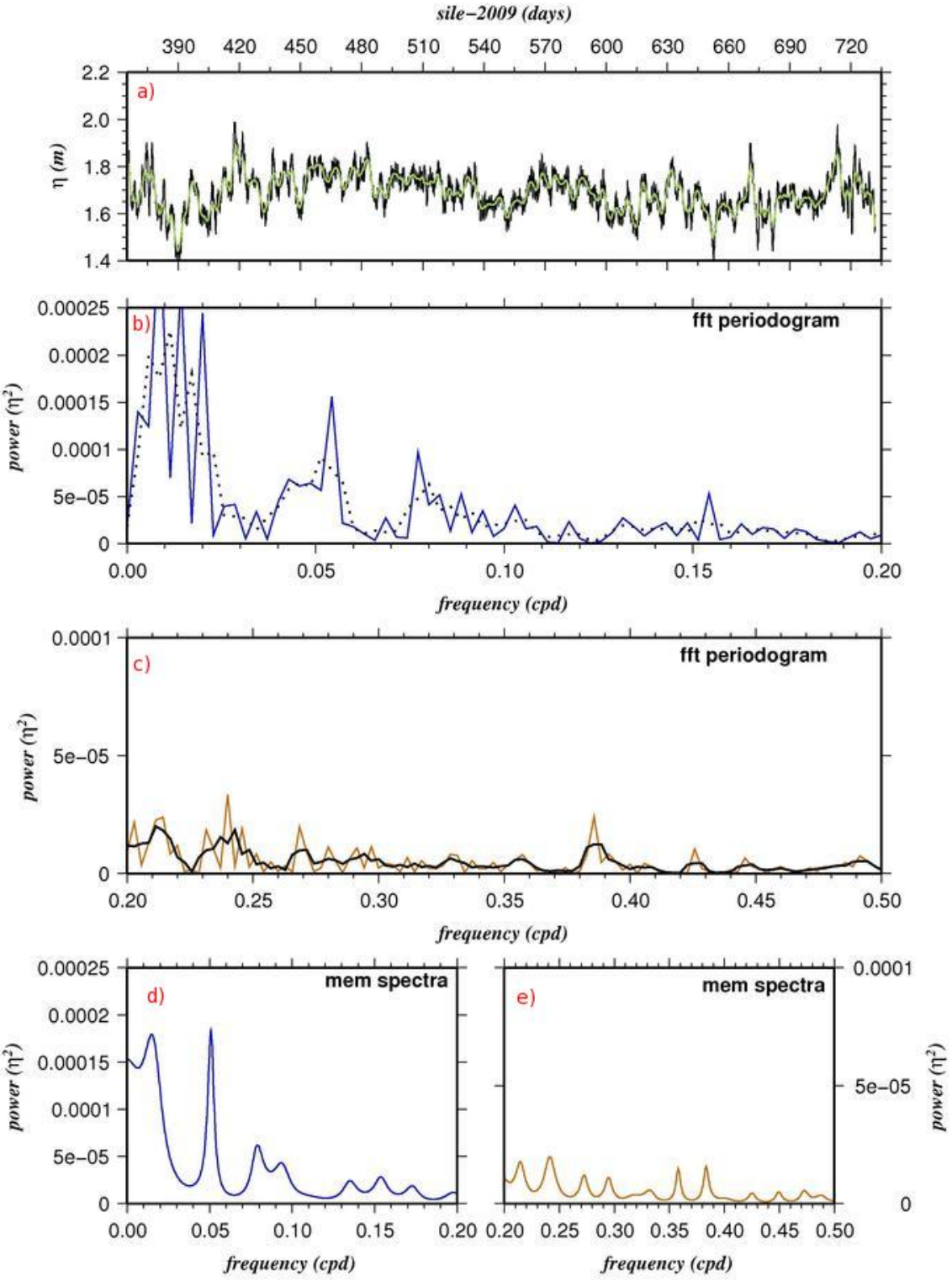

Figure 3.87: Sile sea level spectra in 2009; a) time series, FFT power spectrum between b) 0 - 0.2 cpd, c) 0.2 - 0.5 cpd , MEM power spectrum between d) 0 - 0.2 cpd, e) 0.2 - 0.5 cpd

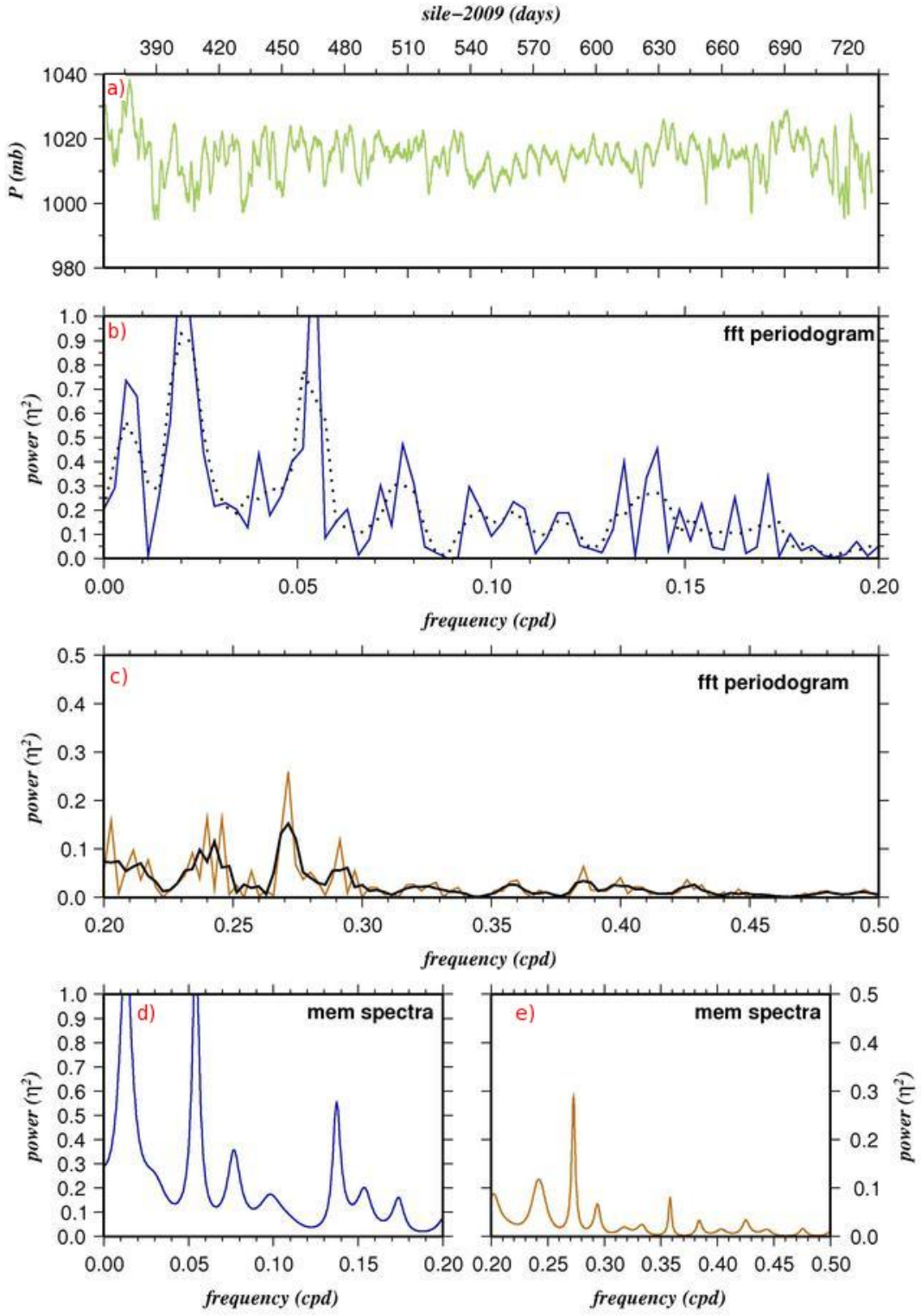

Figure 3.88: Sile atmospheric pressure spectra in 2009; a) time series, FFT power spectrum between b) 0 - 0.2 cpd, c) 0.2 - 0.5 cpd , MEM power spectrum between d) 0 - 0.2 cpd, e) 0.2 - 0.5 cpd

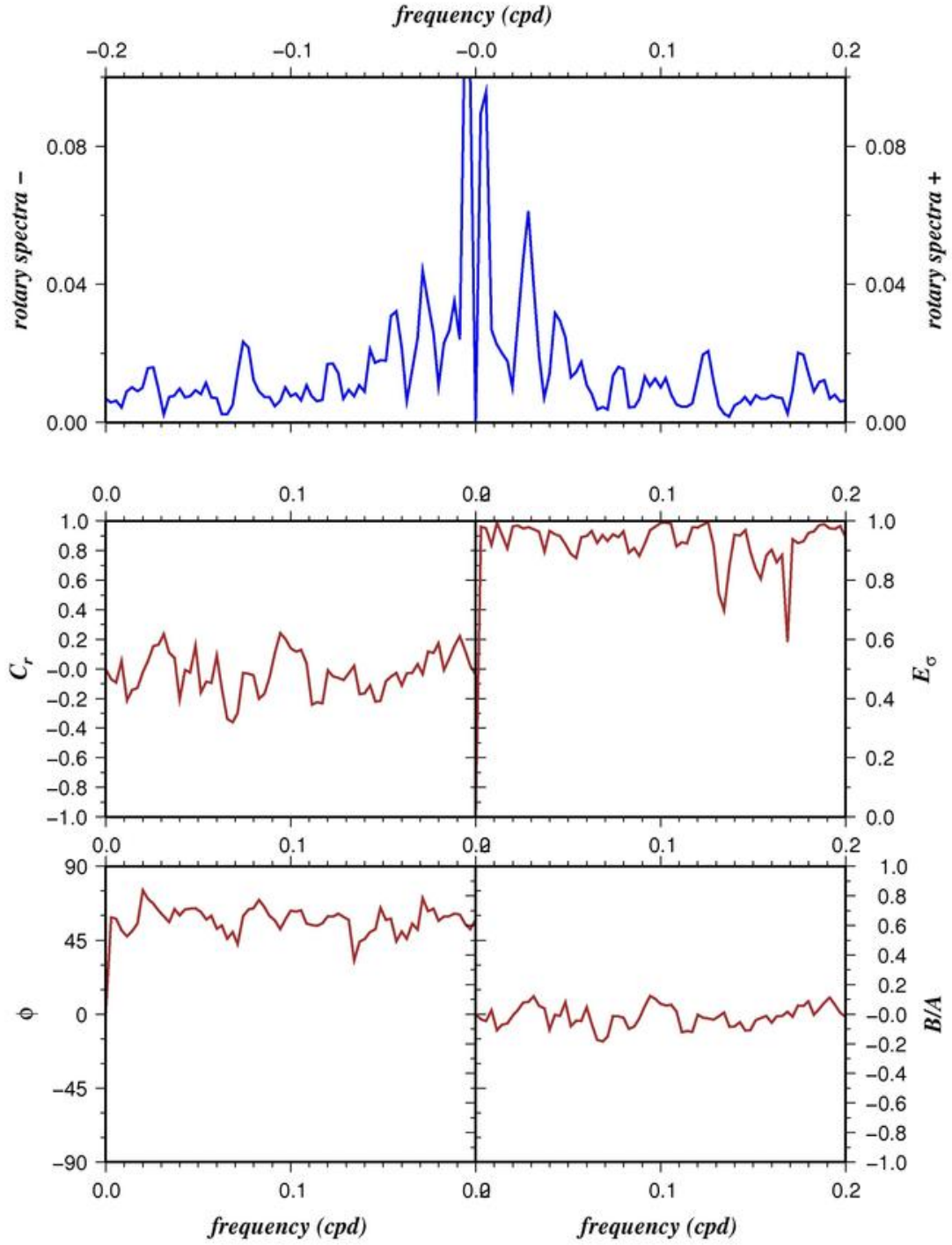

Figure 3.89: Sile wind rotary spectra in 2009; Power spectrum in 0 - 0.2 cpd range (upper panel), rotary coefficent (middle left), ellipse stability (middle right), orientation angle (lower left), the ratio of major axis to minor axis (lower right)

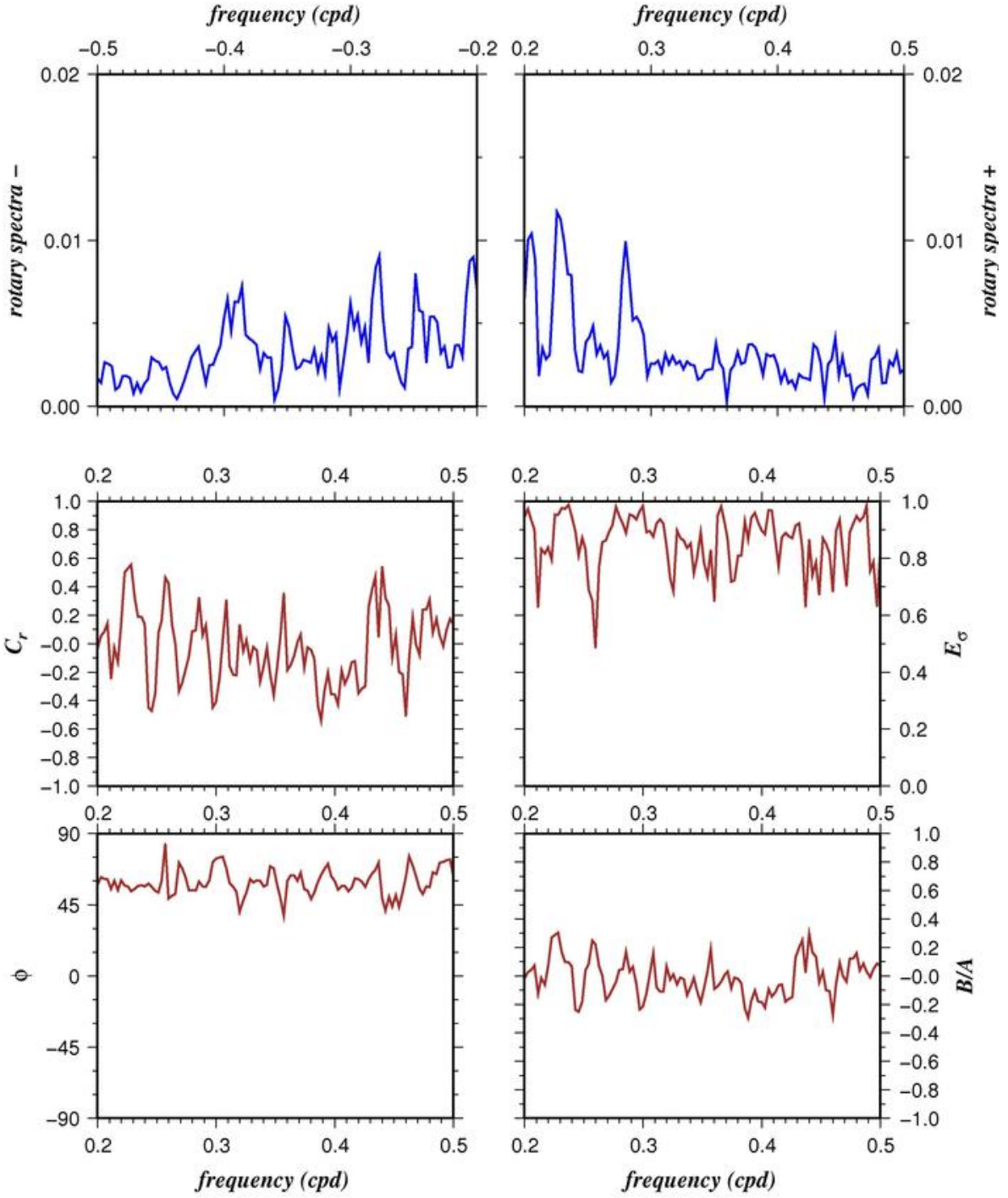

Figure 3.90: Sile wind rotary spectra range in 2009; Power spectrum in 0.2 - 0.5 cpd range (upper left and right), rotary coefficent (middle left), ellipse stability (middle right), orientation angle (lower left), the ratio of major axis to minor axis (lower right)

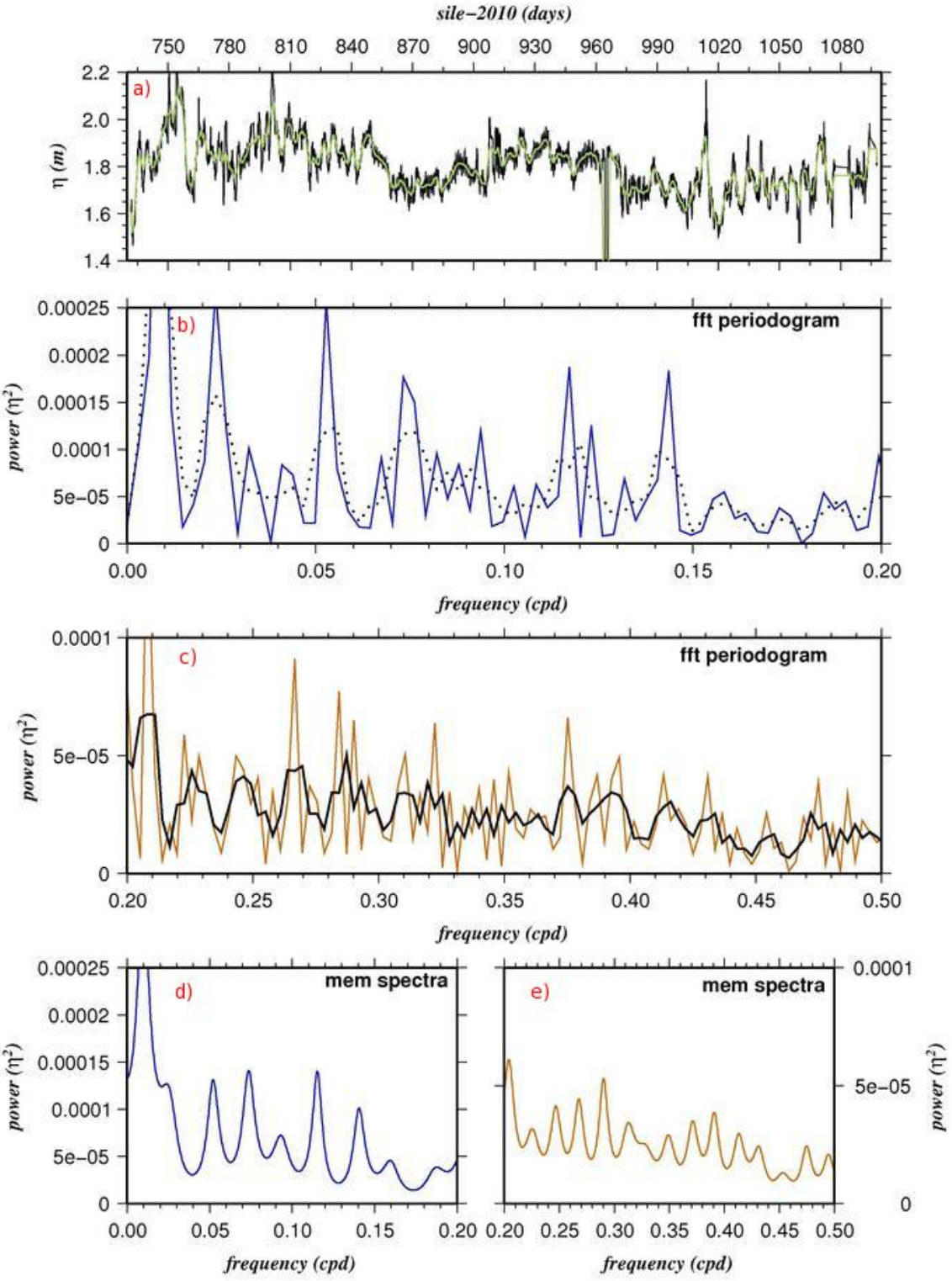

Figure 3.91: Yalova sea level spectra in 2009; a) time series, FFT power spectrum between b) 0 - 0.2 cpd, c) 0.2 - 0.5 cpd , MEM power spectrum between d) 0 - 0.2 cpd, e) 0.2 - 0.5 cpd

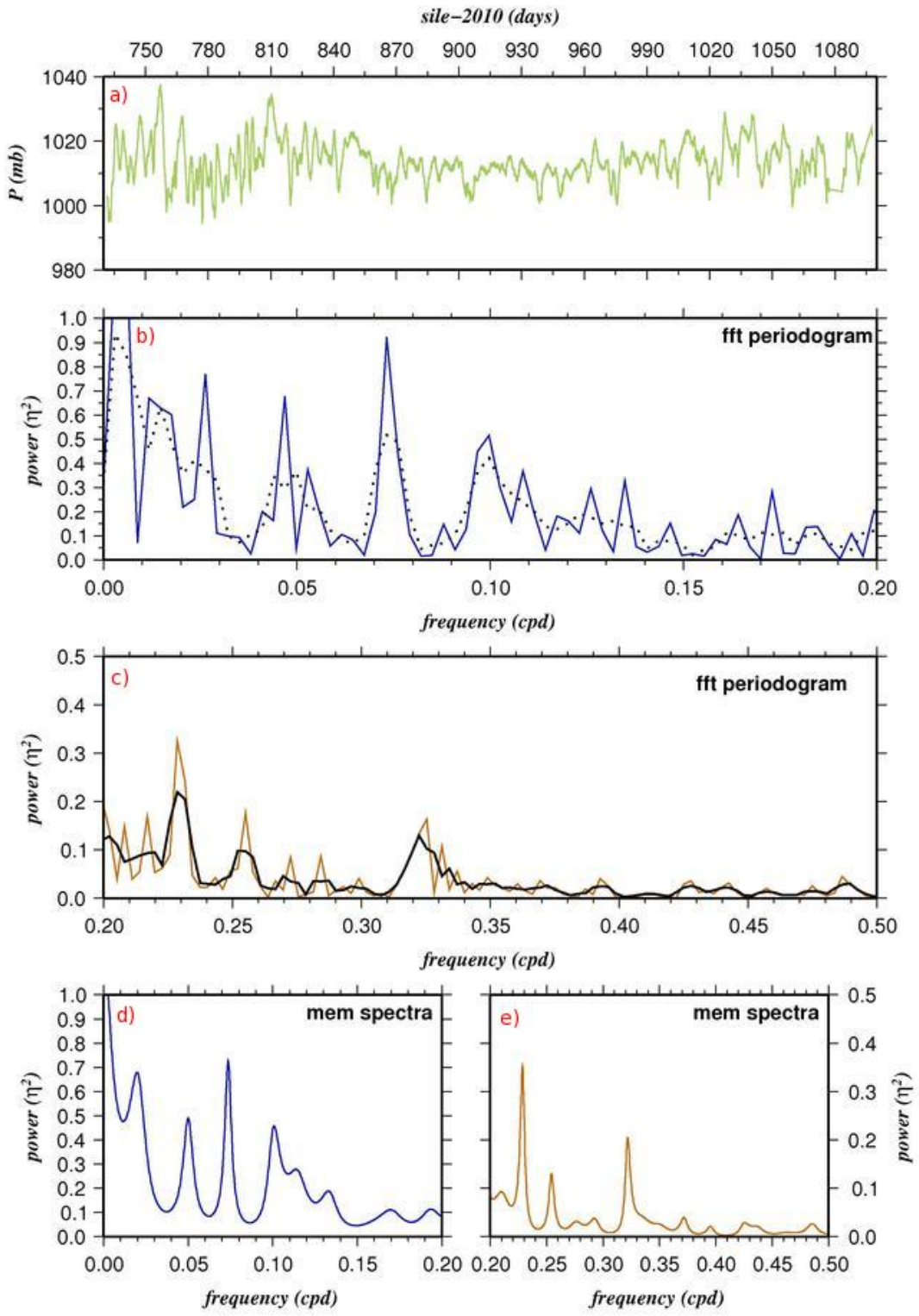

Figure 3.92: Yalova atmospheric pressure spectra in 2010; a) time series, FFT power spectrum between b) 0 - 0.2 cpd, c) 0.2 - 0.5 cpd , MEM power spectrum between d) 0 - 0.2 cpd, e) 0.2 - 0.5 cpd

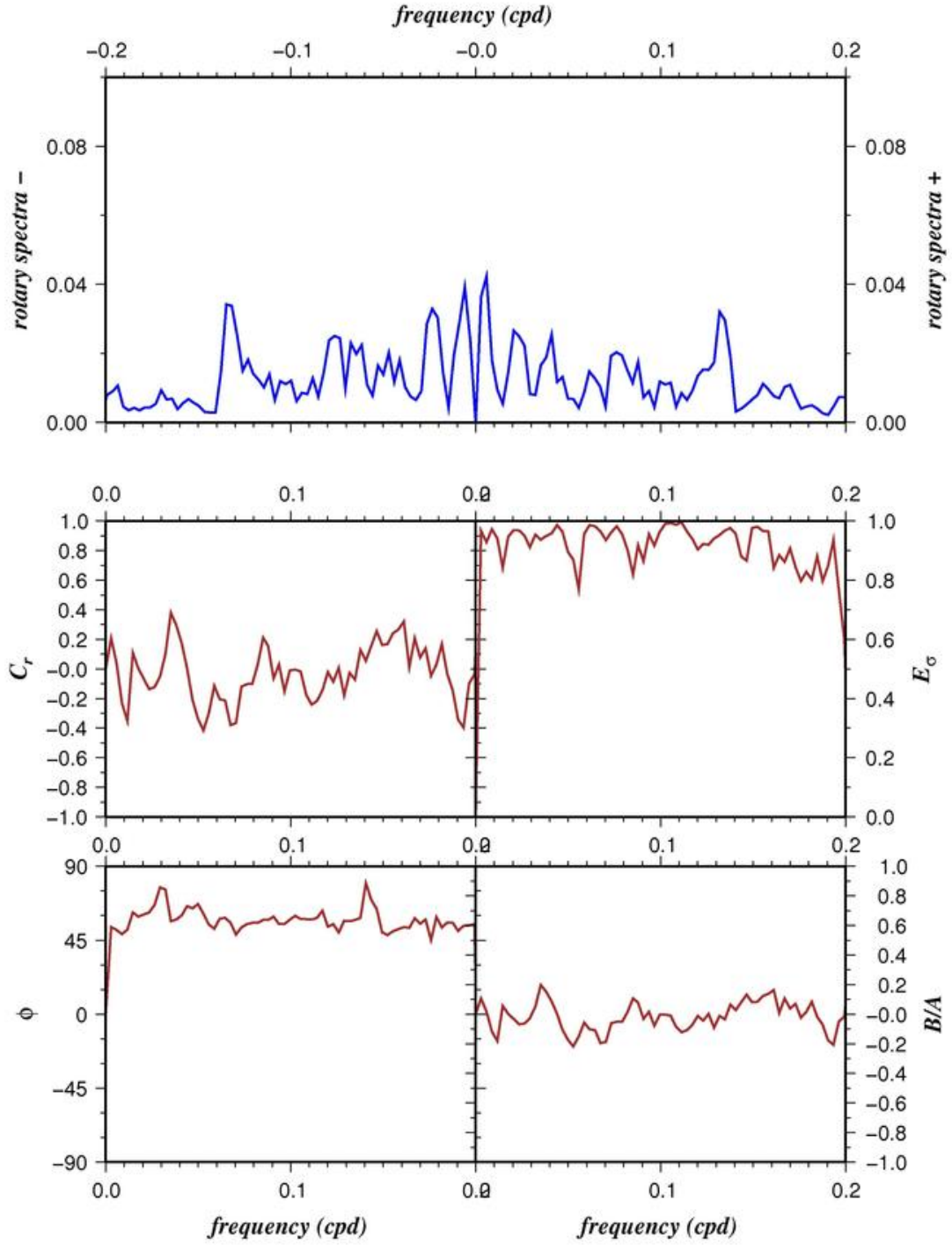

Figure 3.93: Sile wind rotary spectra in 2010; Power spectrum in 0 - 0.2 cpd range (upper panel), rotary coefficent (middle left), ellipse stability (middle right), orientation angle (lower left), the ratio of major axis to minor axis (lower right)

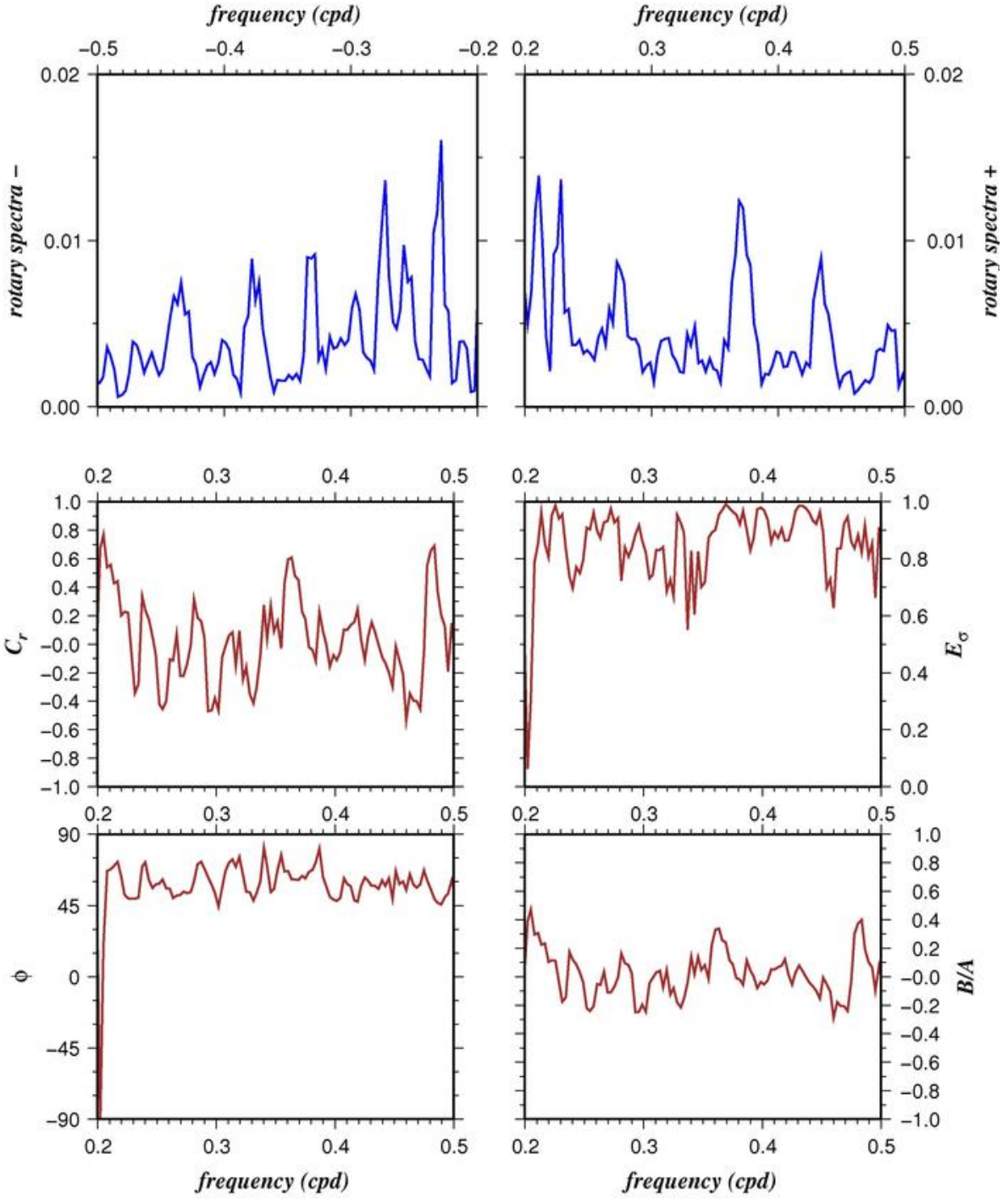

Figure 3.94: Sile wind rotary spectra in 2010; Power spectrum in 0.2 - 0.5 cpd range (upper left and right), rotary coefficent (middle left), ellipse stability (middle right), orientation angle (lower left), the ratio of major axis to minor axis (lower right)

Chapter 4

FINAL REMARKS

In this study, time series of meteorologic and marine data obtained along the Turkish coast yield the conclusions below.

Sea level is highly variable in the Turkish Coasts,especially Turkish Strait System.In addition to diurnal and semidiurnal oscillations in sea level, the analyses of sea level reveals that basin oscillations can vary from several days to weeks owing to winds, barometric pressure differences. Turkish Strait System is influenced by the Black Sea and the Mediterranean oscillations, although there is very limited penetration of tidal oscillations. Sea level changes with a few days scale in Black Sea are dominated by basin-scale winds. Moreover, Black Sea doesn't respond atmospheric pressure as invert barometer at all. On the other hand, In Marmara Sea, both atmospheric pressure and wind effect sea level obviously.Lastly, Mediterranean seems mainly affected by atmospheric pressure.

Annual mean sea level difference between the Black and Marmara Sea is found to be around 26 cm during the study period. However, this difference disappears with the blockage events observed in the upper layer flow of Bosphorus. The blockage events are mainly associated with meteorological parameter such as wind and atmospheric pressure. The lower layer blockages usually occur in spring due to the increasing of sea level in Black Sea whereas the upper layer blockage events occur in winter due to the southwesterly winds.Based on four years observation, upper layer current is well documented in seasonal scale.

Upper layer flux is mainly dominated by sea level differences between Marmara and Black Sea. This study shows that in seasonal scale, the maximum upper layer flux occurs in spring especially March, whereas minimum upper layer transport occurs during winter.

There is drastic sea level rising in 2010, especially in Black Sea and Marmara Sea. it is considered as associated with hydrological cycle and a response to the global climatic variability. Due to the lack of river discharge data during study period,it is not well documented but NAO indexes support this interpretation.

Surface and Internal oscillation which is calculated analytically is not observed during this study, maybe due to their high frequency range or coupling mechanisms between these oscillations.

During the summer, the sea breeze regime dominates along Mediterranean coasts from May to September. However, the regional topography can result in local wind characteristic. Poyraz wind regime observed at Tasucu station is an example of this type effect. Marmara and Agean regions are under influence of northerly and northeastly winds (Etesian winds). During the winter, cyclonic systems lasting from 3 to 5 days frequently are observed.

Chapter 5

REFERENCES

Alhammoud, B., K. Béranger, L. Mortier, M. Crépon and I. Dekeyser, 2005. Surface circulation of the Levantine Basin:Comparison of model results with observations, Progress In Oceanography, 66, 2-4, 299-320, doi:10.1016/j.pocean.2004.07.015

Alpar, B. and Yüce, H., (1998). Sea-Level Variations and their Interactions between the Black Sea and the Aegean Sea. Estuarine, Coastal and Shelf Science, 46, 609-619.

Andersen, S., Jacobsen, F., Alpar, B., (1997). The Water Level in the Bosphorus Strait and its Dependence on Atmospheric Forcing. Deutsche Hydrographische Zeitschrift, 49, 4.

Ataktürk, S.S. (1980). Atmospheric variability and air-sea interactions in the northern margins of Cilician Basin, Ms Thesis, Dept. of Marine science, Middle East Technical University, 84 pp.

Ayoub, N., Le Traon, P. Y., De Mey, P. (1998). A description of the Mediterranean surface variable circulation from combined ERS-1 and TOPEX/POSEIDON altimetric data. Journal of Marine Systems, 18, 3 - 40.

Bartex, Inc. (1995). User's guide 4100 Series Aquatrak, Annapolis, MD, USA.

Beşiktepe, Ş., Sur, H.İ., Özsoy, E., Latif, M.A., Oğuz, T., Ünlüata, Ü., (1994). The Circulation and Hydrography of the Marmara Sea. Prog. Oceanogr. 34, 285-334.

Büyükay, M., (1989). The surface and internal oscillations in the Bosphorus, related to

meteorological forces, M.Sc. Thesis, Institute of Marine Sciences, Middle East Technical University, 169p.

Campbell Scientific, Inc.(1997), PC208W Datalogger Support Software Manual, Logan, Utah, USA.

Çeçen, K., Beyazıt, M., Sümer, M., Güclüer, S., Doğusal, M., Yüce, H., (1981). Oceanographic and hydraulic investigations of the Bosphorus:Section I, Final Report, submitted to the Irrigation Unit of the Turkish Scientific and Technical Research Council, Istanbul Technical University,(in Turkish), Istanbul, 166p.

Dee, D.P., with 35 co-authors., (2011). The ERA-Interim reanalysis: configuration and performance of the data assimilation system. Quart. J. R. Meteorol. Soc., 137, 553-597.

Ducet, N., Le Traon, P.Y. and Gauzelin, P., (1999). Response of the Black Sea mean level to atmospheric pressure and wind forcing. J. Mar. Sys. 22, 311-327.

Hedström, K. S., (1997). Draft User's Manual for an S-Coordinate Primitive Equation Ocean Circulation Model (SCRUM) Version 3.0, Institute of Marine and Coastal Sciences, Rutgers University, Rutgers University.

Hurrell, J.W., Kushnir, Y., Ottersen, G., Visbeck, M., (2003). An overview of the North Atlantic Oscillation. In: Hurrell, W., Kushnir, Y., Ottersen, G., Visbeck, M. (Eds.), The North Atlantic Oscillation: Climatic Significance and Environmental Impact. Geophysical Monograph, vol. 134. American Geophysical Union, Washington DC, pp. 1-36.

Gregg, M. C., Ozsoy, E. and Latif, M. A., 1999. Quasi-steady exchange flow in the Bosphorus Geophysical Research Letters, 26, 83-86.

Gregg, M. C. and Ozsoy, E., (2002). Flow, water mass changes, and hydraulics in the Bosphorus, J. Geophys. Res.,107(C3).

Gonella, J.,(1972). A rotary-component method for analysing meteorological and oceanographic vector time series, Deep Sea Res., 19, 833-846.

Gunnerson, C.G., Özturgut, E., (1974). The Bosphorus,in Degens, E.T. and D.A. ROSS (Eds).The Black Sea - Geol., Chem. and Biol., American Assoc. Pet. Geol. Memoir 20, 99-113.

Karaca M, Deniz A, Tayanç M (2000). Cyclone track variability over Turkey in association with regional climate. Int J Climatol 20:1225-1236

Latif,M.A.,E. Ozsoy,T.Oguz and U. Unluata(1991).Observations of the Mediternean inflow into Black Sea, Deep Sea Research,38,Suppl. 2,S711-S723.

Larnicol, G., Ayoub, N., Le Traon, P. Y. (2002). Major changes in Mediterranean sea-level variability from 7 years of TOPEX/ Poseidon and ERS-1/2 data. Journal of Marine Systems, 33 - 34, 63 - 89.

LeBlond, P.H. and L.A. Mysak, 1978, Waves in the Ocean, Elsevier, Amsterdam.

MFS team (2001). Mediterranean Forecast System Pilot Project, final scientific report-I/II of the EU-MAST Project, contract MAS3- CT98-0171. Available from: http://www.cineca.it/ mf-spp000/documents/documents.html.

Ovchinnikov, I. M., 1966. Circulation in the surface and intermediate layers of the Mediterranean, Oceanology, 6, 48-57

Özsoy, E., (1981). On the atmospheric factors affecting the Levantine Sea, European Centre for Medium Range Weather Forecasts, Tech. Rep. 25, 29p.

Özsoy E., Di Iorio D., Gregg, M., Backhaus, J., (2001). Mixing in the Bosphorus Strait and the Black Sea Continental Shelf: Observations and a Model of the Dense Water Outflow. J. Mar. Sys. 31, 99-135.

Özsoy, E. and Ünlüata, Ü., (1997). Oceanography of the Black Sea: A Review of Some Recent Results. Earth Sci. Rev. 42 (4), 231-272.

Özsoy, E., Latif, M.A., Beşiktepe, Ş., Çetin, N., Gregg, N., Belokopytov, V., Goryachkin, Y., Diaconu, V., (1998). The Bosphorus Strait: Exchange Fluxes, Currents and Sea-Level Changes. in: L. Ivanov and T. Oğuz (editors), Ecosystem Modeling as a Management Tool for the Black Sea, NATO Science Series 2: Environmental Security 47, Kluwer Academic Publishers, Dordrecht, 1395 vol. 1, 367 pp + vol. 2, 385 pp.

Özsoy, E., Latif, M. A., Sur, H. I. and Goryachkin, Y., 1996. A review of the exchange flow regimes and mixing in the Bosphorus Strait, in: Briand, F. (editor), Mediterranean Tributary Seas, Bulletin de l'Institut Oceanographique, Monaco, Special Number 17, CIESM Science Series No. 2, Monaco.

Oğuz, T., Ş., Beşiktepe, (1999). Observations on the Rim Current structure, CIW Formation and transport in the western Black Sea. Deep-Sea Research.I, 46, 1733.1753

O'Brien J. J., Pillybury D. R., (1974). Rotary Wind Spectra in a Sea Breeze Regime. Journal of Metrorology, Vol. 13, No. 7, pp. 820-825.

Ulrych T.J., Bishop T.N. (1975). Rev. Geophys. Space Phys., 13 183.

Ünlüuata, O., Oğuz, T., Latif, M.A., Özsoy, E., (1990). On the physical oceanography of the Turkish Straits. In: Pratt, L.J. (Ed.), The Physical Oceanography of Sea Straits.NATO/AS1 Series, Kluwer, Dordrecht, pp. 25-60.

Pekarova P., Miklanek P., Onderka M., Halmova D. ,Mitkova B. V., Meszaros I., Skoda P., (2008). Flood Regime of Rivers in the Danube river basin: A case study of the Danube at Bratislava. National Report for the IHP UNESCO Negional Cooperation of Danube Countries.

Reiter, E.R. (1975). Handbook for Forecasters in the Mediterranean, Naval Postgraduate School, Monterey, California,Techinal Paper No. 5-75, 344pp.

Robinson, A.R., W.G. Leslie, A. Theocharis and A. Lascaratos. 2001. Mediterranean Sea Circulation Encyclopedia of Ocean Sciences. Academic Press, 1689-1706, doi:10.1006/rwos.2001.0376

Ross D.A. and E.T. Degens, (1974). Recent sediments of the Black Sea. In: The Black

Sea-Geology, Chemistry, and Biology, Degens.E.T and Ross.D.A, eds, American Association of Petroleum Geologists Memoir Vol.20, Tulsa, Oklahoma, U.S.A., pp. 183-199.

Shchepetkin, A. F., and J. C. McWilliams (2005). The regional oceanic modeling system (ROMS): A split-explicit, free-surface, topography- following-coordinate oceanic model, Ocean Modell., 9, 347-404.

Sözer, A., (2012). Numerical Modeling of the Bosphorus Exchange Flow Dynamics, Institute of Marine Sciences, Middle East Technical University, Erdemli, Mersin, Turkey (unpublished Ph.D thesis, in preparation).

Stanev, E.V. and E.L. Peneva. (2002). Regional sea level response to global climatic change: Black Sea examples. Global and Planetary Change 32:33-47.

Yüce, H., (1993a). Water level variations in the Sea of Marmara. Oceanologica Acta, 16, 4, 335-340.

Yüce, H., (1993b). Analysis of the water level variations in the eastern Black Sea. J. Coastal Res., 9, 4, 1075-1082.

Yüce, H. (1996). Mediterranean water in the Strait of İstanbul (Bosphorus) and the Black Sea exit. Estuarine, Coastal and Shelf Science, 43 (5), 597-616.

Wunsch, C. (1972), Bermuda sea level in relation to tides, weather, and baroclinic fluctuations, Rev. Geophys., 10(1), 1-49, doi:10.1029/RG010i001p00001.

Zavatarelli M., Mellor G. L. 1995. A numerical study of the Mediterranean Sea circulation. Journal of Physical Oceanography,25(6), 1384-1414.

Chapter 6

APPENDIX

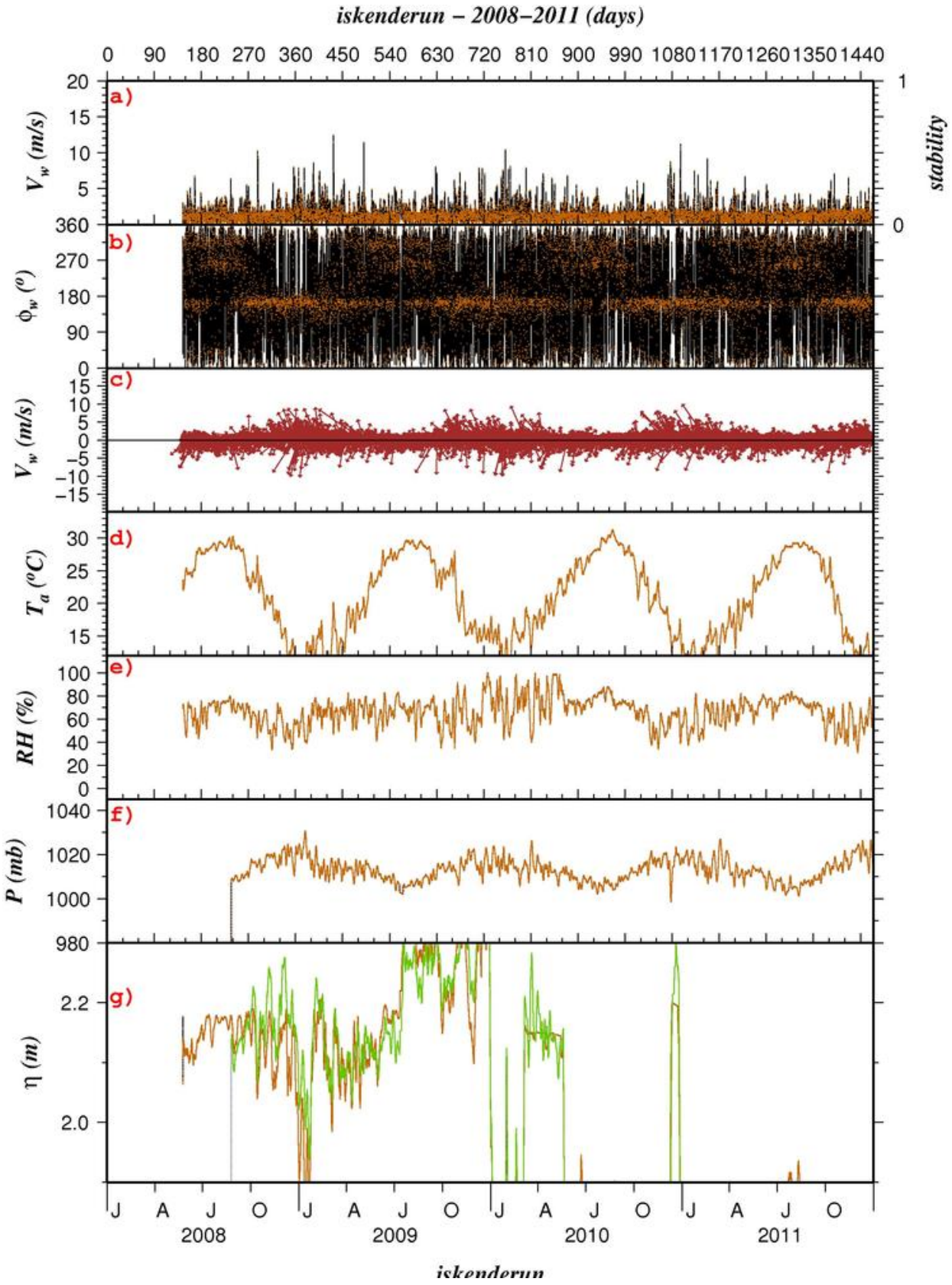

Figure 6.1: Iskenderun station time-series from 2008 to 2012; a)Wind speed, b)wind direction, c)downwind vector diagram, d)air temperature, e)relative humidity, f)atmospheric pressure and g)sea level

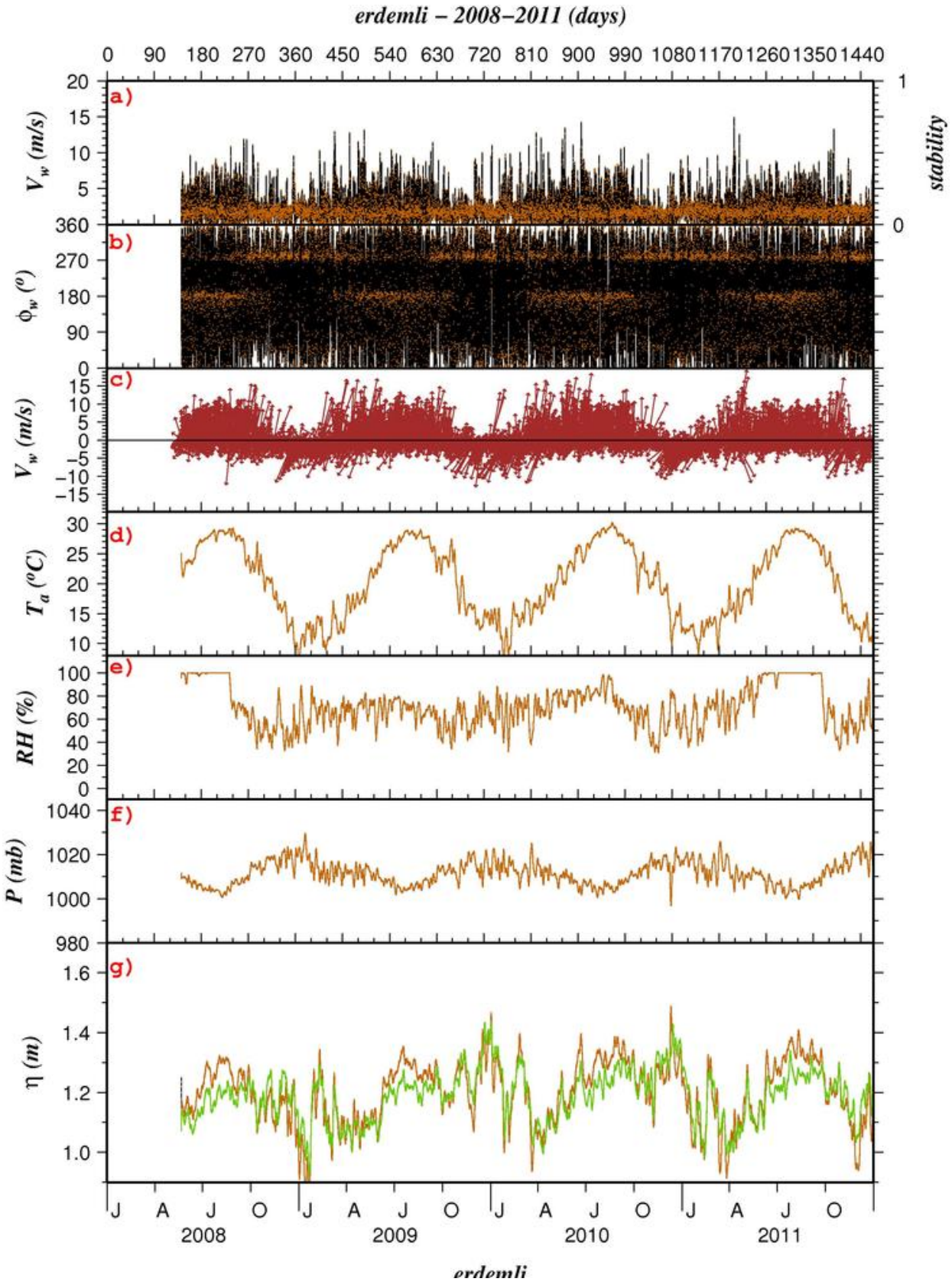

Figure 6.2: Erdemli station time-series from 2008 to 2012; a)Wind speed, b)wind direction, c)downwind vector diagram, d)air temperature, e)relative humidity, f)atmospheric pressure and g)sea level

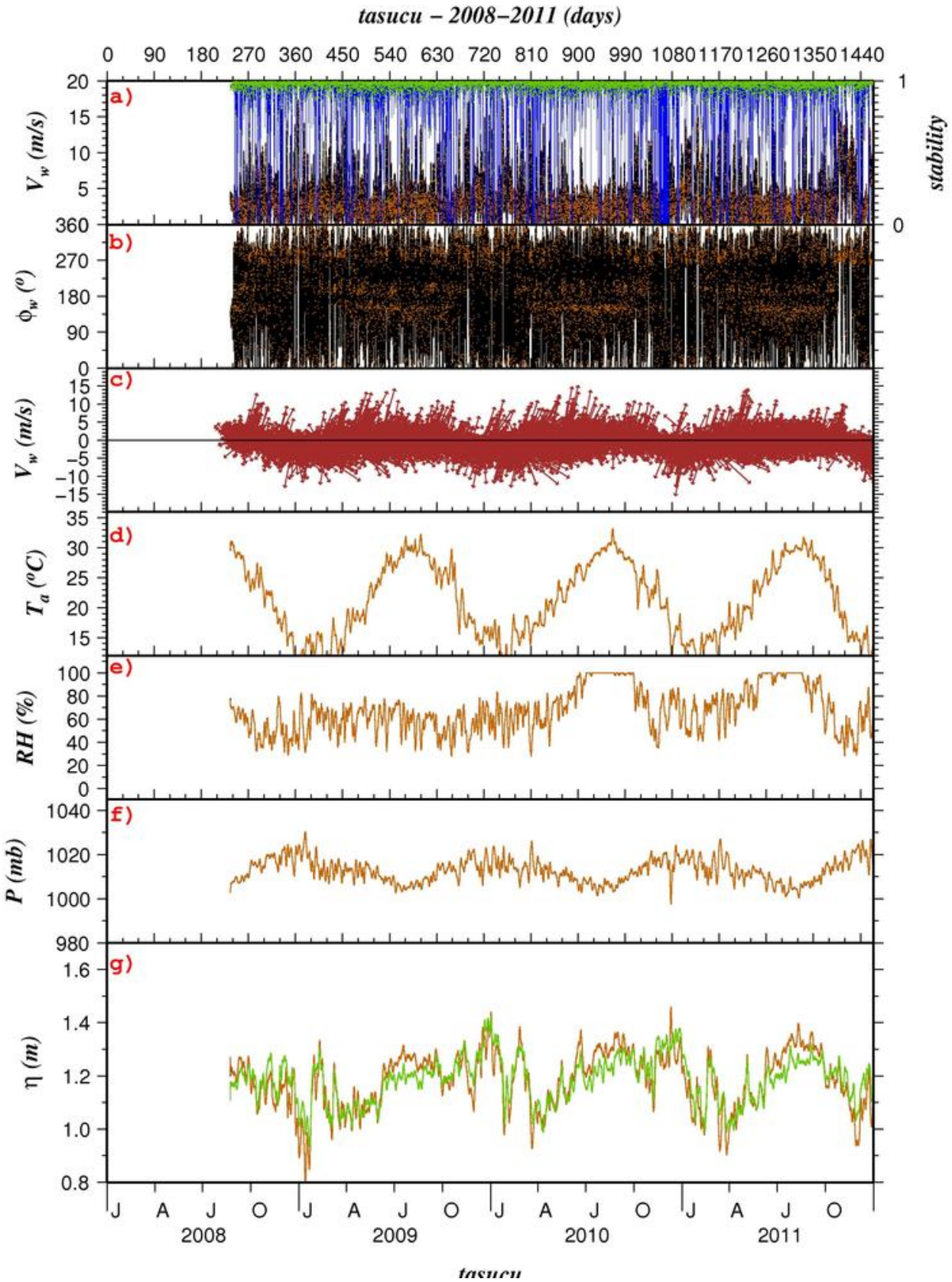

Figure 6.3: Tasucu station time-series from 2008 to 2012; a)Wind speed, b)wind direction, c)downwind vector diagram, d)air temperature,e)relative humidity, f)atmospheric pressure and g)sea level

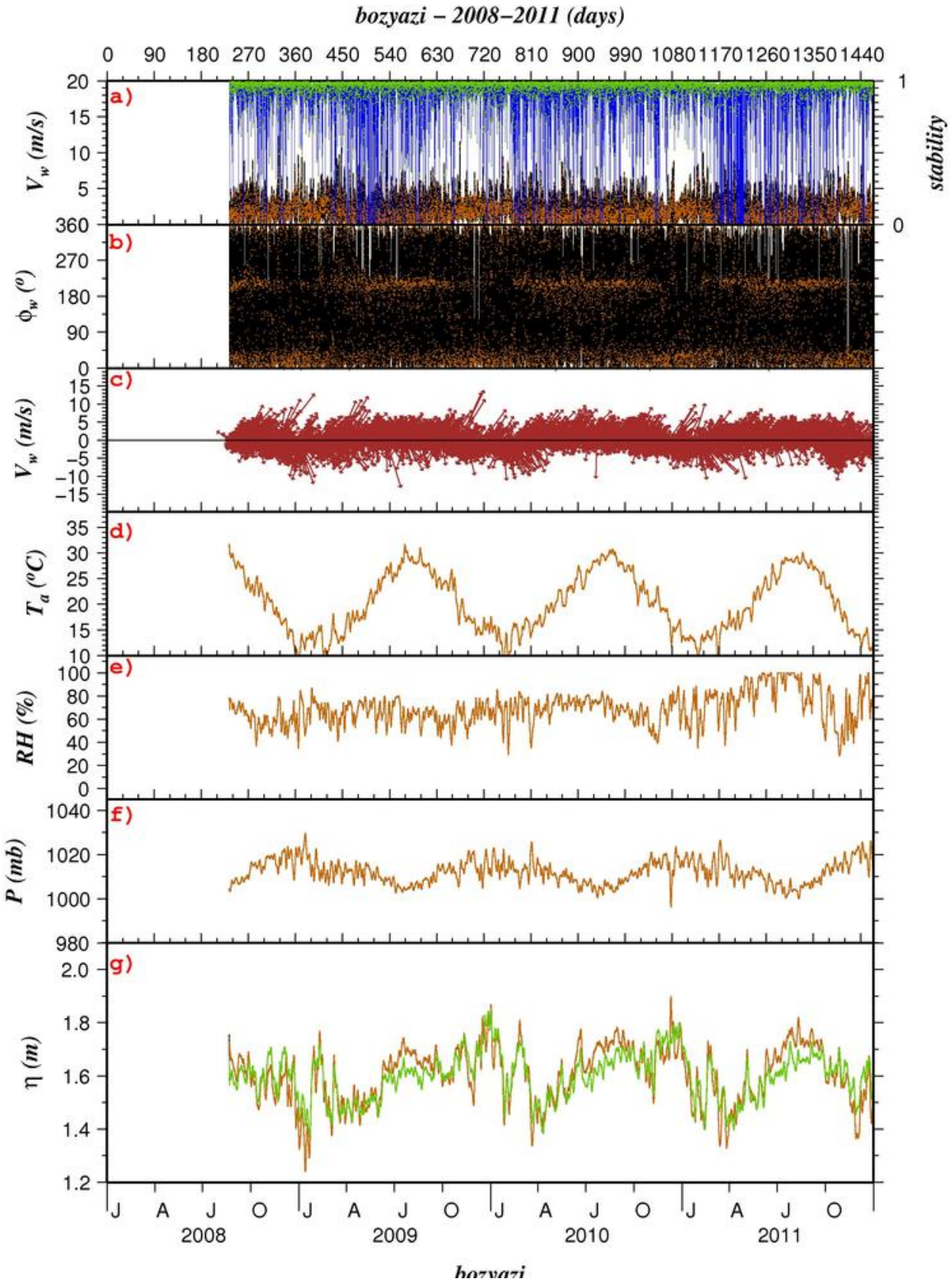

Figure 6.4: Bozyazi station time-series from 2008 to 2012; a)Wind speed, b)wind direction, c)downwind vector diagram, d)air temperature, e)relative humidity, f)atmospheric pressure and g)sea level

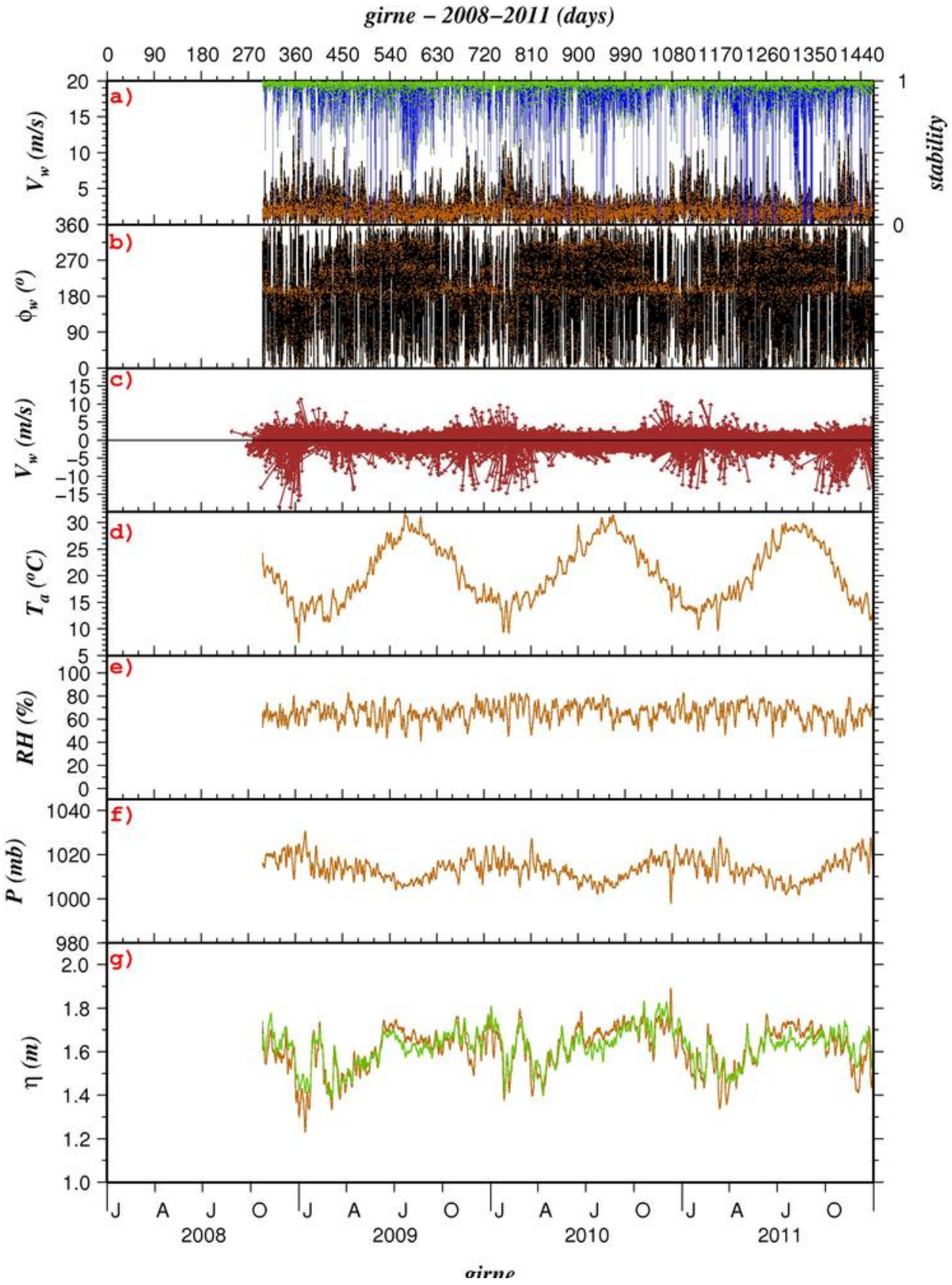

Figure 6.5: Girne station time-series from 2008 to 2012; a)Wind speed, b)wind direction, c)downwind vector diagram, d)air temperature, e)relative humidity, f)atmospheric pressure and g)sea level

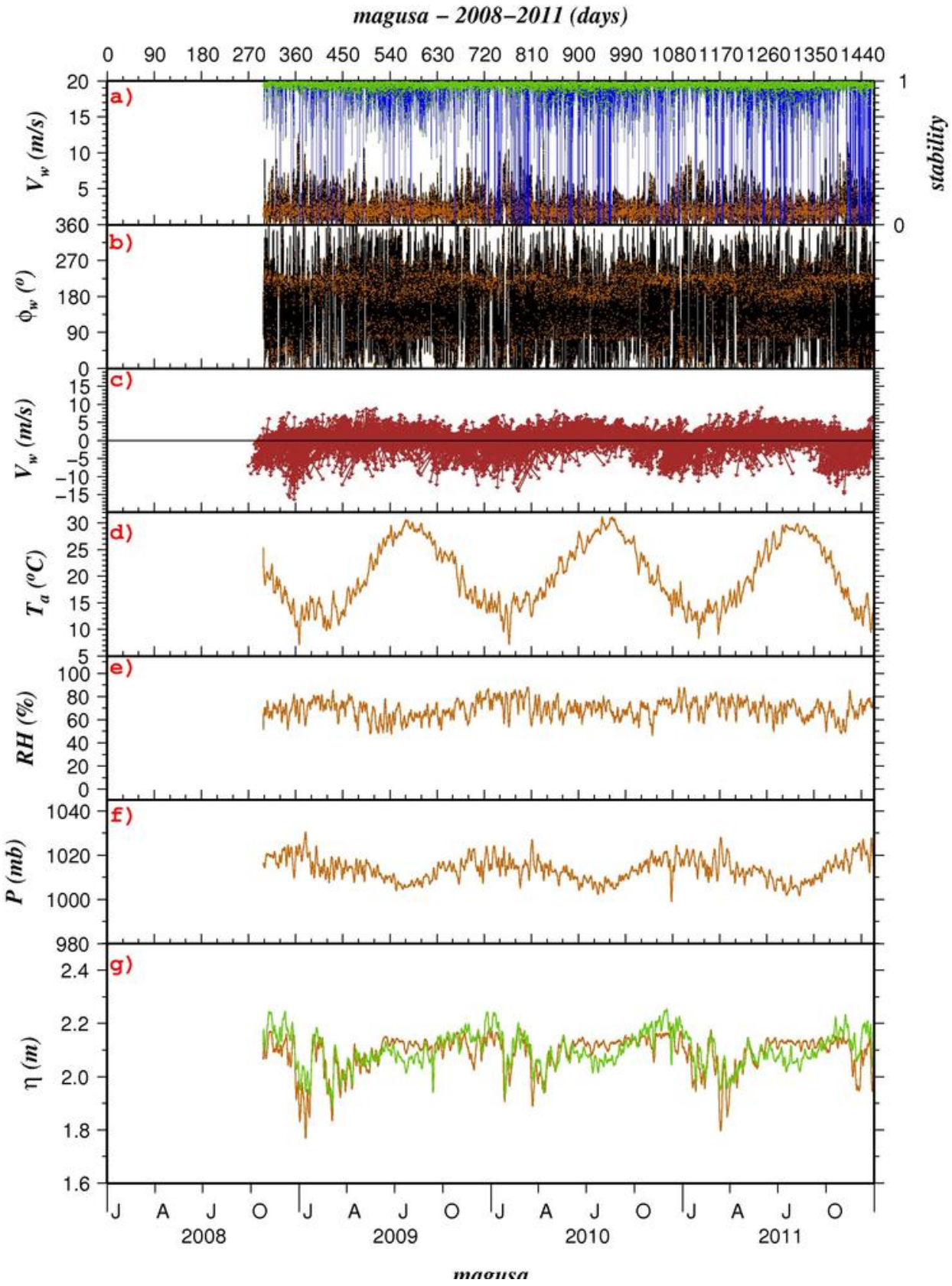

Figure 6.6: Magusa station time-series from 2008 to 2012; a)Wind speed, b)wind direction, c)downwind vector diagram, d)air temperature,e)relative humidity, f)atmospheric pressure and g)sea level

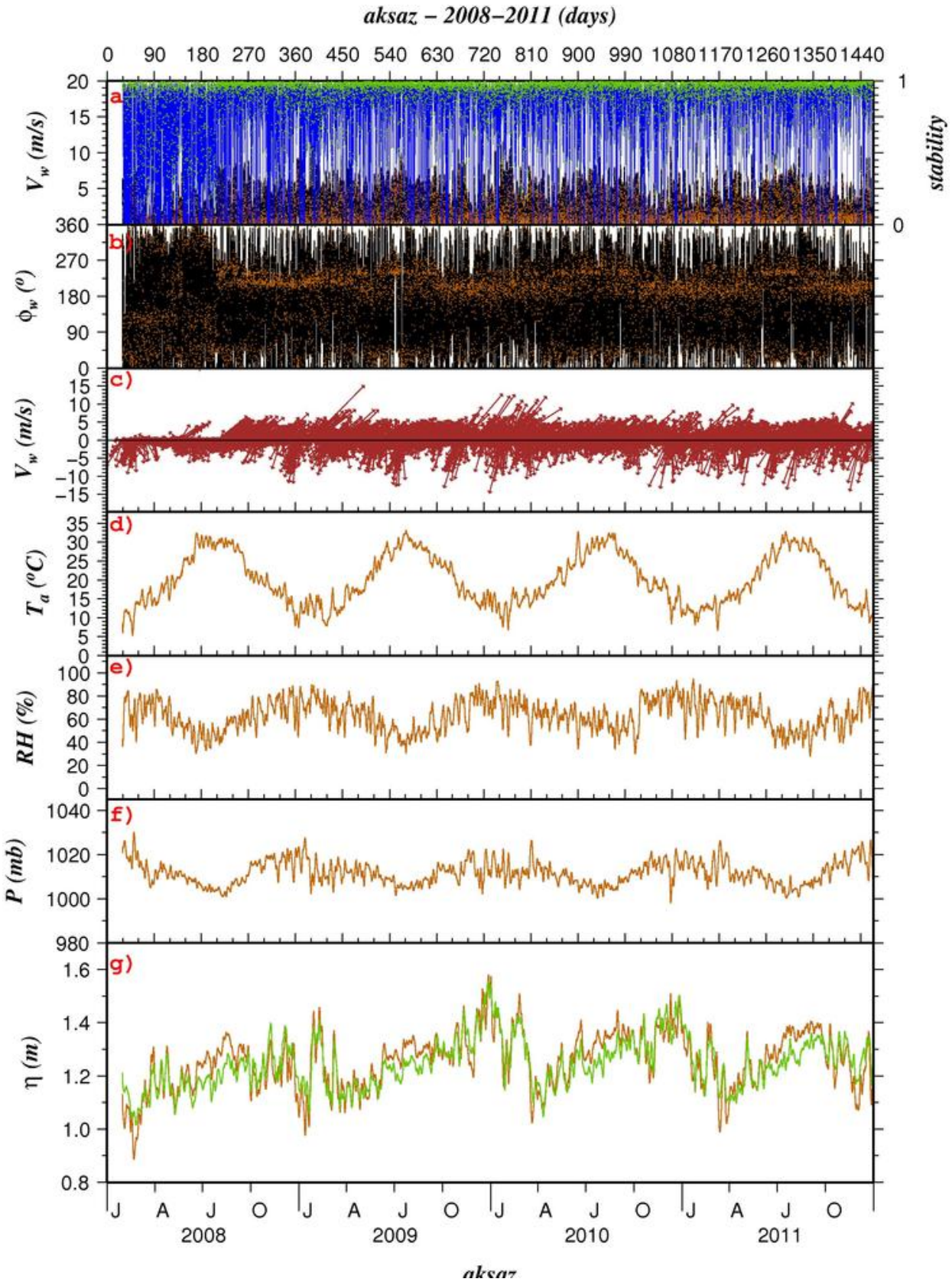

Figure 6.7: Erdemli station time-series from 2008 to 2012; a)Wind speed, b)wind direction, c)downwind vector diagram, d)air temperature,e)relative humidity, f)atmospheric pressure and g)sea level

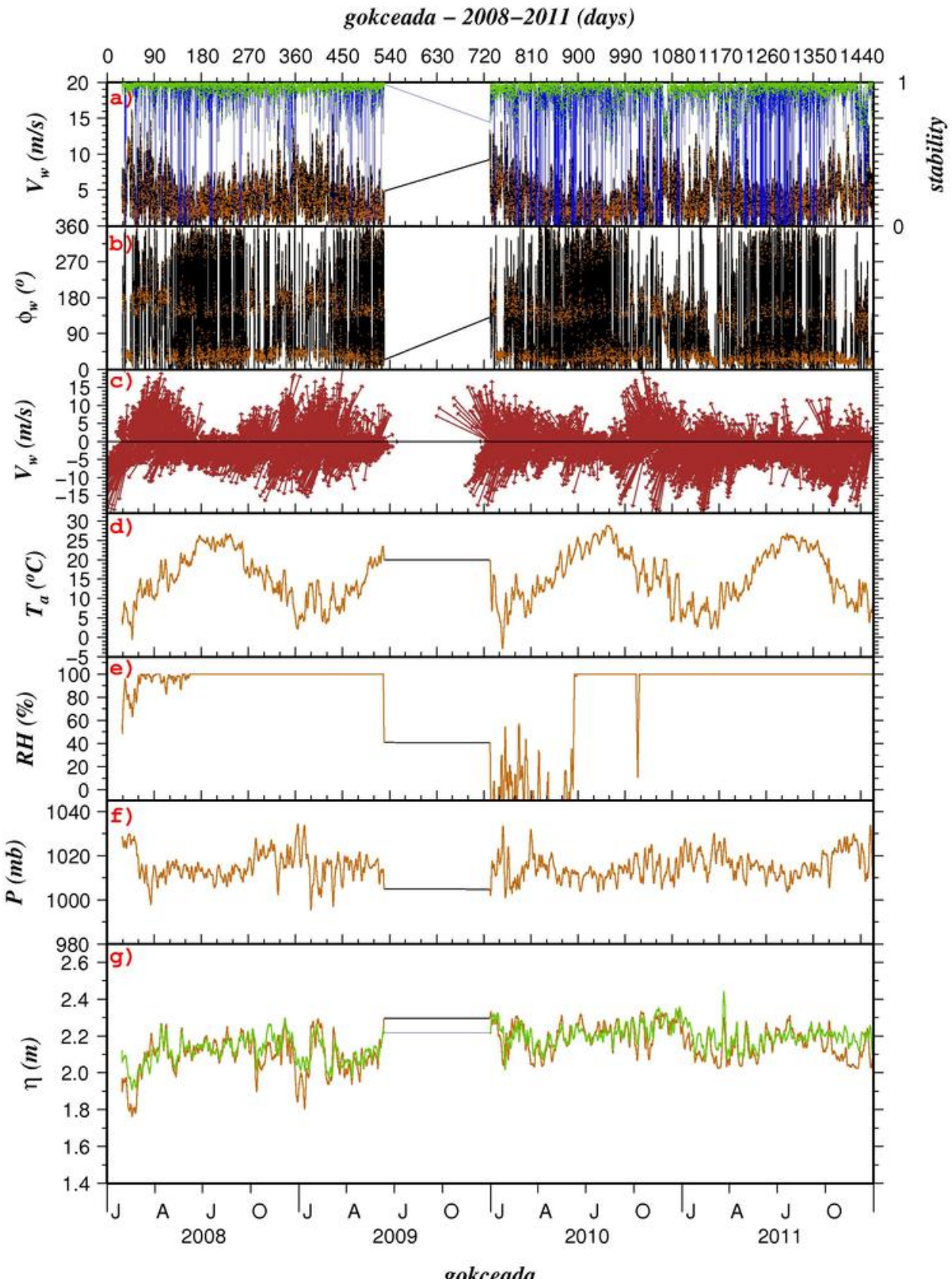

Figure 6.8: Gokceada station time-series from 2008 to 2012; a)Wind speed, b)wind direction, c)downwind vector diagram, d)air temperature, e)relative humidity, f)atmospheric pressure and g)sea level

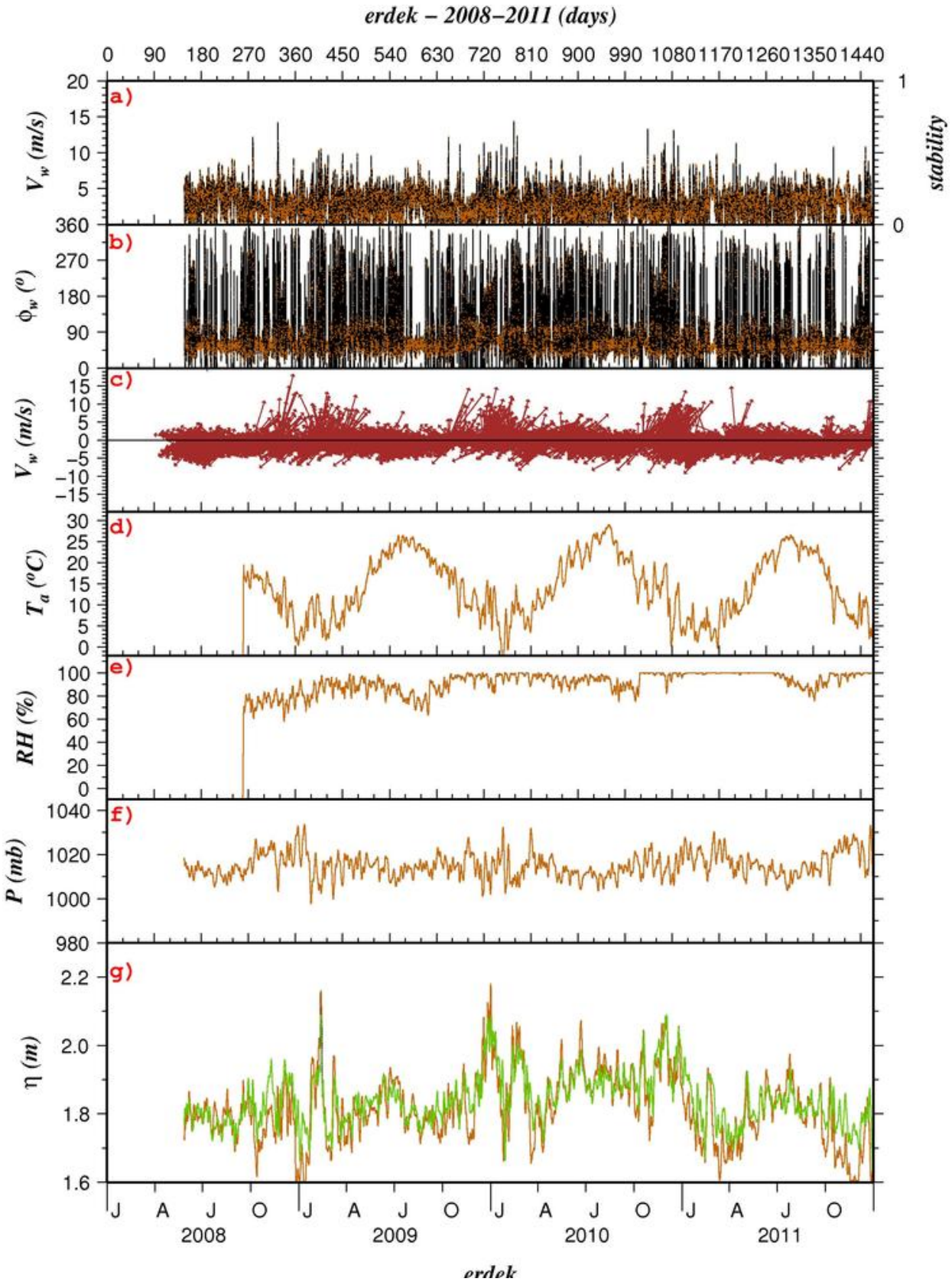

Figure 6.9: Erdek station time-series from 2008 to 2012; a)Wind speed, b)wind direction, c)downwind vector diagram, d)air temperature, e)relative humidity, f)atmospheric pressure and g)sea level

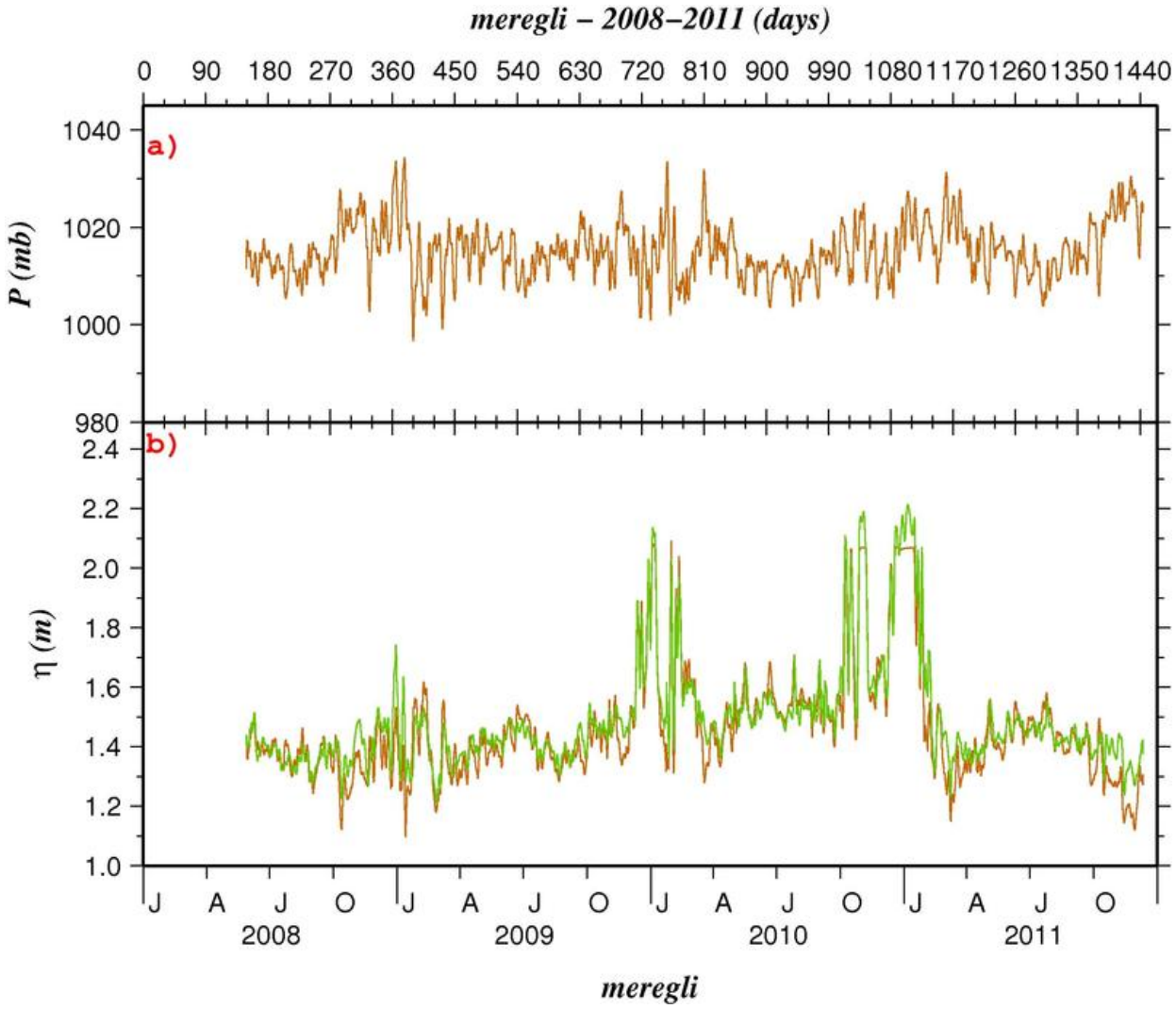

Figure 6.10: Meregli Station time-series from 2008 to 2012; a)atmospheric pressure b)sea level

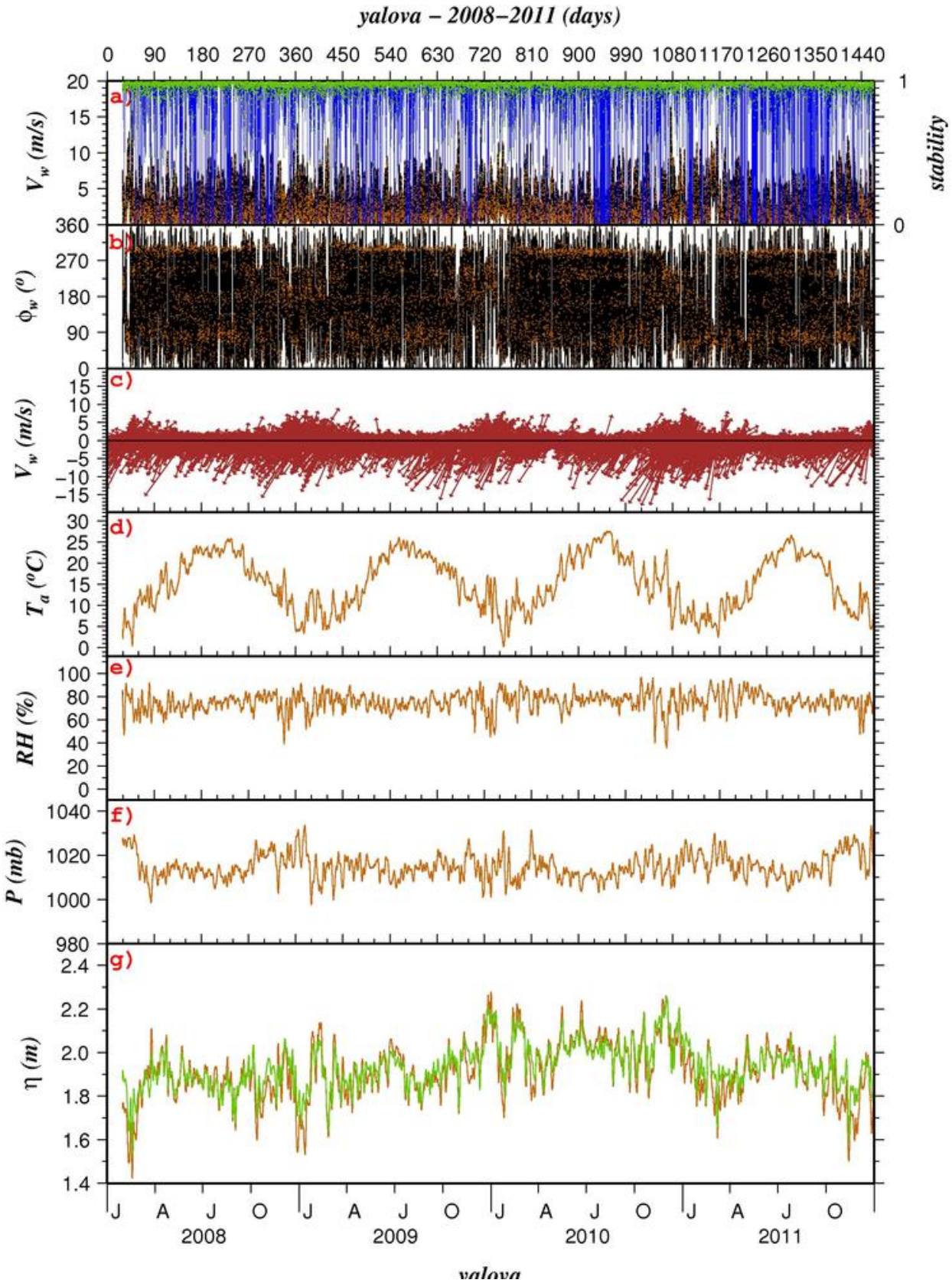

Figure 6.11: Yalova Station time-series from 2008 to 2012; a)Wind speed, b)wind direction, c)downwind vector diagram, d)air temperature, e)relative humidity, f)atmospheric pressure and g)sea level

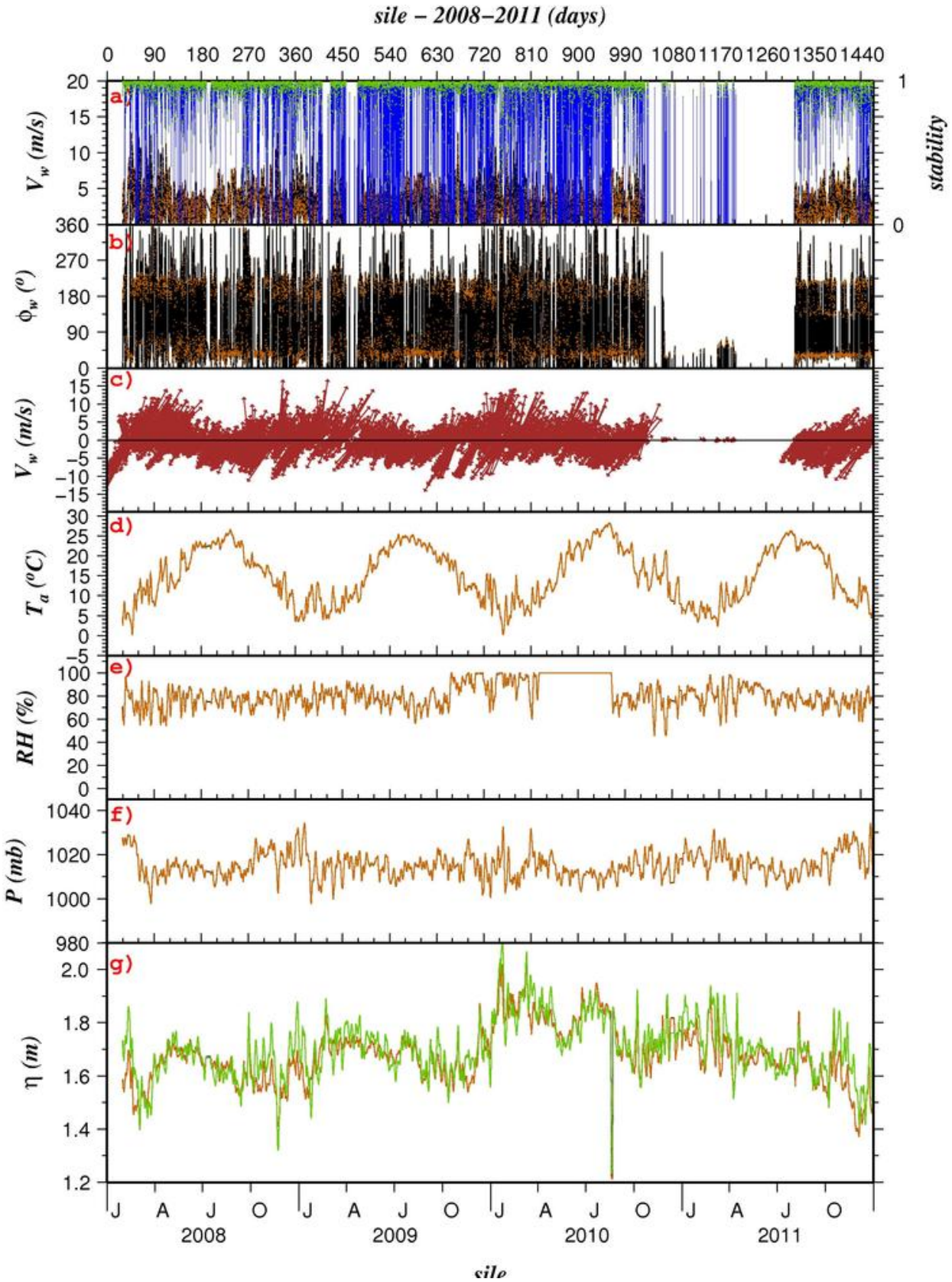

Figure 6.12: Sile Station time-series from 2008 to 2012; a)Wind speed, b)wind direction, c)downwind vector diagram, d)air temperature, e)relative humidity, f)atmospheric pressure and g)sea level

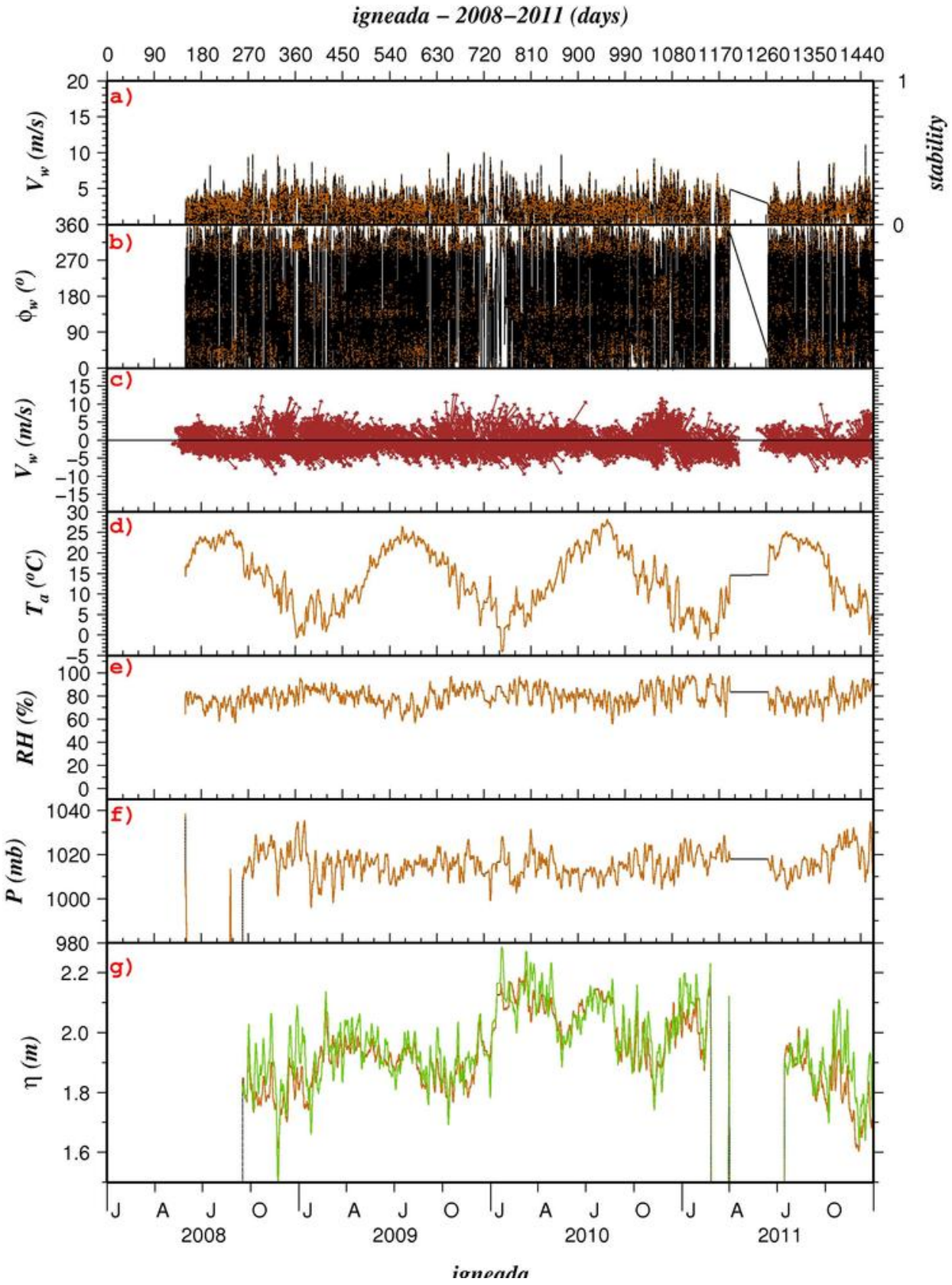

Figure 6.13: Igneada Station Time-series from 2008 to 2012; a)Wind speed, b)wind direction, c)downwind vector diagram, d)air temperature, e)relative humidity,f)atmospheric pressure and g)sea level